NASA TECHNICAL NOTE

NASA TN D-5541

NASA TN D-5541

INFINITE PERIODIC MINIMAL SURFACES WITHOUT SELF-INTERSECTIONS

by Alan H. Schoen

Electronics Research Center
Cambridge, Mass. 02139

NATIONAL AERONAUTICS AND SPACE ADMINISTRATION • WASHINGTON, D. C. • MAY 1970

1. Report No.	2. Government Accession No.	3. Recipient's Catalog No.
NASA TN D-5541		

4. Title and Subtitle	5. Report Date
Infinite Periodic Minimal Surfaces without Self-Intersections	May 1970
	6. Performing Organization Code

7. Author(s)	8. Performing Organization Report No.
Alan H. Schoen	C-98

9. Performing Organization Name and Address	10. Work Unit No.
Electronics Research Center Cambridge, Mass.	125-21-06-14
	11. Contract or Grant No.
	13. Type of Report and Period Covered
12. Sponsoring Agency Name and Address	Technical Note
National Aeronautics and Space Administration	14. Sponsoring Agency Code

15. Supplementary Notes

16. Abstract

A preliminary account of a study of the partitioning of three-dimensional Euclidean space into two interpenetrating labyrinths by intersection-free infinite periodic minimal surfaces (IPMS) is given. A construction algorithm for deriving such surfaces leads to the identification of the five cases already known, plus a number of new examples.

By the use of this algorithm and other methods, a total of seventeen intersection-free IPMS have been identified. Photographs of plastic models and computer-generated drawings of examples of such surfaces are shown. Also described and illustrated is an example of a non-orientable IPMS, generated from a skew pentagonal surface module. A counterpart to Schoenflies' proof that there exist only six quadrilateral modules of IPMS is mentioned: There exist only eight pentagonal modules of IPMS having non-cubic Bravais lattices.

17. Key Words	18. Distribution Statement
•Partitions of Space •Interpenetrating Labyrinths •Infinite Periodic Minimal Surfaces (IPMS) •Skeletal Graphs	Unclassified – Unlimited

19. Security Classif. (of this report)	20. Security Classif. (of this page)	21. No. of Pages	22. Price*
Unclassified	Unclassified	92	$3.00

*For sale by the Clearinghouse for Federal Scientific and Technical Information
Springfield, Virginia 22151

TABLE OF CONTENTS

LIST OF ILLUSTRATIONS*

*Most of the stereoscopic views included in the illustrations are arranged to accommodate both the reader who prefers *cross-eyed* stereo viewing and also the reader who prefers *parallel* stereo viewing. The stereo pairs labelled *right-left* are arranged for *cross-eyed* viewing, while the *left-right* pairs are arranged for *parallel* viewing. Because of the correlation between *accommodation* and *convergence*, a reader who is somewhat near-sighted may find it easiest to see a fused stereo image in sharp focus if he chooses the *left-right* pairs for viewing without eyeglasses. These pairs may also be viewed satisfactorily with a suitable binocular stereoscope. A reader who is somewhat far-sighted may be able to see a fused stereo image in sharp focus if he chooses the *right-left* pairs for viewing without eyeglasses. A reader with strong ocular accommodation is usually able to see satisfactory stereo images with either *left-right* or *right-left* pairs. If a *right-left* pair is viewed in *parallel* fashion, or a *left-right* pair is viewed in *cross-eyed* fashion, the perspective becomes inverted, and a pseudoscopic image is seen.

Because of a computer coding error, the stereoscopic drawings in Figure 13 provide only a fraction of the full depth illusion which was intended.

LIST OF TABLES

INFINITE PERIODIC MINIMAL SURFACES WITHOUT SELF-INTERSECTIONS

Alan H. Schoen
Electronics Research Center
Cambridge, Mass.

SUMMARY

A preliminary account of a study of the partitioning of three-dimensional Euclidean space into two interpenetrating labyrinths by intersection-free infinite periodic minimal surfaces (IPMS) is given. A construction algorithm for deriving such surfaces leads to the identification of the five cases already known, plus a number of new examples.

By the use of this algorithm and other methods, a total of seventeen intersection-free IPMS have been identified. Photographs of plastic models and computer-generated drawings of examples of such surfaces are shown.

Also described and illustrated is an example of a non-orientable IPMS, generated from a skew pentagonal surface module.

A counterpart to Schoenflies' proof that there exist only six quadrilateral modules of IPMS is mentioned: There exist only eight pentagonal modules of IPMS having non-cubic Bravais lattices.

I. INTRODUCTION

The five published examples of infinite periodic minimal surfaces (IPMS) which are free of self-intersections are as follows. In 1865, the first published example of an *infinite periodic minimal surface* (IPMS) was described by H. A. Schwarz (ref. 1). This surface was also studied in memoirs published independently by Riemann and by Weierstrass. In Schwarz's analysis, which is described by Darboux (ref. 2) as deeper and more comprehensive than that of his contemporaries, the analytic solution for the surface is expressed in terms of the Weierstrass parametrization for minimal surfaces. We call this surface, which has symmetry related to that of the diamond crystal structure, Schwarz's *diamond surface*, or D. A finite portion of D is shown in Figure 1.

A surface which is adjoint (i.e., conjugate under bending according to Bonnet's transformation (ref. 3)) to D, which we call the *primitive surface*, or P, was also described by Schwarz. P, illustrated in Figure 2, has symmetry related to that of the

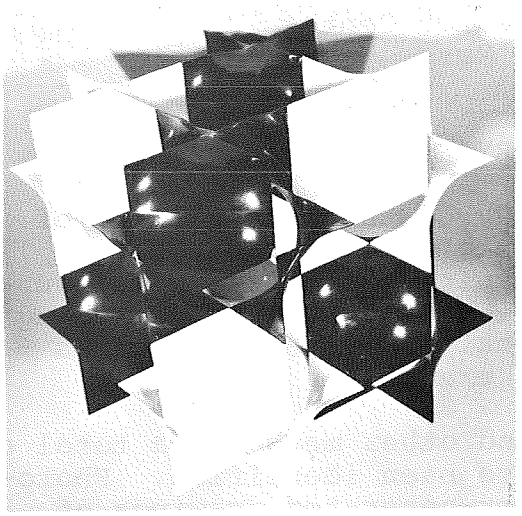

a. Oblique view.

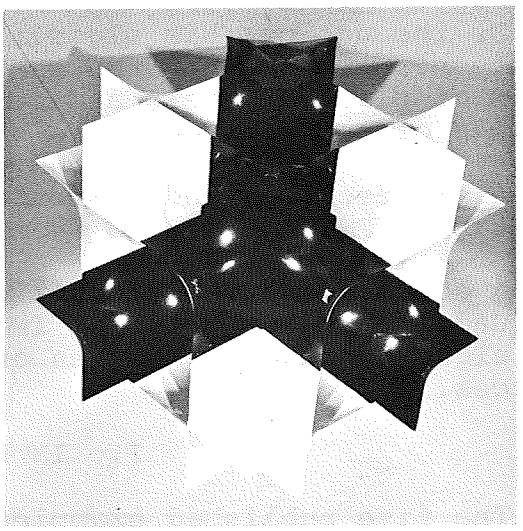

b. View along (111) axis.

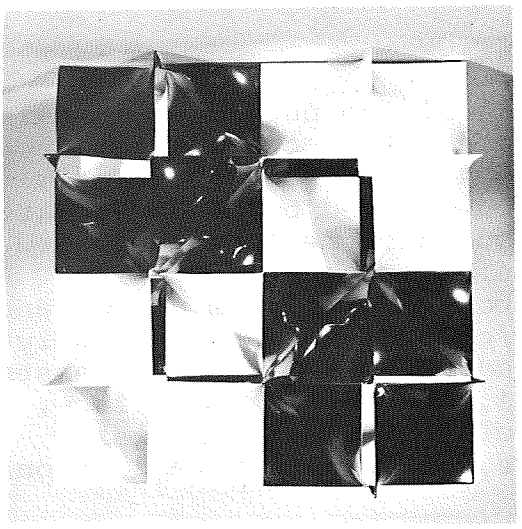

c. View along (100) axis.

Figure 1.- Schwarz's *diamond* surface (D); faces are those of the regular map $\{6,4|4\}$.

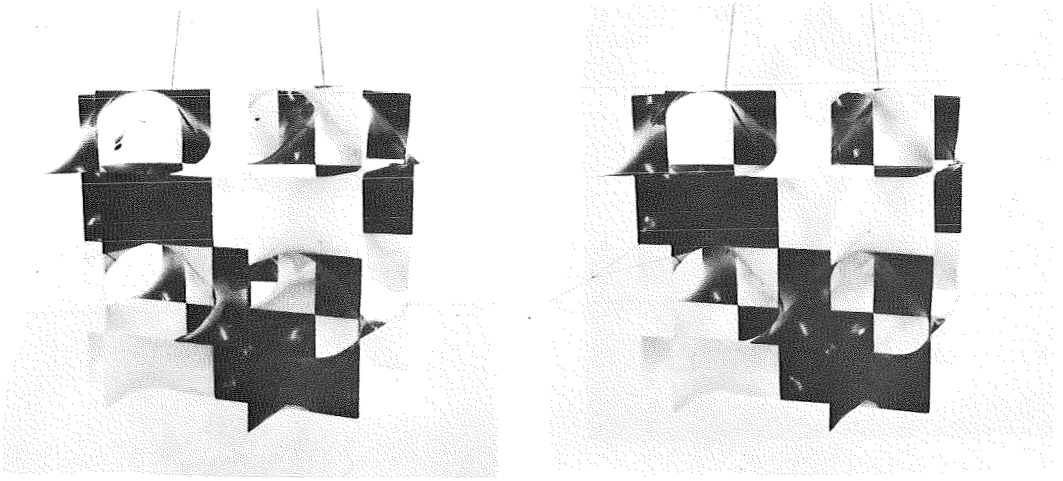

d. Right-left stereoscopic views of D.

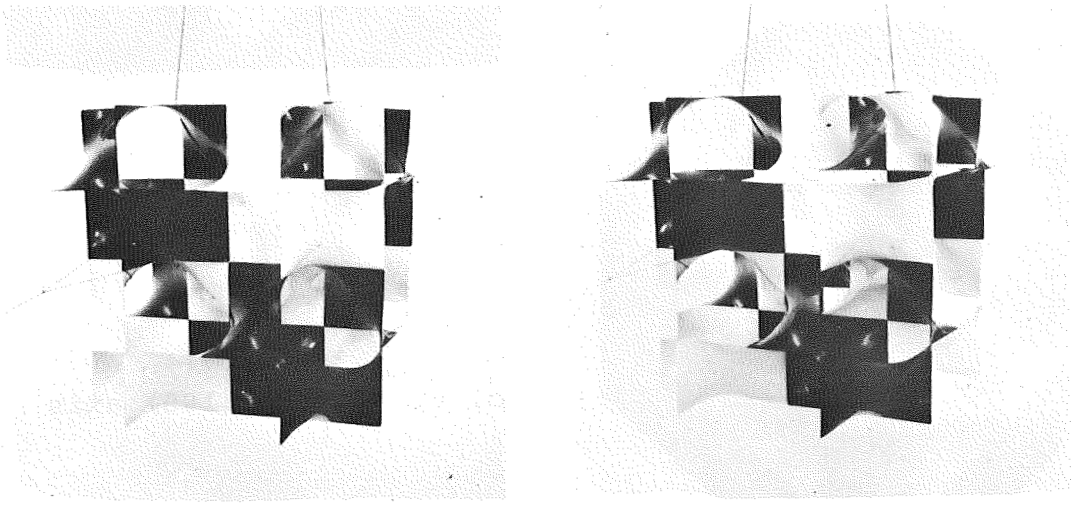

Figure 1.- Concluded.

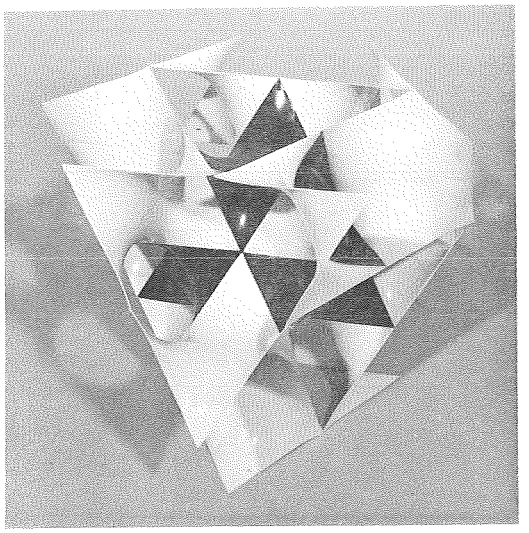

a. Oblique view

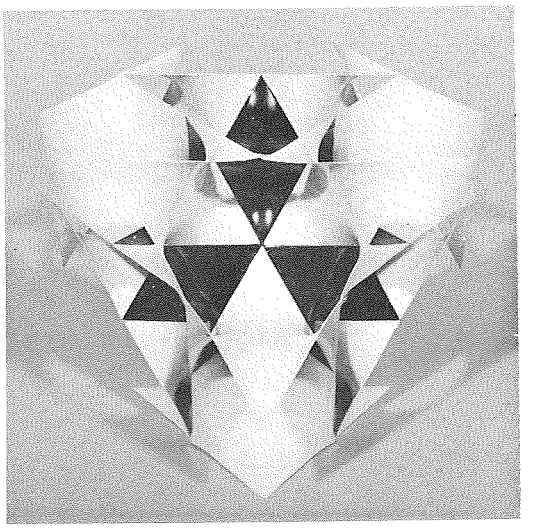

b. View along (111) axis

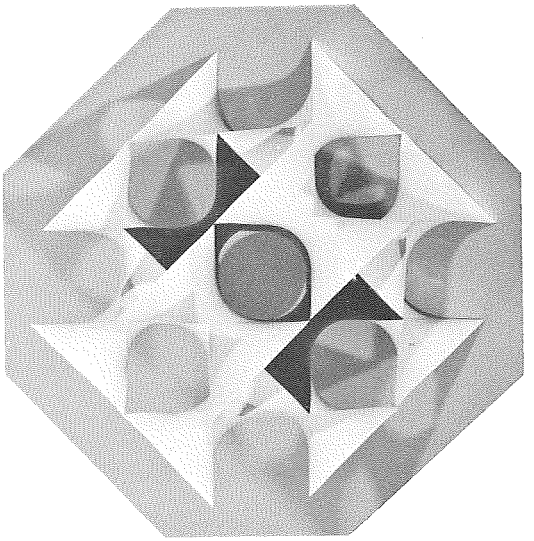

c. View along (100) axis

Figure 2.- Schwarz's *primitive* surface P;
faces are those of the regular map {6,6|3}.

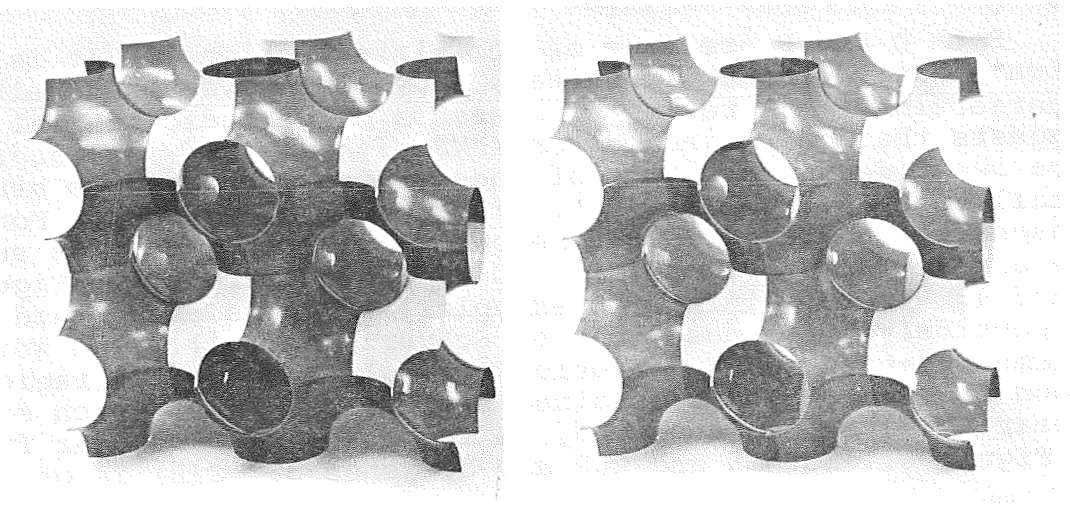

d. Right-left stereoscopic views of P; faces are those of the regular map {6,4|4}.

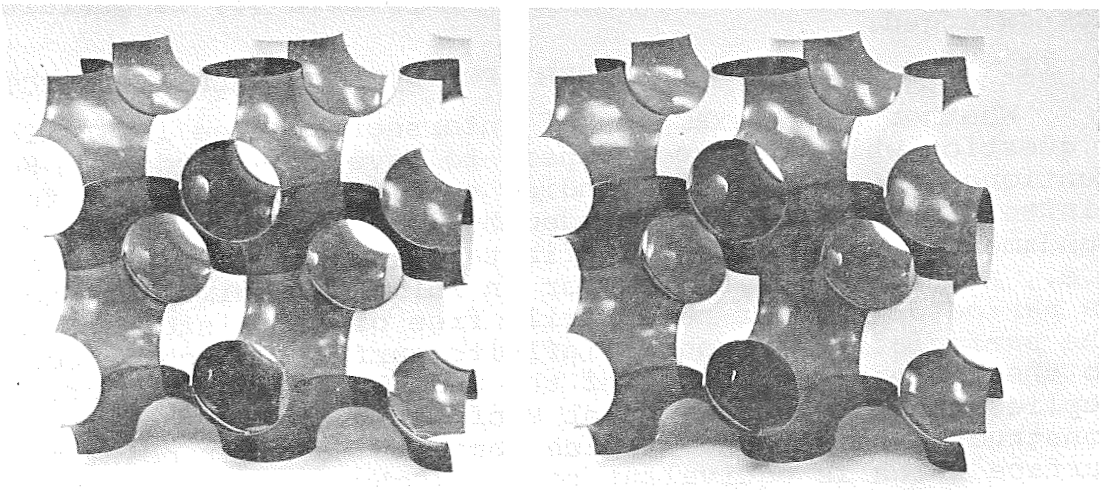

e. Left-right stereoscopic views of P; faces are those of the regular map {6,4|4}.

Figure 2.- Concluded.

primitive cubic lattice. The Bravais lattice (lattice of translational symmetry) for D is face-centered-cubic (F); the Bravais lattice for P is the primitive cubic lattice (P). A fundamental region of P or D is of genus 3.

Both D and P are free of self-intersections. (It is readily shown* that there are infinitely many IPMS which have self-intersections.) A review of research on periodic minimal surfaces suggests that *only three other IPMS without self-intersections have been identified*. One of these three surfaces was studied in detail by E. R. Neovius (ref. 4), a pupil of Schwarz. For reasons which are explained below, we call this Neovius surface *the complement of P*, or C(P). C(P) is illustrated in Figures 3 and 4. The remaining two examples, which we call H and CLP, respectively, were described by Schwarz (ref. 1). The Weierstrass parametrization for H, of which a single fundamental region is shown in Figure 5, was obtained by Schwarz. CLP, which does not appear to have been analyzed, is shown (in an irregular fragment) in Figure 6. Both H and CLP are of genus 3. C(P) is of genus 9.

The author would like to express his special thanks to H.B. Lawson, Jr. and to J.C.C. Nitsche, for helpful discussions of the associate surface transformation and other topics. Thanks are due also to N.W. Johnson for a discussion of the theory of regular maps, and to P. Pearce, whose investigations of curved polyhedra ("saddle polyhedra"), with minimal surface faces, led the author to the study of Schwarz's surfaces. The help of Robert N. Davis, in the preparation of the computer films from which selected frames are shown in Appendix II, is gratefully acknowledged.

II. THE EXISTENCE OF OTHER IPMS WITHOUT SELF-INTERSECTIONS

Whether other examples of intersection-free IPMS exist is a question which does not appear to have been studied. Schwarz mentioned the problem of finding sufficient conditions for a finite minimal surface, bounded by line segments, to serve as a fundamental region for an infinite *discrete* group of rotations — i.e., a fundamental region for an infinite minimal surface which is *periodic* (but not necessarily free of self-intersections). The *periodicity* of such an infinite surface, which is equivalent to the *discrete* character of the underlying rotation group, implies that around any point P of the surface, one can always construct a neighborhood which contains no other point of the surface which is equivalent to P. (Schwarz also discussed the question of whether the solution for such a surface can be expressed in terms of elliptic functions of the coordinates. These questions will not be discussed here.)

In this technical note, we present an introductory description of twelve new examples of IPMS which we find to be free of

*To be published

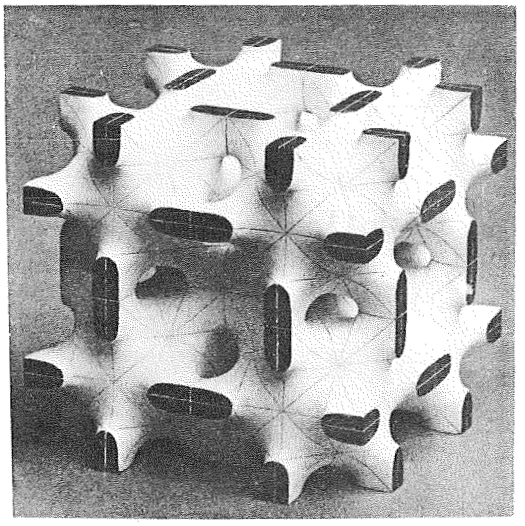

a. C(P) (from a photograph of Neovius' model, shown in his Ph.D. thesis, 1883, ref. 4).

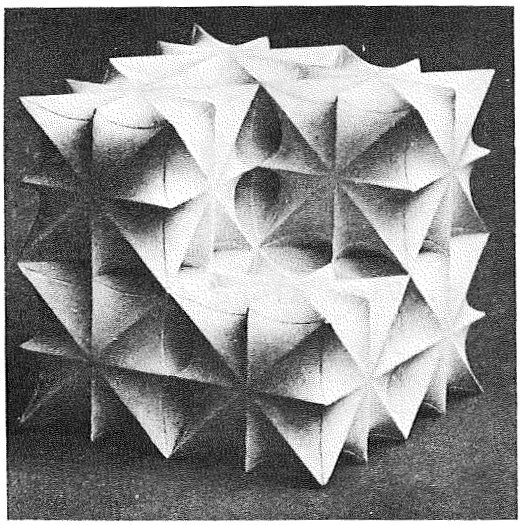

b. The surface adjoint to C(P) (ref. 4).

Figure 3.- The two surfaces analyzed by Neovius: C(P) (the complement of P) and the surface adjoint to C(P).

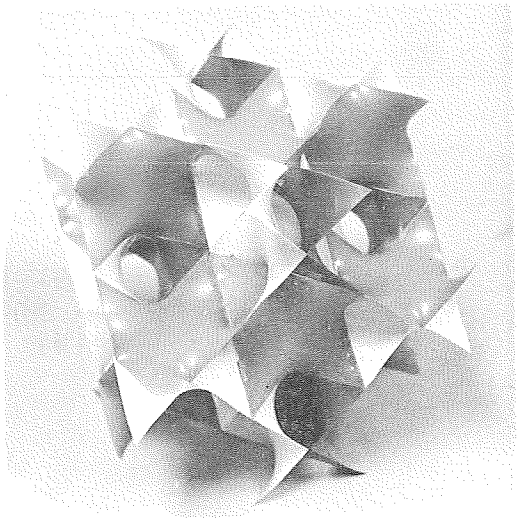

a. Oblique view.

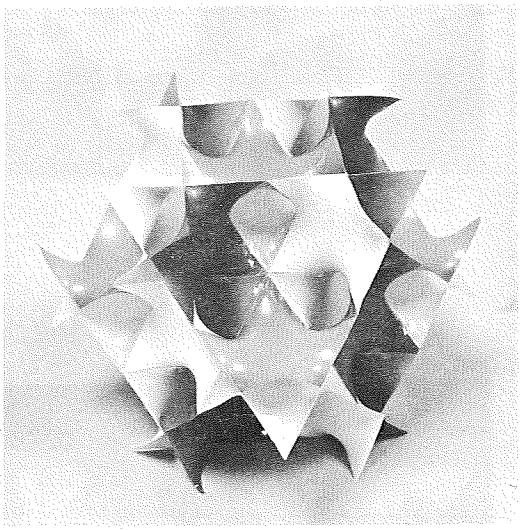

b. View along (111) axis.

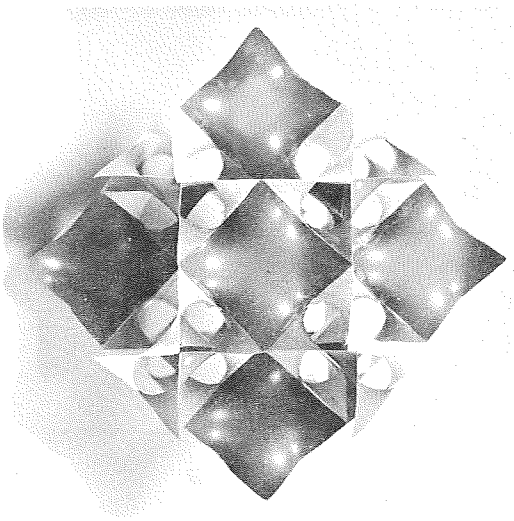

c. View along (100) axis.

Figure 4.- Views of C(P).

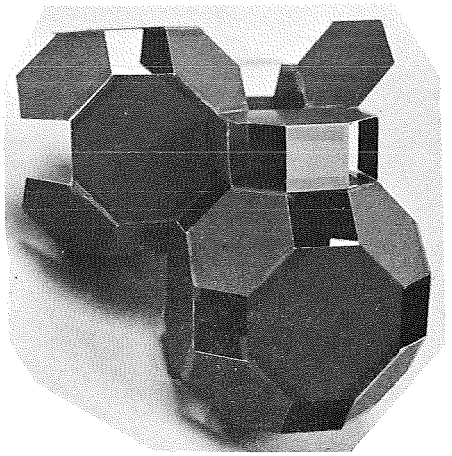

d. Oblique view of a fragment of an *infinite uniform skew polyhedron* which has a labyrinth structure homeomorphic to that of C(P). This polyhedron is described by the symbol $(8^2 \cdot 6 \cdot 4)$. Its vertices are all symmetrically equivalent, and its faces are all regular polygons.

e. The two symmetry domains associated with the two distinct kinds of vertices of the skeletal graph of either labyrinth of C(P) (cf. ref. 10). These *saddle polyhedra* form a binary space-filling arrangement (honeycomb) in which there exists a one-to-one correspondence between the edges of either skeletal graph of C(P) and the faces of the honeycomb (Appendix II).

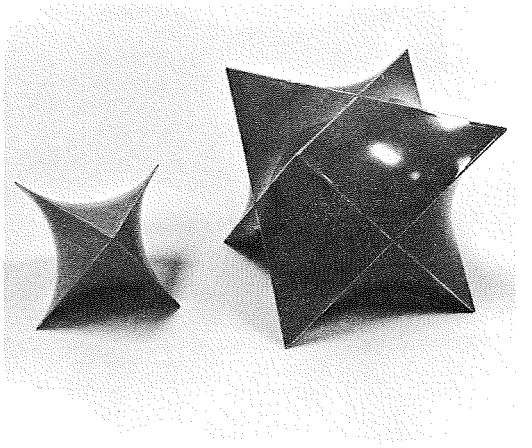

Figure 4.- Concluded.

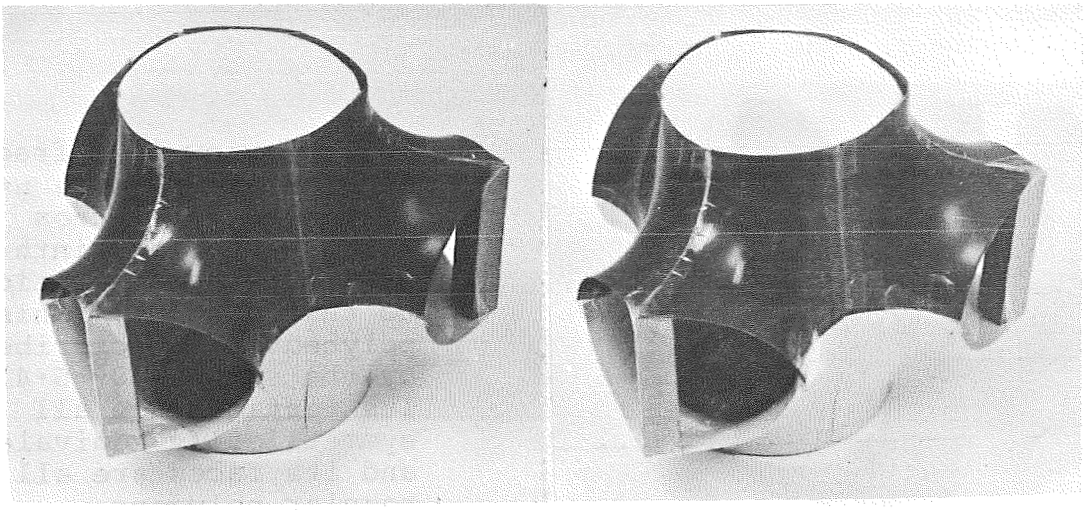

a. Right-left stereoscopic views of H.

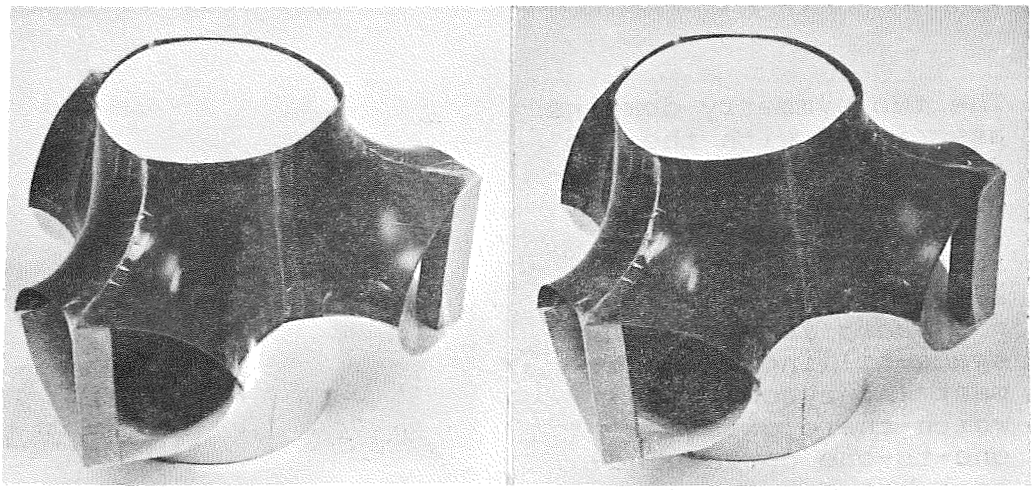

b. Left-right stereoscopic views of H.

Figure 5.- Schwarz's *hexagonal* surface H. A single lattice fundamental region is shown. (The model was assembled from pentagonal plastic modules, formed in the shape of pieces of the self-intersecting surface which is adjoint to H, which were then bent into the desired shape.)

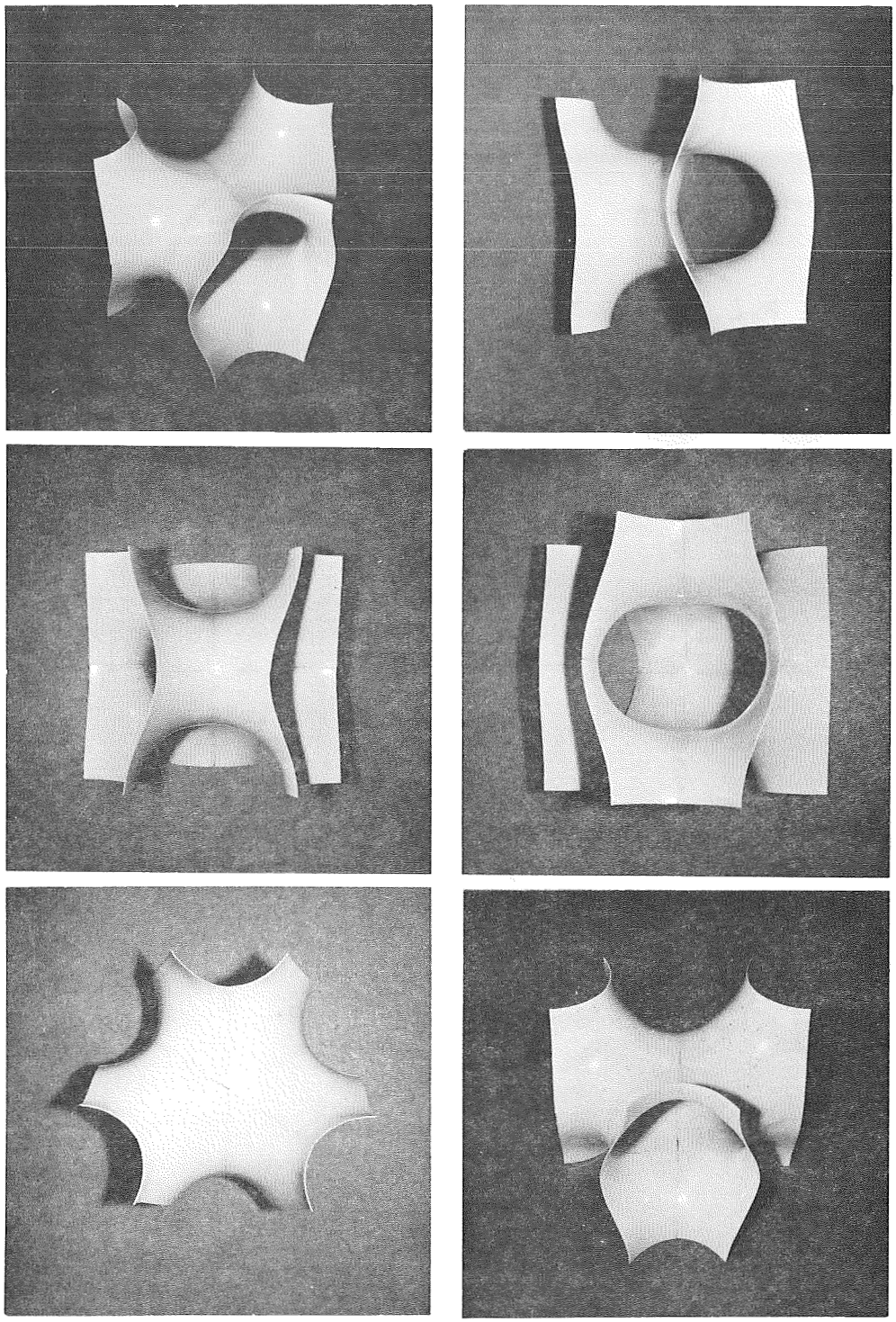

Figure 5c (Concluded).- An alternative form of a lattice fundamental region of H; the convex hull of this assembly of pentagonal faces is also a regular hexagon right prism (cf. Figures 5a and 5b).

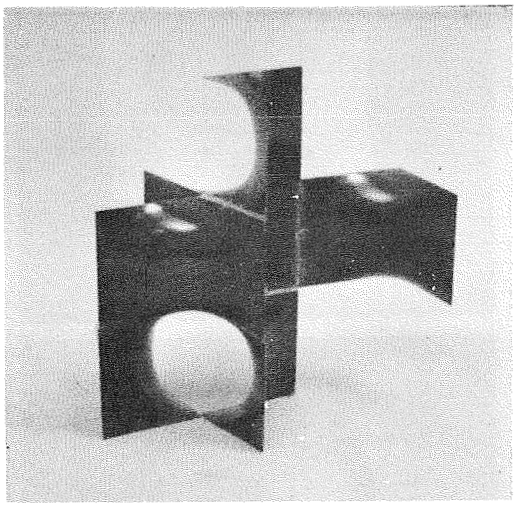

a.

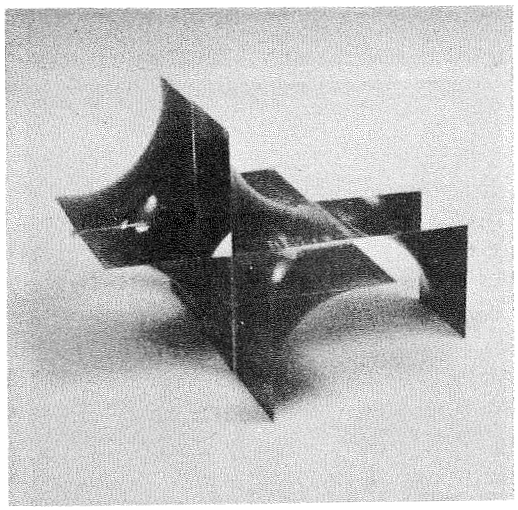

b.

Figure 6.- Two oblique views of a fragment of the Schwarz surface CLP.

self-intersections. Several of these examples are derived from a construction algorithm which was suggested by a study of Bonnet's associate surface (bending) transformation (ref. 3), and especially by a study of the example, described by Kummer and Schwarz (ref. 1), of the dual relationship between the free plane boundary curves of a quadrilateral module of P and the line-segment boundaries of the adjoint quadrilateral module of D. An elementary discussion of this duality, and also of its significance in the construction of intersection-free IPMS, is provided in Appendix I.

An explicit solution has been found, thus far, for only one of these twelve new surfaces. This surface, which is associate to P and D, has been named the *gyroid* (refs. 5 and 6), or G, and it is illustrated in Figure 7. Concerning the remaining eleven new IPMS, a proof of existence and of the absence of self-intersections is elementary for one surface (Figure 8), which we call the complement of D, or C(D) (ref. 6). For six others, which have been named H'-T, H"-R, T'-R', S'-S", I-WP, and F-RD, respectively, the existence proof is based on elementary properties of the adjoint transformation and on the properties of kaleidoscopic groups (ref. 7). Because of limits on the orientation of the normal vector along the boundary of a minimal surface, which follow from the fact that a minimal surface is wholly contained within the convex hull of its boundary curve, H'-T and C(D) can both be proved to be free of self-intersections. Complete analysis of the surfaces H"-R, T'-R', S'-S", I-WP, and F-RD would be required to prove rigorously that they have no self-intersections. For two of these cases, F-RD and I-WP, much of the required analysis was performed by Stessmann (ref. 8), in an incomplete study of their respective self-intersecting adjoint surfaces. I-WP and F-RD are shown in Figures 9 and 10, respectively. For two other cases, which we have named R_{II} and R_{III} (these are also described below), both existence and freedom from self-intersections are guaranteed, for a finite range of proportions of an elementary Flächenstück, by known results (ref. 9) concerning existence conditions for finite doubly-connected minimal surfaces of this general type. Finally, for the two remaining examples, which we have named C(H) (Figure 11) and O,C-TO (Figure 12), respectively, the absence of self-intersections can be "proved", at present, only by invoking the results of experimental demonstrations performed with soap films and with the bending of thin plastic models of surfaces proved to be minimal surfaces.

Because of the diversified and complex character of these examples, a full acount of the subject will be deferred until an extended report* is completed. In that report, each of these

*To be published

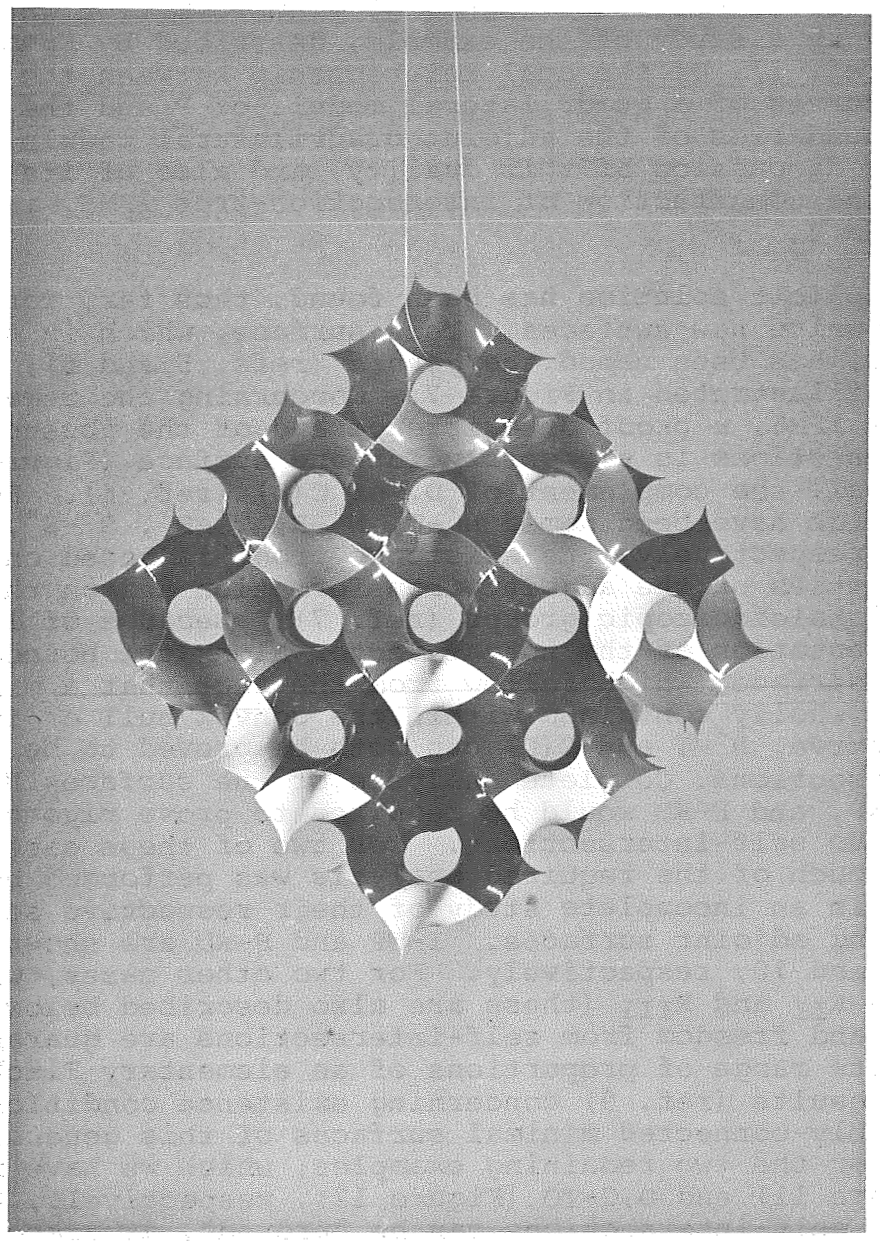

a. View is along (100) axis of G.

Figure 7.- The gyroid (G); faces are those of the regular map $\{6,4|4\}$.

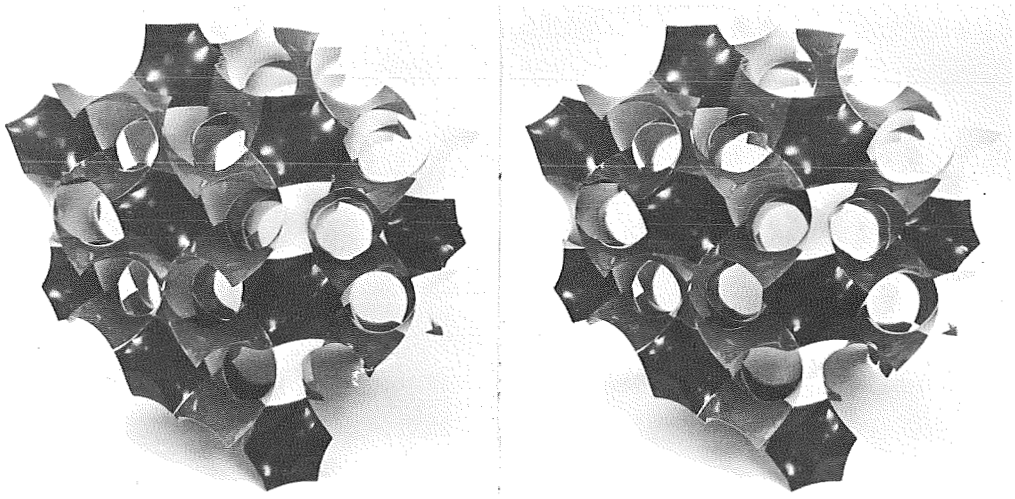

b. Right-left stereoscopic views of G.
View is along (111) axis.

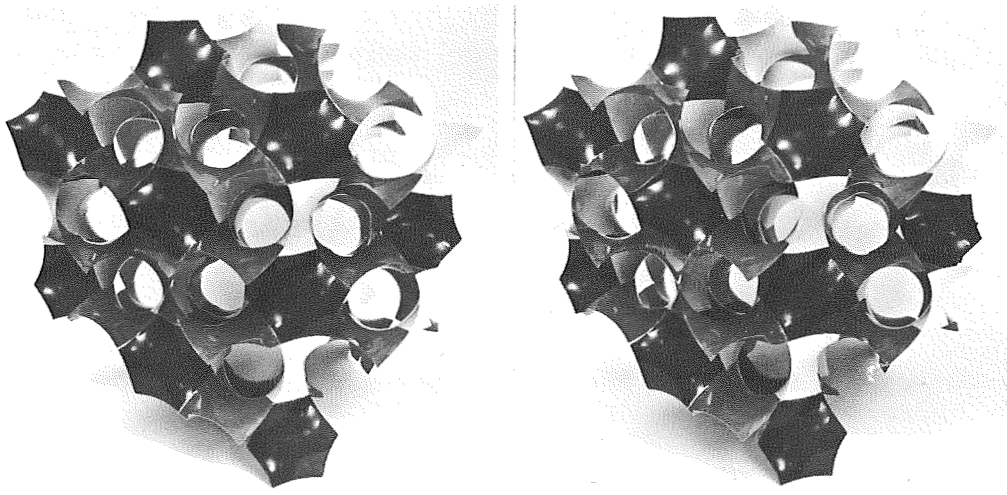

c. Left-right stereoscopic views of G.
View is along (111) axis.

Figure 7. Continued.

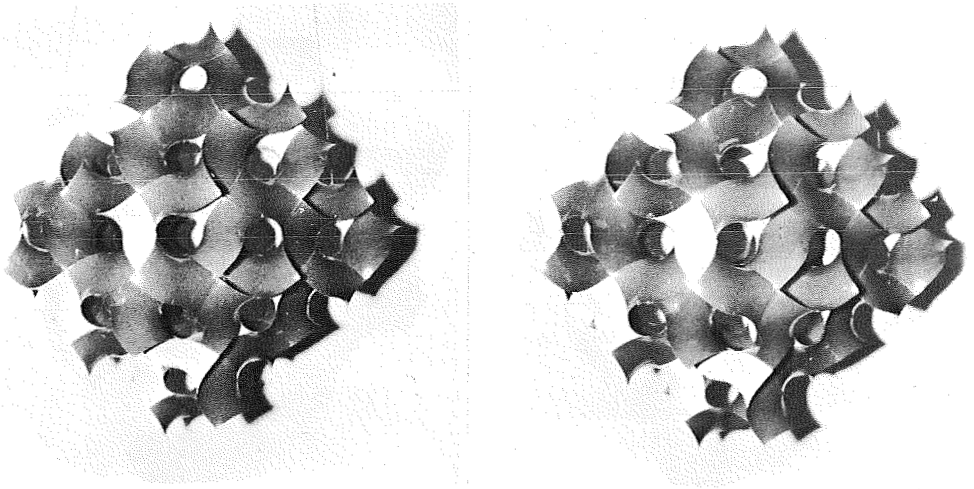

d. Right-left stereoscopic views of G.
View is along (100) axis.

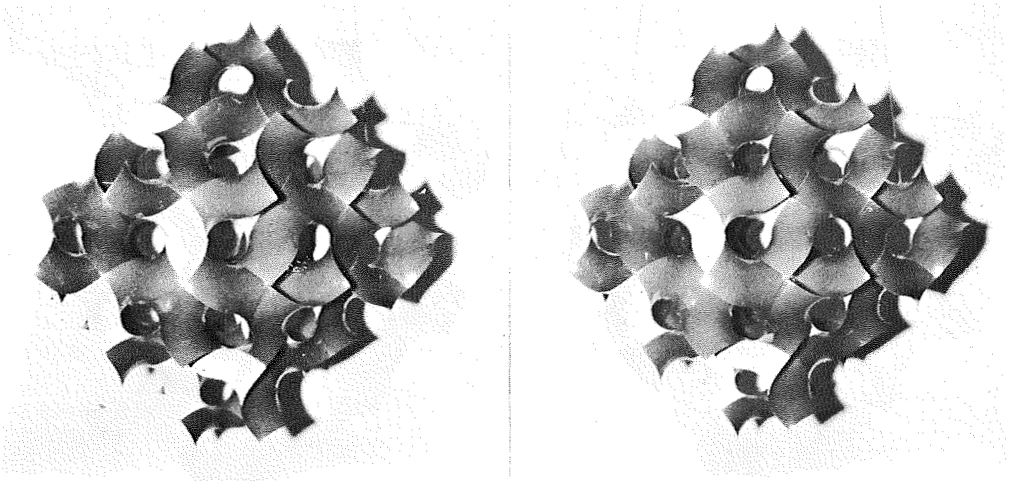

e. Left-right stereoscopic views of G.
View is along (100) axis.

Figure 7.- Continued

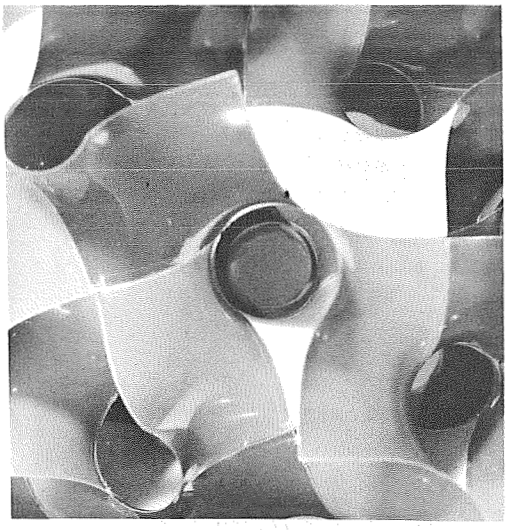

f. Close-up view of the approximately helical tunnel in one labyrinth of G. View is along (100) axis.

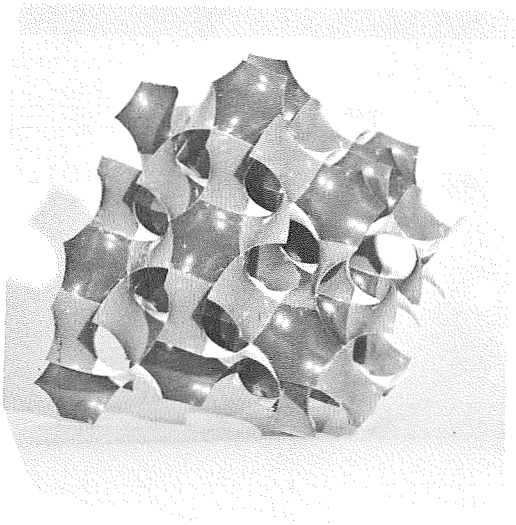

g. View of G along (110) axis.

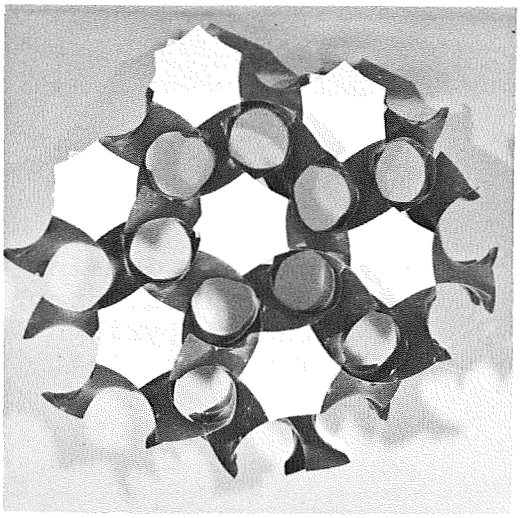

h. View of G along (111) axis.

Figure 7.- Concluded.

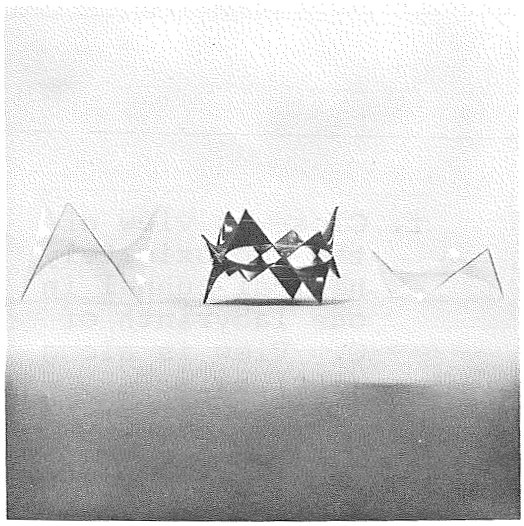

a. Two 12-gon faces (center) of C(D), with the Petrie polygon faces (left and right, respectively) of the two dual regular maps on D: $\{4,6|4\}$ and $\{6,4|4\}$ (cf. ref. 6).

b. Oblique view of C(D).

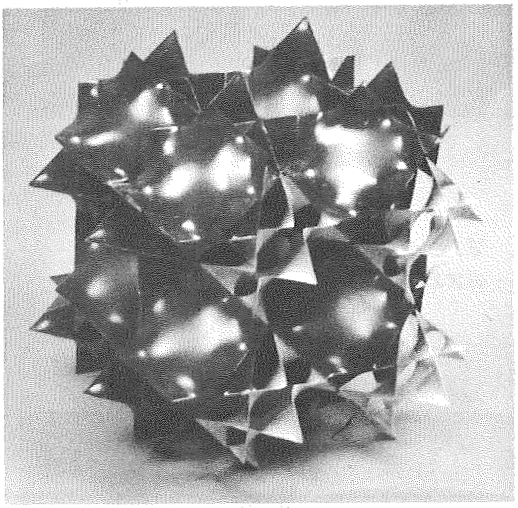

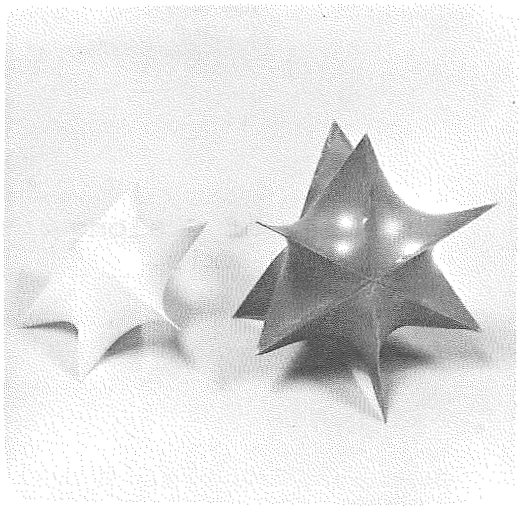

c. The symmetry domains of the skeletal graph of either labyrinth of C(D) (cf. Fig. 4e).

Figure 8.- The complement of Schwarz's diamond surface D: C(D).

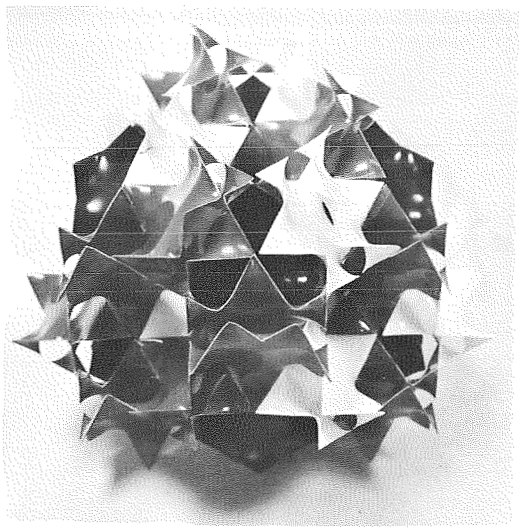

d. View of C(D) along (111) axis.

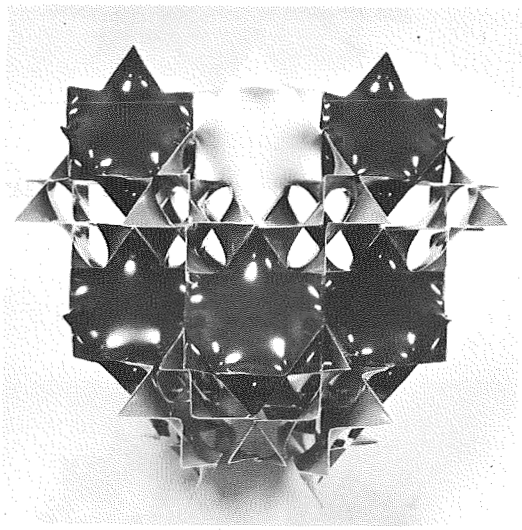

e. View of C(D) along (110) axis.

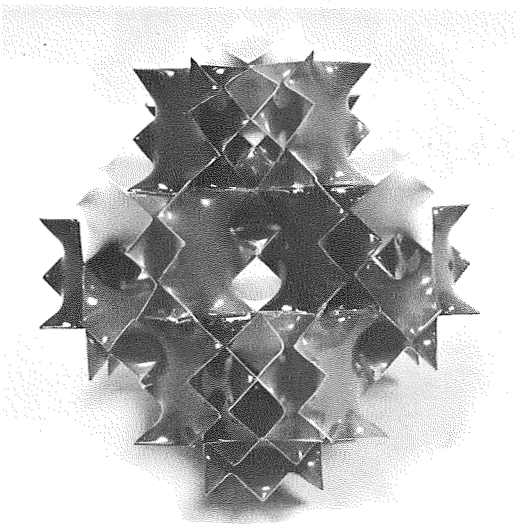

f. View of C(D) along (112) axis.

Figure 8.- Continued.

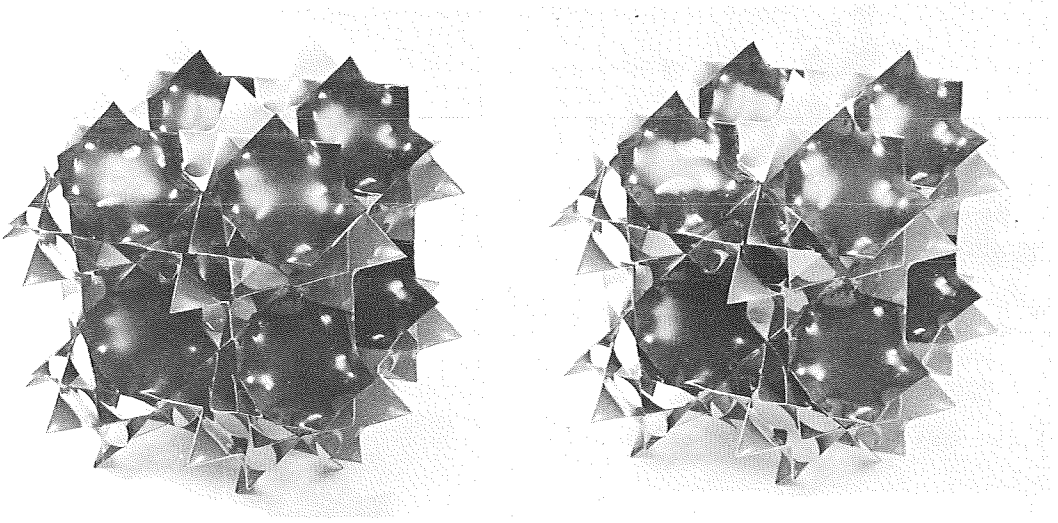

g. Right-left stereoscopic views of C(D).

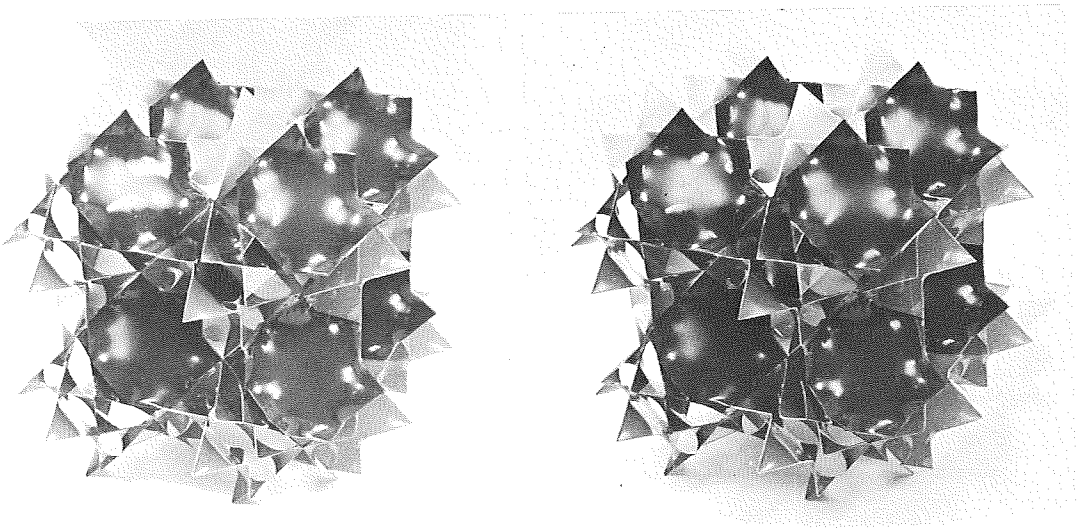

h. Left-right stereoscopic views of C(D).

Figure 8.- Concluded

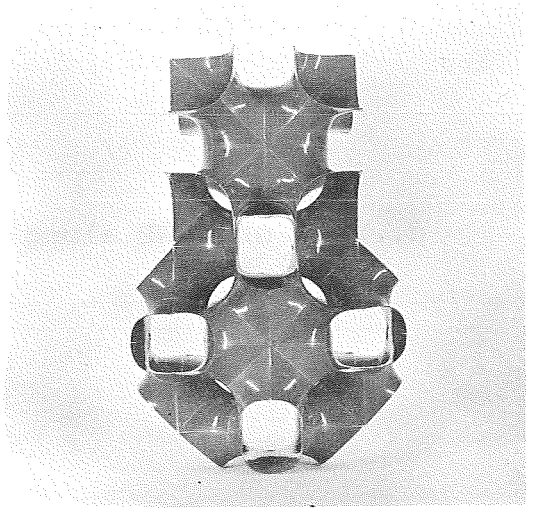

a. View along (100) axis. The assembly of 48 faces appearing in the upper half of the picture contains two lattice fundamental regions of I-WP. Its convex hull is a cube. For the assembly of 96 faces in the lower half of the picture, the convex hull is a rhombic dodecahedron.

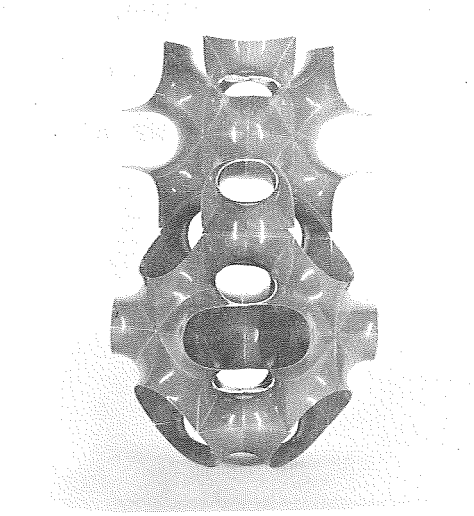

b. View along (110) axis.

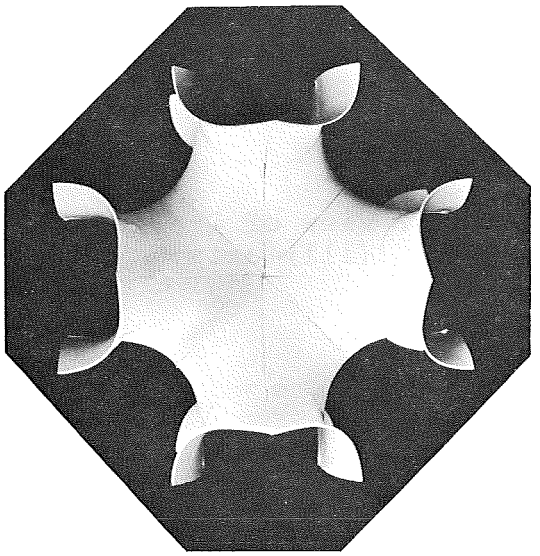

c. View along (100) axis.

Figure 9.- The surface I-WP.

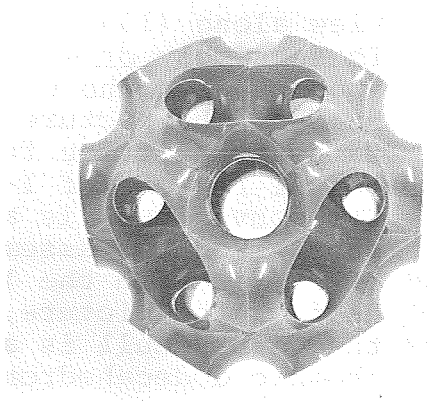

d. View of I-WP along (111) axis.

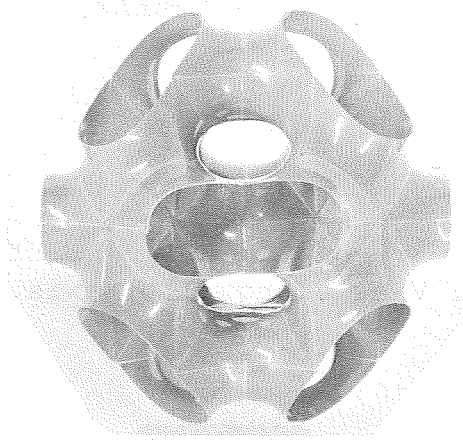

e. View of I-WP along (110) axis.

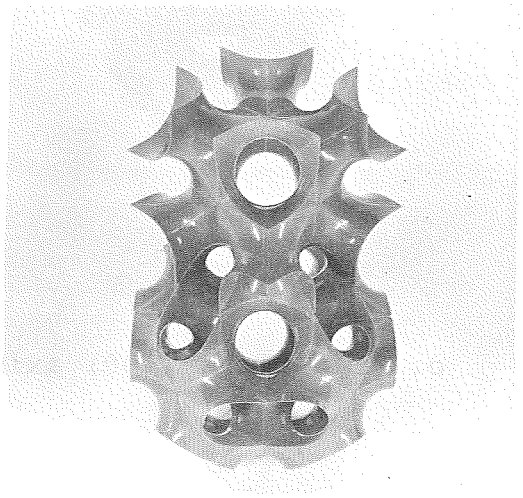

f. View of I-WP along (111) axis.

Figure 9.- Continued.

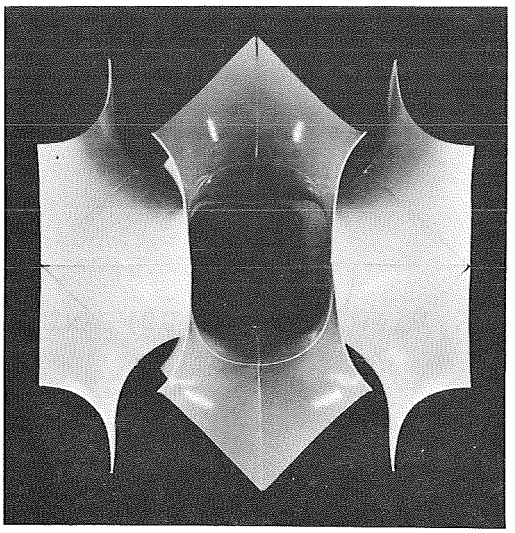

g. View of I-WP along (100) axis.

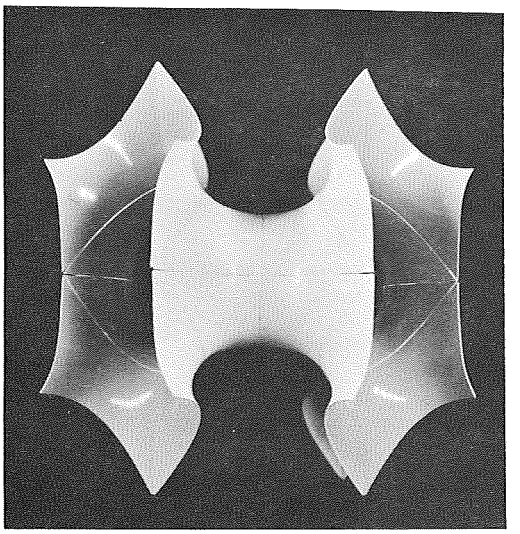

h. View of I-WP along (110) axis.

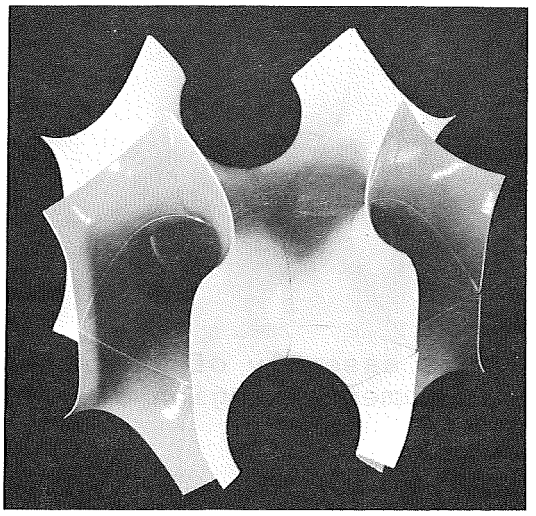

i. Oblique view of I-WP.

Figure 9.- Concluded.

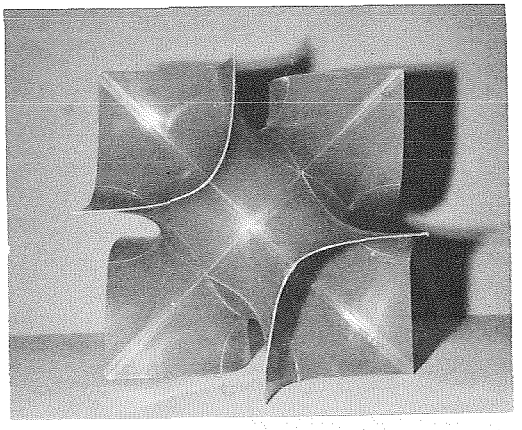

a. View along (100) axis.

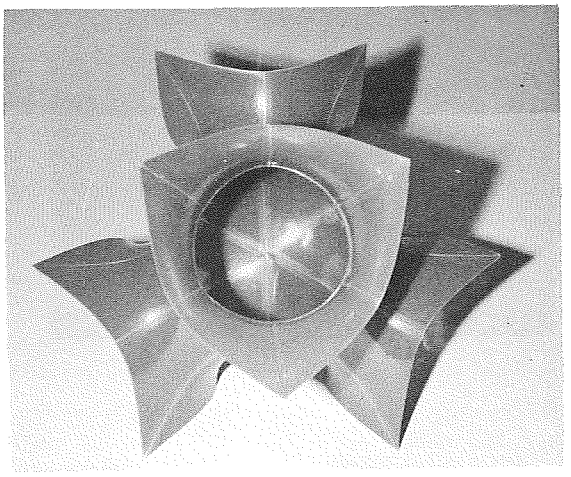

b. View along (111) axis.

Figure 10.- The surface F-RD. This assembly of 24 faces contains one-half of a lattice fundamental region of F-RD. Its convex hull is a cube.

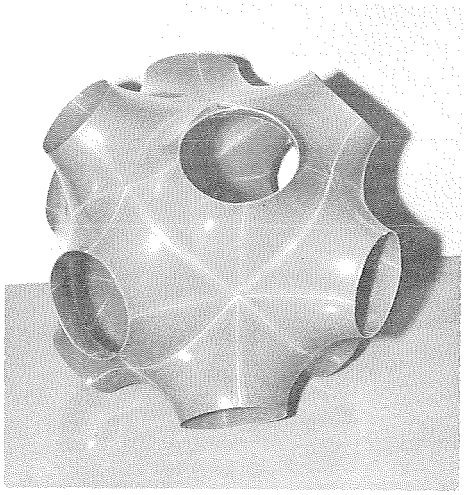

c. Oblique view of F-RD.

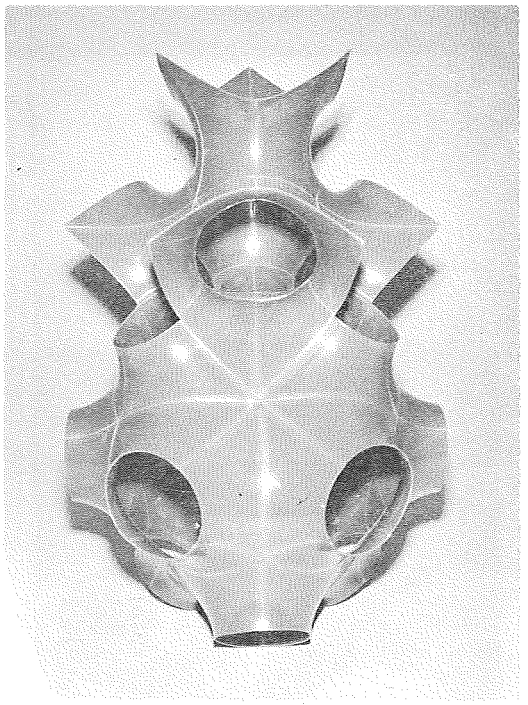

d. Oblique view of F-RD.

Figure 10 (Concluded).- The convex hull of the lattice fundamental region shown in Figure 10c is a rhombic dodecahedron.

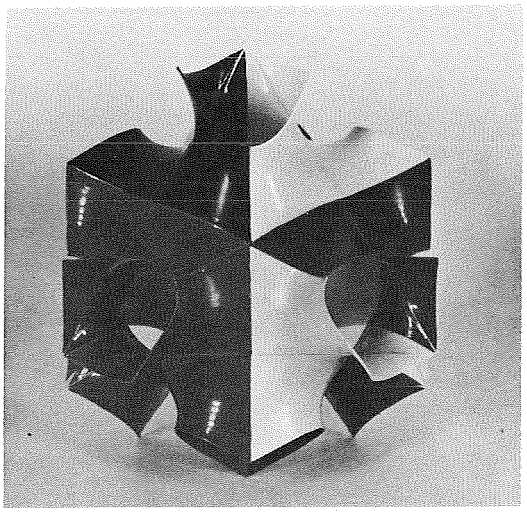

a. View along c-axis.

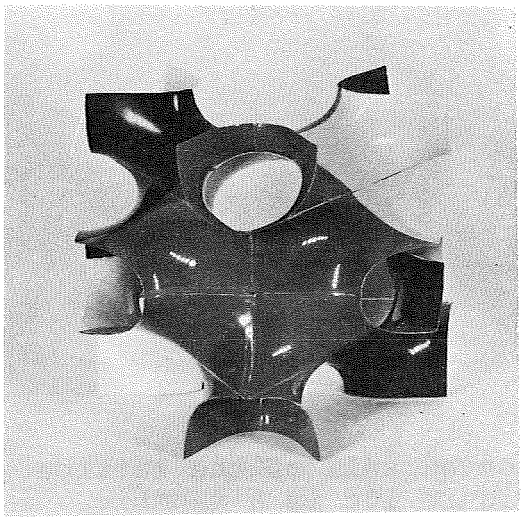

b. Oblique view.

Figure 11.- The complement of Schwarz's hexagonal surface H: C(H). A single lattice fundamental region is shown.

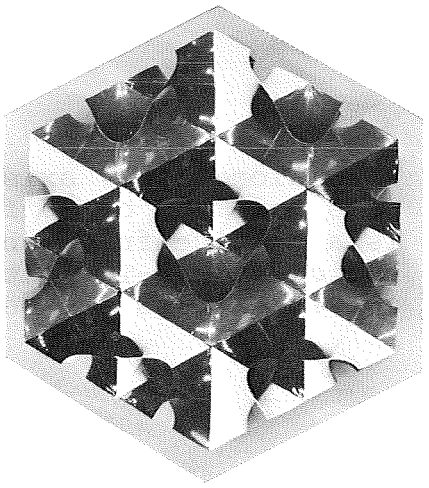

c. View along c-axis.

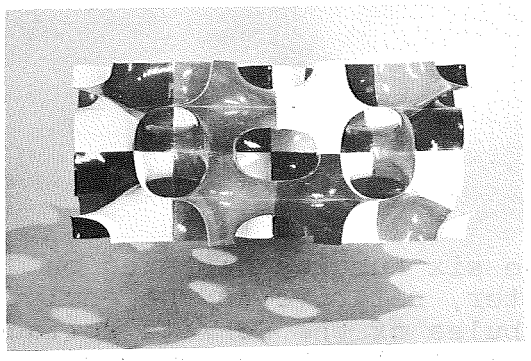

d. View along a-axis.

Figure 11.- C(H): Assembly of four lattice fundamental regions (concluded).

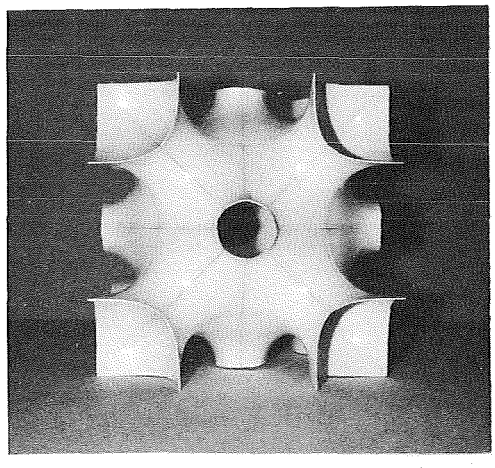

a. View along (100) axis. This assembly of 48 faces is a lattice fundamental region of O,C-TO. Its convex hull is a cube.

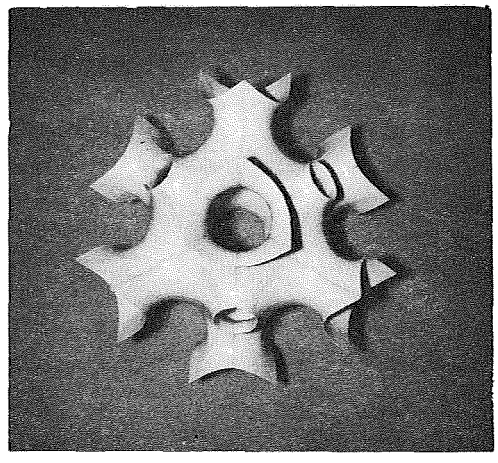

b. View along (111) axis.

Figure 12.- The surface O,C-TO. The six tubules centered on the (100) axes are of smaller diameter, relative to the enclosing cube, than the corresponding six tubules of the Schwarz surface P (cf. Figures 2d and 2e). The eight (111) tubules of O,C-TO are smaller than the corresponding eight in I-WP (cf. Figure 9). (The eight (111) tubules of I-WP are smaller than the four corresponding ones in F-RD (cf. Figure 10).)

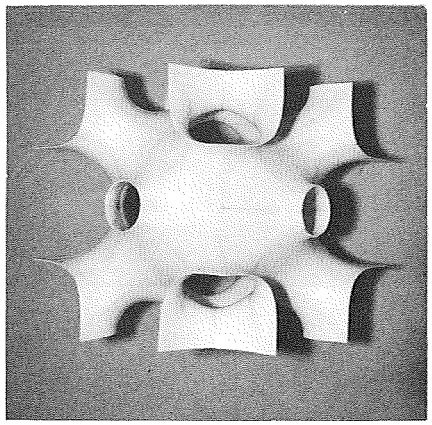

c. View of O,C-TO along (110) axis.

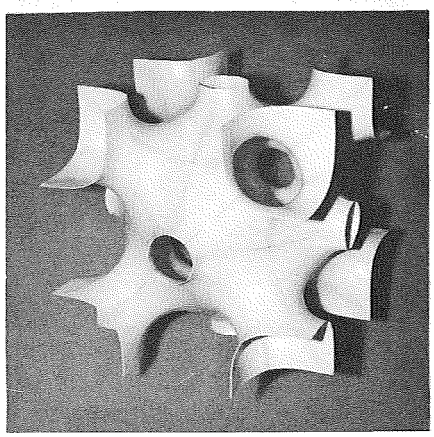

d. Oblique view of O,C-TO.

Figure 12.- Continued.

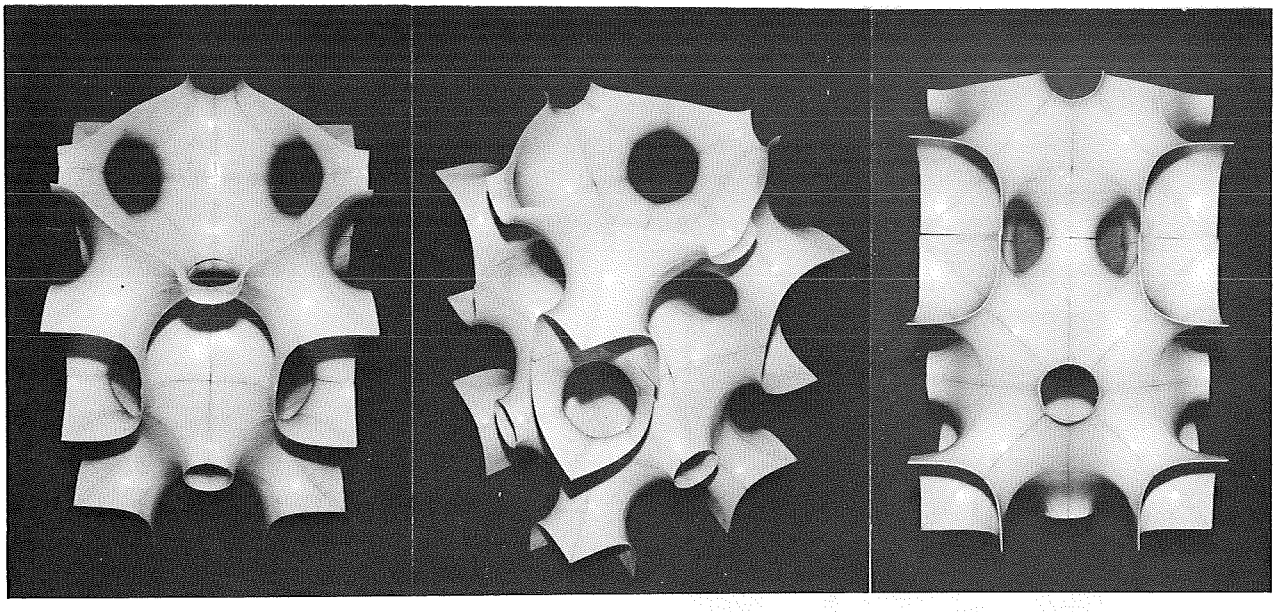

e. f. g.

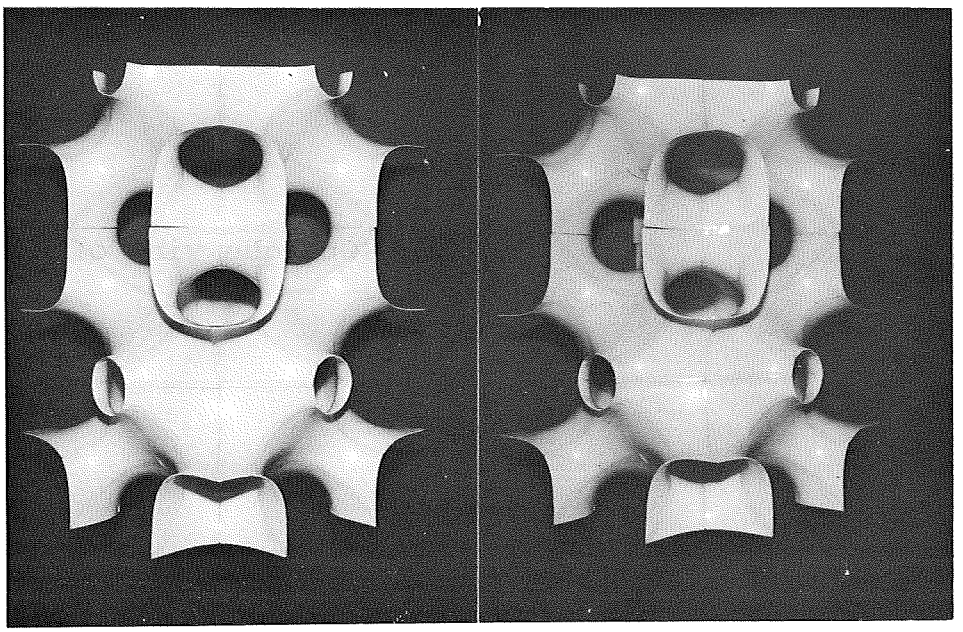

h. Right-left stereoscopic views.

Figure 12 (Concluded).- Assorted views of the surface O,C-TO: one and one-half lattice fundamental regions.

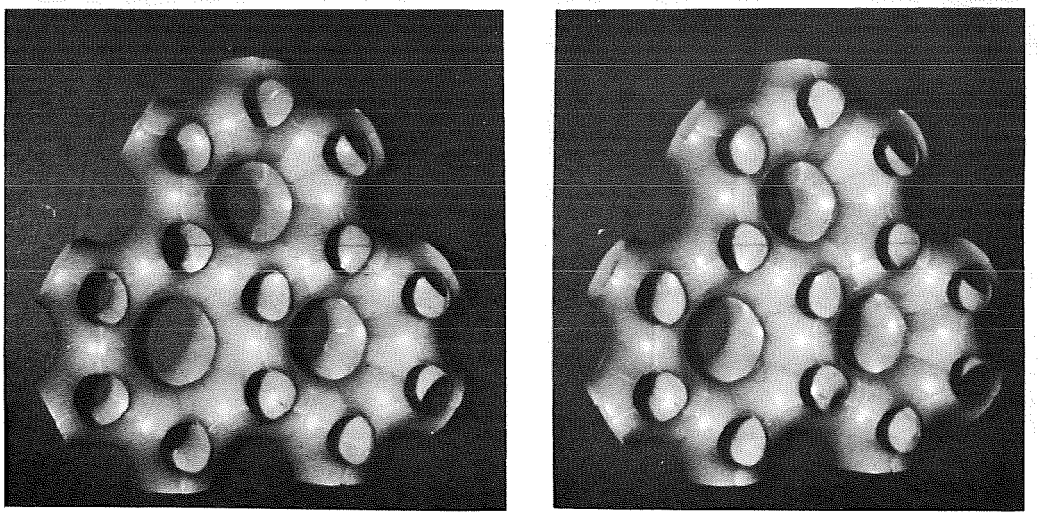

a. Right-left stereoscopic views.

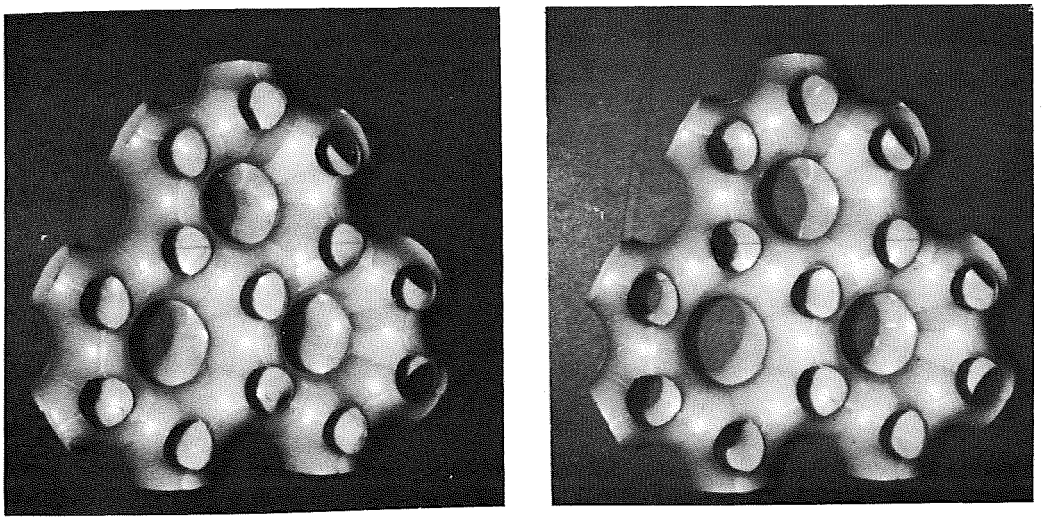

b. Left-right stereoscopic views.

Figure 13.- Stereoscopic views of the surface H'-T.

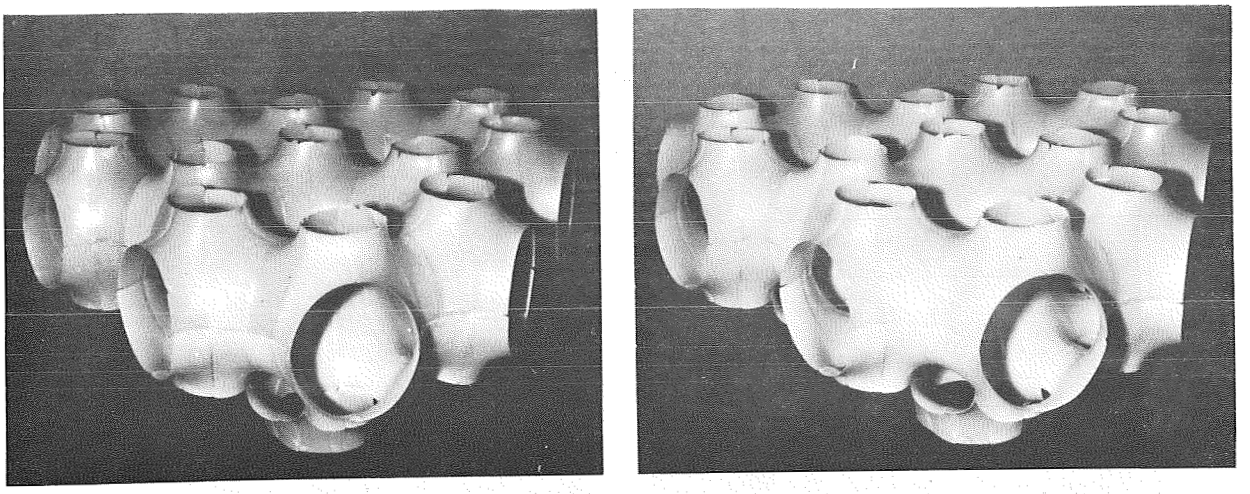

c. Right-left stereoscopic views.

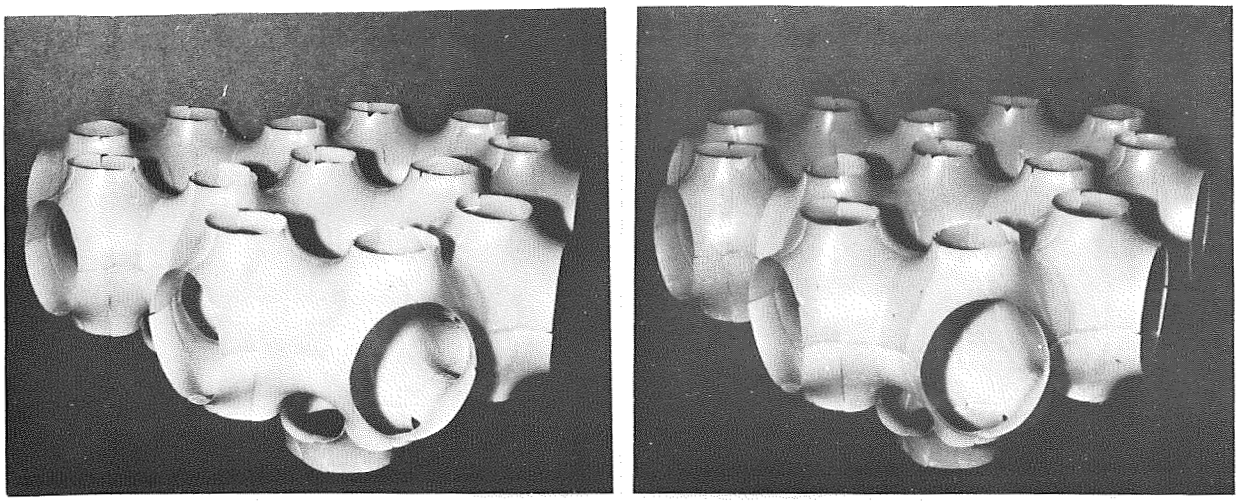

d. Left-right stereoscopic views.

Figure 13.- Continued

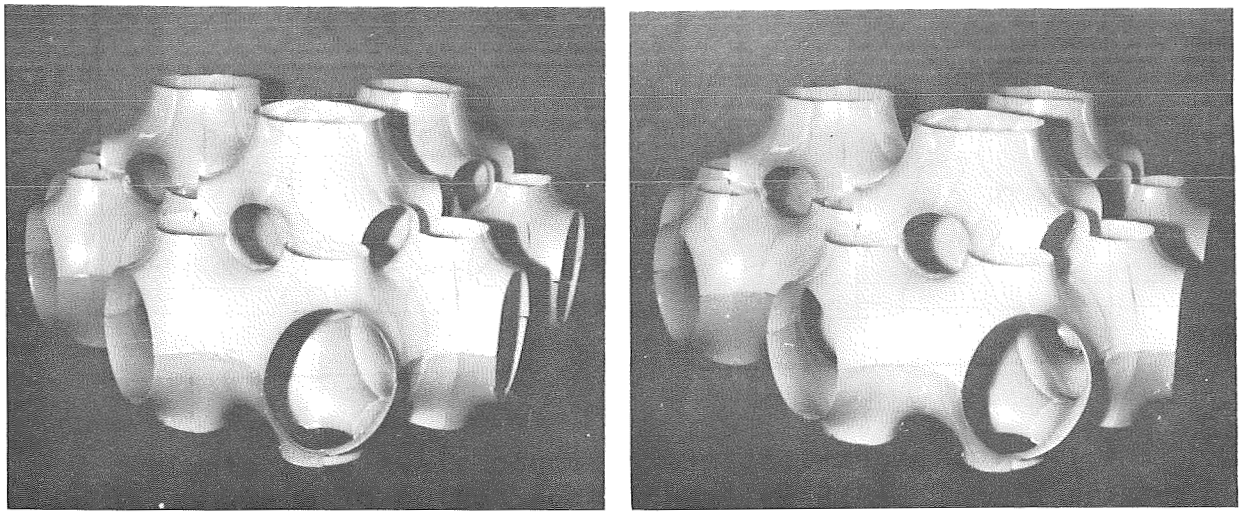

e. Right-left stereoscopic views.

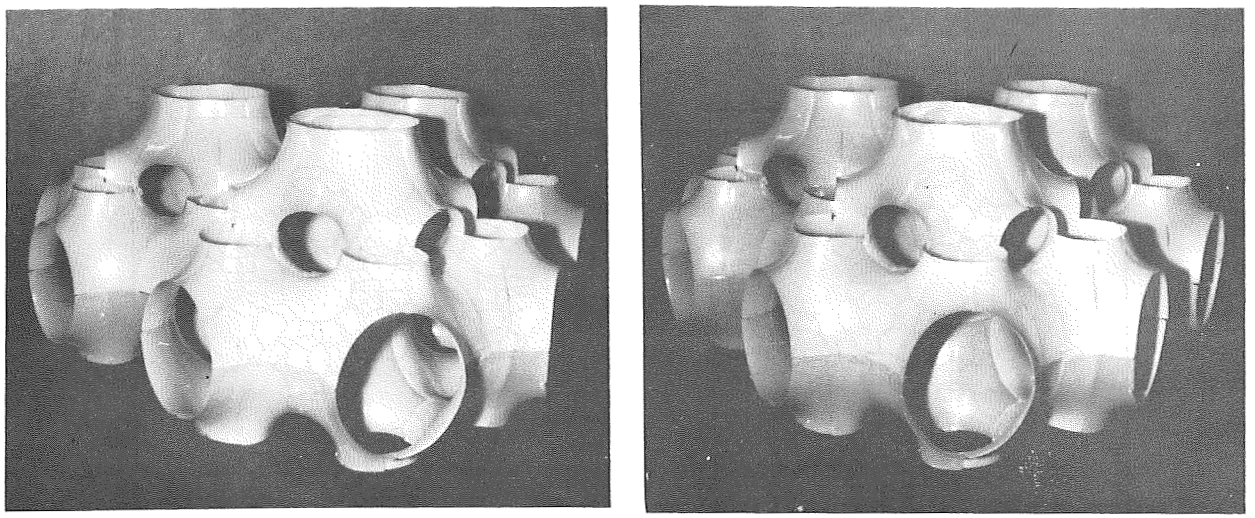

f. Left-right stereoscopic views.

Figure 13.- Continued.

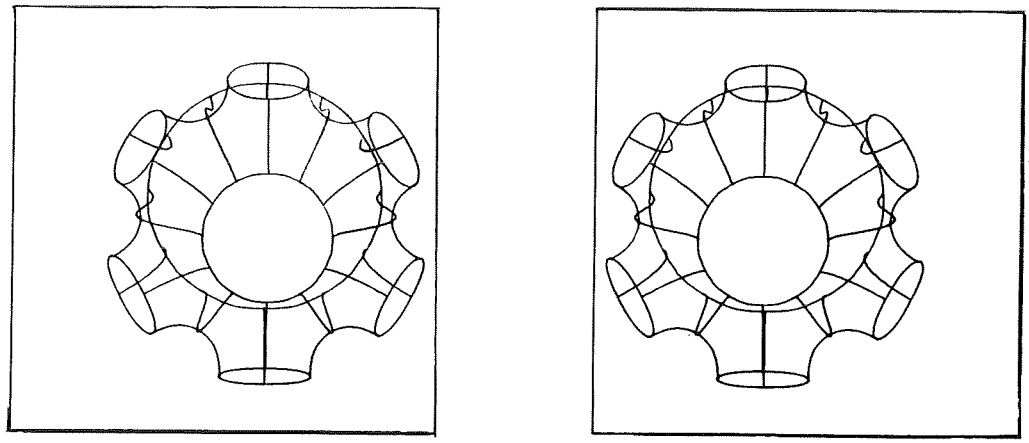

g. Right-left stereoscopic views of a single lattice fundamental region of H'-T.

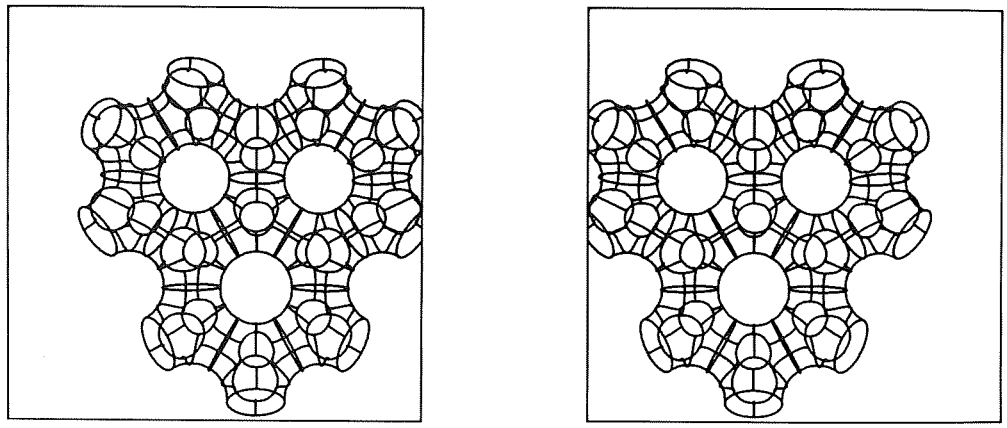

h. Right-left stereoscopic views.

Figure 13.- Continued.

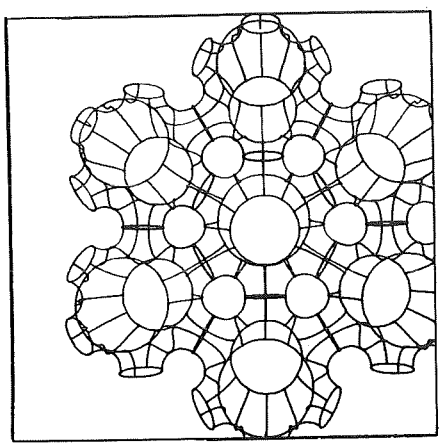

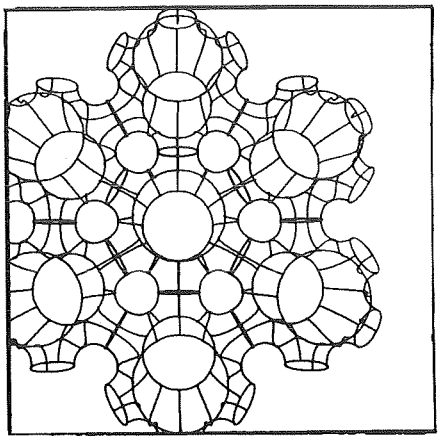

i. Right-left stereoscopic views

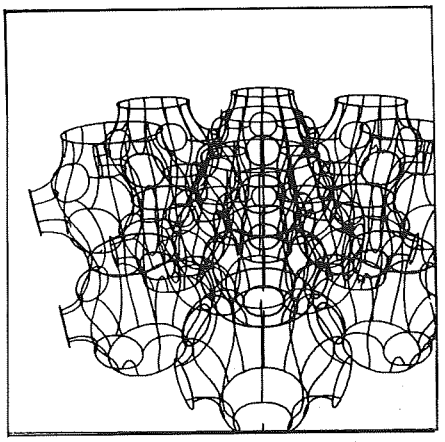

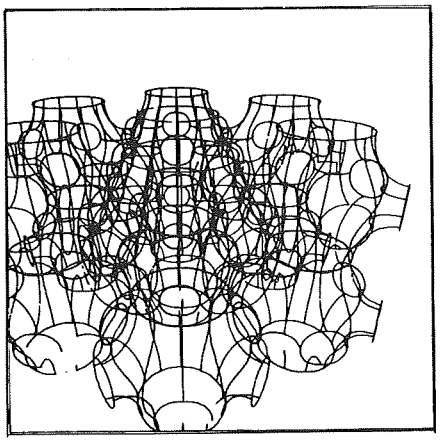

j. Right-left stereoscopic views

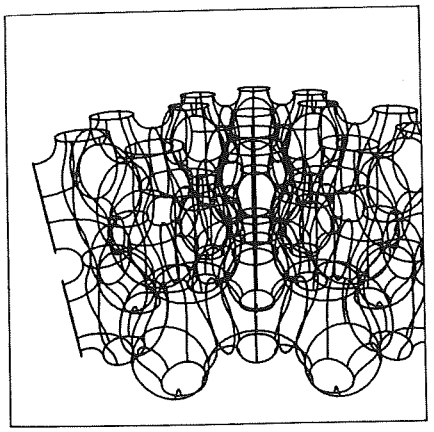

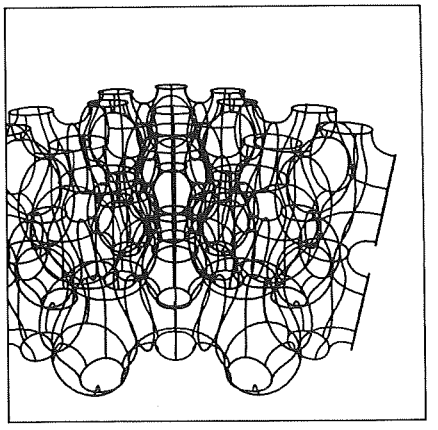

k. Right-left stereoscopic views

Figure 13.- Continued.

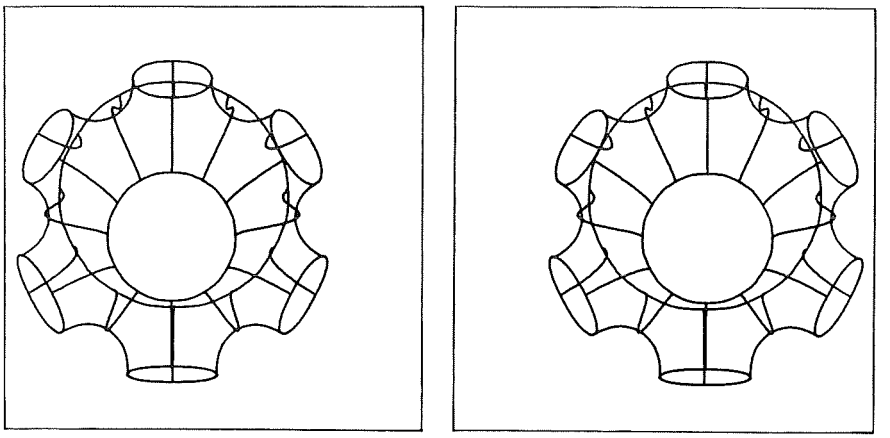

l. Left-right stereoscopic views of a single lattice fundamental region of H'-T.

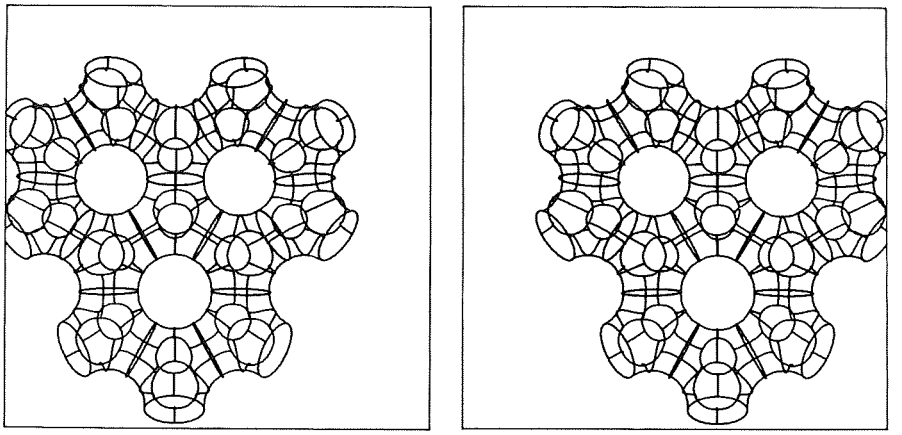

m. Left-right stereoscopic views of H'-T.

Figure 13.- Continued.

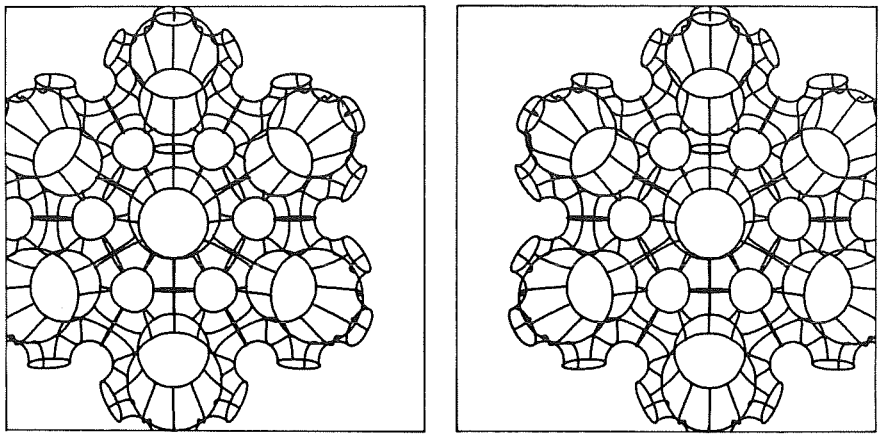

n. Left-Right Stereoscopic Views

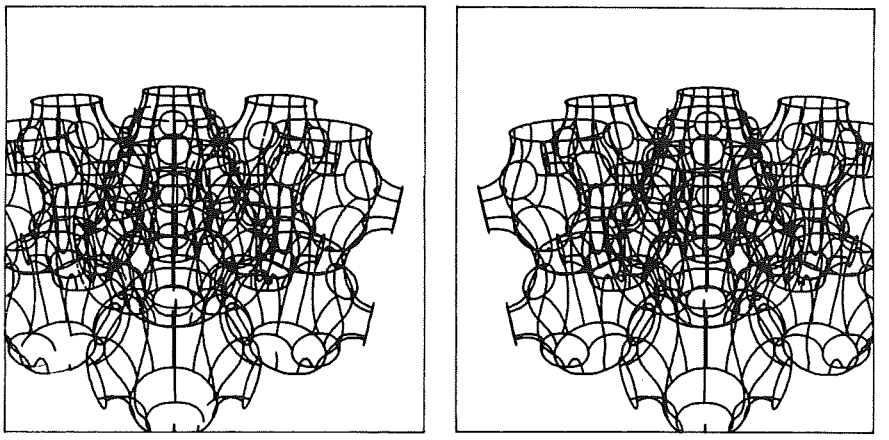

o. Left-Right Stereoscopic Views

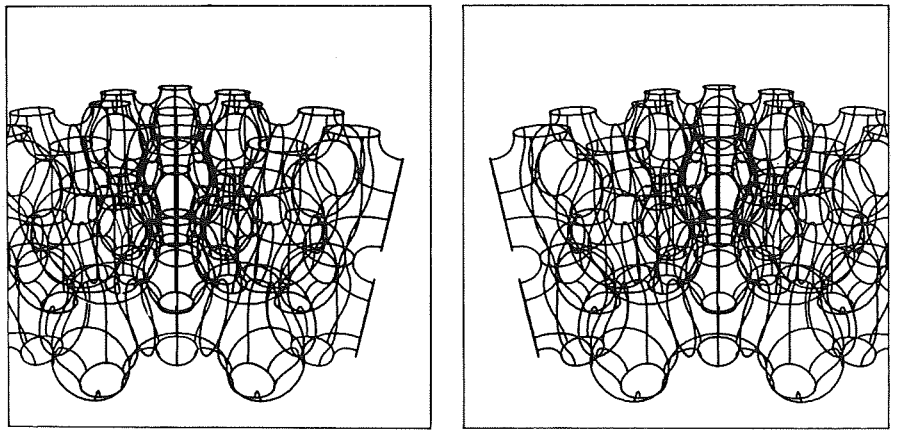

p. Left-Right Stereoscopic Views

Figure 13.- Concluded.

IPMS will be described in detail. Meanwhile, we describe an algorithm which may be used to construct eleven of the seventeen IPMS discussed in this note. These eleven examples include the five surfaces already known to Schwarz and Neovius. We will also describe how the existence of specific additional examples of intersection-free IPMS can be investigated, using (a) an extension of the construction algorithm and (b) experimental methods based either on the associate surface bending of thin plastic models of surfaces proved to be minimal surfaces, or on the construction of soap films bounded by the interior faces of appropriate convex polyhedra (or on both).

An elementary discussion of some aspects of Bonnet's associate surface transformation, and of its significance in the construction of intersection-free IPMS, is given in Appendix I. Some other related topics are also briefly discussed there.

III. LABYRINTHS, SKELETAL GRAPHS OF LABYRINTHS, AND THE NAMING OF INTERSECTION-FREE IPMS ACCORDING TO SKELETAL GRAPH

Each IPMS is identified here by a specially coined name. In several cases, including Schwarz's surfaces D, P, H (hexagon), and CLP, this name is an abbreviation of the name assigned to a certain infinite periodic graph. Each such graph may be considered as the *skeletal graph* of an infinite *labyrinth*; each intersection-free IPMS partitions R^3 into two such labyrinthine regions, and, therefore, two such graphs are associated with each IPMS. When the labyrinths are congruent, the graphs are congruent, and we then adopt the convention that the name of the IPMS is the same as the name of the graph (cf. Schwarz's D, P, H, and CLP). (In several cases, a different convention is used for naming such surfaces, partly because the structure of the labyrinths does not suggest simple familiar names for their skeletal graphs.) When the labyrinths — and also their skeletal graphs — are not congruent, the name of the IPMS is composed of abbreviations which describe *each* of the skeletal graphs, these abbreviations being separated by a hyphen. For example, a certain IPMS, called H'-T (Figure 13), can be said to be based on two skeletal graphs which we call H' (hexagon) and T (triangle), respectively.

These associated pairs of skeletal graphs can be considered as *dual* graphs. By means of an empirically developed algorithm† which is a refinement of an algorithm described elsewhere (ref. 10) for establishing a dual relationship between two infinite symmetric graphs (i.e., graphs with equivalent edges and equivalent vertices), it has been found possible to construct a

†See Appendix II

[symmetrical] dual relationship between the two skeletal graphs associated with every one of the seventeen IPMS discussed in this note. Not all of the seventeen IPMS have labyrinths for which the skeletal graphs are *symmetric* graphs; nevertheless, this dual graph construction algorithm leads to unique self-consistent results in all seventeen cases.

The utility of the concept of skeletal graph may be illustrated by mentioning that given an associated [dual] pair of infinite periodic graphs which are interchanged by the action of appropriate two-fold rotational isometries, or given a pair of distinct dual infinite periodic graphs which have appropriate mirror-plane isometries, the question of the existence of an intersection-free IPMS for which the graphs in question may be regarded as labyrinth skeletal graphs can be immediately transformed into a question which is amenable to investigation by mathematical methods. This point will be discussed further in Section VI. Although the isometries of the skeletal graphs and those of the corresponding IPMS are identical for each of the intersection-free surfaces considered in this note, it is not true that the topological structure of a given IPMS implies the existence of a *unique* pair of dual skeletal graphs for that surface, unless it is stipulated that *the two skeletal graphs of an IPMS have the same space group as the IPMS*. For example, consider Schwarz's D and P surfaces: these two adjoint surfaces have the same genus: 3; their skeletal graphs are of degree 4 (D) and 6 (P), respectively. As noted by Schwarz, either of these infinitely multiply-connected IPMS may be transformed into the other by a continuous deformation, the surface at all stages of the deformation being a minimal surface. (This deformation may be described rather simply in terms of a continuous change in the separation of every pair of parallel "crossed" triangles which bound a doubly-connected minimal surface module of the IPMS.) Hence, the concept of a skeletal graph would be somewhat ambiguous, if we did not require that a surface have the same space group as the pair of skeletal graphs which belong to it. The concept of skeletal graphs appears to be a useful one. It provides a picturesque model of both the symmetry and connectedness of each IPMS. Furthermore, the concept of skeletal graph can also be usefully applied to the qualitative consideration of a number of different examples of infinite periodic surfaces of constant (but non-zero) mean curvature, which are deformable into the examples of IPMS described here. A detailed discussion of the concept of skeletal graphs is included in Appendix II.

The five examples of intersection-free IPMS known to Schwarz and Neovius all contain an infinite number of straight lines. A straight line lying in a minimal surface is an axis

of two-fold rotational symmetry. Because the effect of such an isometry is to interchange the two *sides* of an orientable surface and, therefore, also to interchange the two labyrinths into which R^3 is partitioned by the surface, the labyrinth pairs for these five examples are *directly congruent*. Among the twelve new examples of IPMS discussed here, one — the gyroid — has inversion symmetry and *oppositely congruent labyrinths*. Of the remaining eleven cases, four contain straight lines and have *directly congruent* labyrinths; the remaining seven examples have mirror-plane symmetries, contain no straight lines, and their labyrinths are *non-congruent*. (These remarks should, of course, be considered with due regard for the unproved state — for some of these surfaces — of the assertion that the surfaces are free of self-intersections.)

IV. KALEIDOSCOPIC CELLS, OR FUNDAMENTAL REGIONS FOR GROUPS OF REFLECTIONS IN R^3

We now describe the convex polyhedra which provide plane boundaries for finite minimal surfaces which can be replicated by reflection to yield IPMS without self-intersections.

Coxeter (ref. 7) has shown that there are seven convex polyhedra Π_i which are fundamental regions of discrete groups generated by reflections. These polyhedra, which will be called *kaleidoscopic cells*, are described in the following list:

Π_1: *Rectangular parallelopiped*.

Π_2: *Tetragonal disphenoid*, an isogonal, isohedral tetrahedron with isosceles triangle faces; the four vertices of the tetrahedron have Cartesian coordinates proportional to (1 2 0), (1 - 2 0), (- 1 0 2), and (- 1 0 - 2), respectively.

Π_3: *Trirectangular tetrahedron* (one-half of Π_2); its four vertices have coordinates proportional to (- 1 0 0), (1 - 2 0), (1 2 0), and (- 1 0 2), respectively. Π_3 is called "trirectangular" by Coxeter, because its face angles include three right angles.

Π_4: *Quadrirectangular tetrahedron* (one-half of Π_3); its four vertices have coordinates proportional to (1 0 0), (- 1 0 0), (1 - 2 0), and (- 1 0 2), respectively. Π_4 is called "quadrirectangular" by Coxeter, because its face angles include four right angles.

Π_5: *(333) prism*, a triangular (right) prism, each of the three angles of the base triangle being $\pi/3$.

Π_6: *(244) prism*, a triangular (right) prism, the three angles of the base triangle being $\pi/2$, $\pi/4$, and $\pi/4$, respectively.

Π_7: *(236) prism*, a triangular (right) prism, the three angles of the base triangle being $\pi/2$, $\pi/3$, and $\pi/6$, respectively.

The three tetrahedra, Π_2, Π_3, and Π_4, which are fundamental regions of groups of reflections having *cubic* Bravais lattices, necessarily have invariant proportions. On the other hand, each of the remaining four examples of Π_i may be chosen with some arbitrariness with respect to relative proportions. Thus, Π_1 (*monoclinic* Bravais lattice) may have any set of relative values whatever of height, depth, and width; the three prisms, Π_5, Π_6, and Π_7 (*hexagonal* and *tetragonal* Bravais lattices) may have arbitrary values of height with respect to lateral dimensions. In the context of minimal surface boundary conditions, however, the relative proportions of the cells Π_1, Π_5, Π_6, and Π_7 must satisfy certain inequalities. These inequality relations arise because the existence of a non-simply-connected minimal surface with a specific type of boundary is subject to limitations on the allowed separation of the fixed curves or free boundaries (here planes) which bound the surface. The familiar examples of the catenoid and of doubly-connected minimal surfaces bounded by parallel coaxial "aligned" regular polygons of finite order (this latter case was investigated in detail by H. A. Schwarz (ref. 1)) illustrate this kind of limiting behavior on boundary separation.

V. ALGORITHM FOR CONSTRUCTING AN INTERSECTION-FREE MIRROR-SYMMETRIC IPMS, WHICH IS ADJOINT TO A TWO-FOLD ROTATIONALLY-SYMMETRIC IPMS (NOT NECESSARILY FREE OF SELF-INTERSECTIONS) COMPOSED OF CONGRUENT REPLICAS OF A SIMPLY-CONNECTED MINIMAL SURFACE SPANNED BY A STRAIGHT-EDGED POLYGON

Consider a kaleidoscopic cell Π. Π is a convex polyhedron with m faces F_r $(r = 1,2,\ldots,m)$.

Construct the set of vectors $\{\hat{U}_r\}$ $(r = 1,2,\ldots,m)$: the direction of each $\hat{U}_r$ is chosen to coincide with the outward normal to F_r, and the magnitudes of the $\{U_r\}$ need only satisfy the relation

$$\sum_{r=1}^{m} \hat{U}_r = 0. \tag{1}$$

Let Π' be a polyhedron dual to Π. Each distinct Hamilton line H_α in Π' corresponds to a distinct permutation T_α of the

set $\{F_r\}$ of faces of Π. In each such permutation T_α, only *adjoining* faces of Π (faces which intersect in an edge of Π) correspond to consecutive elements in T_α.

Now construct the polygon W_α with edges $\{\hat{U}_r\}$, which are ordered consecutively in W_α according to the sequence corresponding to the Hamilton line H_α. Let M_α be the minimal surface spanned by W_α. (M_α is unique, since W_α is found to have a convex projection in every case which arises.) The minimal surface M_α^*, which is the adjoint of M_α, is bounded by plane lines of curvature $C_{\alpha,r}$. Each curve $C_{\alpha,r}$, which lies in the plane of the face f_r of a polyhedron Π^* which is of type Π, is the image, under the adjoint transformation, of the edge $\hat{U}_r$ of M_α.

Except in the case of the three tetrahedral cells Π_2, Π_3, and Π_4, which have invariant proportions, the polyhedron Π^* has proportions which are determined — as discussed below — by the proportions of W_α. The exact relation between the proportions of Π^* and the proportions of W_α can be determined only from a complete analytic solution for the adjoint surfaces M_α and M_α^*.

(The directions of the vectors $\hat{U}_r$ could equally well have been chosen to lie along the *inward* normals to the faces F_r of Π. This freedom of choice for the *sense* of the $\hat{U}_r$ is simply an expression of the fact that if θ is the transformation angle in the associate surface transformation of a minimal surface, then adjoint surfaces exist both for $\theta = \pi/2$ and for $\theta = -\pi/2$; two such adjoint surfaces are simply mirror images of one another.)

For each of the three tetrahedra, Π_2, Π_3, and Π_4, the invariant proportions of the cell allow only one solution of Eq. (1) (aside from a multiplicative constant). The five skew quadrilateral solutions W_α found, for these three cells, by application of the above rule for deriving all distinct polygons W_α associated with a cell, belong to the set of six Schoenflies quadrilaterals (ref. 8) from which IPMS can be generated. (The sixth Schoenflies quadrilateral contains one vertex angle of $2\pi/3$; associated with this vertex, there is a branch point corresponding to self-intersection in the IPMS obtained by analytic continuation of the minimal surface module M_α spanned by the quadrilateral. A simplified model of the adjoint surface, based on M_α^*, is shown, in an assembly constructed from flat pieces of cardboard, in Figure 14.

For each of the three prism cells Π_5, Π_6, and Π_7, the edges $\hat{U}_r$ of the skew pentagons W_α are found to be a subset of the edges of a prism Q_α of the same type as the kaleidoscopic prism cell itself. The two edges of equal length in W_α, each of which lies at the intersection of a pair of lateral faces of the prism ("altitude" edges), may be chosen to be of arbitrary

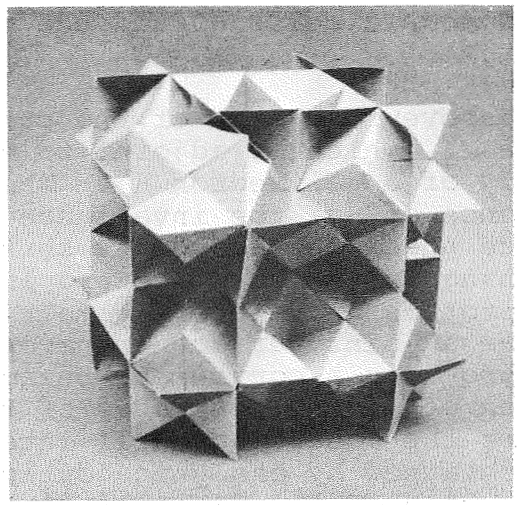

Figure 14.- A simplified model of a self-intersecting infinite periodic minimal surface. This surface is constructed from congruent replicas of a quadrilateral bounded by plane lines of curvature. The quadrilateral is adjoint to that straight-edged quadrilateral, among the six such polygons enumerated by Schoenflies, which contains a face angle of 120^{o} (cf. ref. 8).

magnitude with respect to the lengths of the remaining edges of W_α. For each of the six solutions W_α which are obtained from the three prisms, Π_5, Π_6, and Π_7, there is a unique inverse relation between the *relative altitude* of the prism Q_α (i.e., the ratio of the altitude of Q_α to the length of one of the transverse edges of Q_α) and the *relative altitude* of the corresponding kaleidoscopic prism cell Π^* (i.e., the ratio of the altitude of Π^* to the length of one of the transverse edges of Π^*): as the relative altitude of Q_α increases without limit, the relative altitude of Π^* approaches zero; as the relative altitude of Q_α approaches zero, the relative altitude of Π^* increases, approaching a limiting finite value.

For the rectangular parallelopiped kaleidoscopic cell, Π_1, the edges $\hat{U}_r$ of the two derived skew hexagons W_α are subsets of the edges of rectangular parallelopipeds Q_α which have different proportions, in general, from those of the adjoint cells Π^*. Inverse relations hold here, also, between the relative dimensions of the kaleidoscopic cells Π^* and the relative dimensions of the cells Q_α.

It was stated above that each of the curved edges $C_{\alpha,r}$ of the minimal surface M_α^*, which is adjoint to M_α, lies in the plane of the face f_r of a polyhedron Π^*. This result is an elementary consequence of (a) the invariance of the Gauss map of a minimal surface under the associate surface transformation, and (b) the interchange of asymptotics and lines of curvature (here, *linear* asymptotics and mirror-symmetric *plane* lines of curvature) under the adjoint surface transformation (ref. 11). While this result provides a convenient phenomenological method for the construction of minimal surfaces of type M_α^*, it is not sufficient to insure the absence of self-intersections in the IPMS M_α^*, which is obtained by analytic continuation of M_α^* (i.e., by reflecting M_α^* in each of the faces of Π^*, then reflecting the *reflected* surfaces in each of the faces of the replicas of Π^*, etc.). Thus, without proof to the contrary, it is necessary to allow for the possibility that one or more of the curved edges $C_{\alpha,r}$ extends beyond an edge of the face f_r in whose plane it lies, to form what we will call an "extended loop". The existence of such an extended loop implies that the IPMS M_α^* intersects itself. In each of the examples which arise from the algorithm described here, it is not difficult to present a convincing demonstration that such extended loops do not occur, by (a) examining the behavior of the normal to a soap-film model of the adjoint surface M_α, thereby showing the "impossibility" of an assignment to the faces of Π^* of a self-consistent set of edge curves $C_{\alpha,r}$ which include any extended loops; (b) bending thin models of the surface M_α into the configuration of the adjoint surface M_α^*; and (c) constructing M_α^* in the form of a

soap film (in unstable equilibrium) in Π^* (or in a cell of proportions approximating those of Π^*). Such demonstrations, although quite convincing, do not constitute a mathematical proof of the non-existence of self-intersections. In general, only quantitative information derived from detailed analysis of each surface will afford such proof, and this analysis has not been attempted. (As mentioned in Section II, elementary arguments are sufficient to prove that H'-T is free of self-intersections.)

Meanwhile, it has been found possible to construct models of IPMS of type M_α^* which appear to be fair approximations to the actual form of the desired minimal surface, either by bending thin plastic models of surfaces of type M_α, or by constructing thin plastic models of M_α^* on the basis of measurements of soap film models of M_α^* which are blown in cells Π^*. The fact that such methods lead to results of reasonably good accuracy in the case of the surfaces D, P, and C(P), where the complete solutions are known, lends support to the idea that reasonably correct models can indeed be constructed in this way.

VI. THE CONSTRUCTION OF INTERSECTION-FREE IPMS WHICH HAVE A MORE COMPLICATED FUNDAMENTAL REGION THAN THOSE IPMS OBTAINED BY USE OF THE ALGORITHM OF THE PREVIOUS SECTION

Certain infinite periodic graphs (including several examples of symmetric graphs) for which a fundamental region may be chosen to lie within a kaleidoscopic cell, have been examined with an eye toward the possibility that there may exist an intersection-free IPMS for which such a graph provides a labyrinth skeletal graph. If one makes use of the metaphorical concept of *inflating* the infinite graph (regarded as a flexible hollow tubular graph), so as to transform it into a hypothetical IPMS, it is a straightforward matter to deduce the approximate configuration of the curved edges $C_{\alpha,r}$ of a hypothetical surface of general type M_α^*, these edges lying in the faces of a cell Π^*. (The isometric property of the associate surface transformation, coupled with the requirement that W_α be a closed polygon, constrains the relative lengths of the edges $C_{\alpha,r}$.) In some cases, this hypothetical surface M_α^* is multiply-connected, with no plane lines of curvature or linear asymptotics in the interior of M_α^*. It is believed that several of these cases probably correspond to real examples of intersection-free IPMS, but conclusive evidence on this point is lacking so far.

In several other cases, the hypothetical surface M_α^* is simply-connected, but the number of bounding arcs $C_{\alpha,r}$ is greater than the number of faces of the cell Π^*, i.e., there is at least one face f_r of Π^* containing two arcs: $C_{\alpha,r}$ and $C'_{\alpha,r}$. In such

cases, it is fruitful to investigate the behavior of the normal to the adjoint surface M_α and also, occasionally, the limiting behavior of M_α when it has edge proportions near those of "slightly perturbed" examples of proved minimal surfaces having straight edges. Such perturbed examples are constructed by forming a kind of *linear combination* of the polygonal boundaries of a pair of appropriate minimal surfaces; the boundary of the resulting surface, in each such case, includes some edges common to the pair of surfaces and some edges which are fractional portions of edges unique to each of the pair of surfaces. It is then sometimes possible to prove that there must exist a unique set of proportions of M_α for which the "extra edge" $C'_{\alpha,r}$ in M^*_α actually does lie in a plane which is not merely *parallel* to the face f_r of Π^*, but *coplanar* to it, as in the hypothetical surface. When this situation occurs, the surface M^*_α is a possible intersection-free IPMS; nevertheless, the absence of extended loops of the kind discussed in the previous section must be proved in order to insure that M^*_α does not intersect itself.

While a number of promising examples of such hypothetical IPMS have been identified, only two have been carefully investigated so far.* One of these, which we call the complement of the Schwarz surface H, or C(H), is of genus 7 (Figure 11). The other, which is called O,C-TO (Figure 12), is a surface of genus 10; an explanation of its name and a description of its structure are given in Table II of Section IX.

The existence of C(H) and of O,C-TO, and the absence of self-intersections from these surfaces, have been confirmed by the construction of fundamental regions M^*_α for each surface in the form of soap films in the appropriate kaleidoscopic cells: Π_5 for C(H) and Π_4 for O,C-TO.

VII. COMPLEMENTARY PAIRS OF INTERSECTION-FREE IPMS

It was observed by the author that the intersection-free surface C(P) studied by Neovius (a) contains exactly the same straight lines as does Schwarz's primitive surface P, and (b) has the same set of isometries, or space group, as P. This observation, which accounts for the assignment of the name C(P) to this Neovius surface, led immediately to the construction of the surface C(D) (ref. 6). D and C(D) also contain the same straight lines and share a common space group. P and C(P) have genus 3 and 9, respectively; D and C(D) have genus 3 and 19, respectively.

---

*Note added in proof: A third such IPMS, of genus 5, with hexagonal adjoint module M_α and cell Π_5, has been found. It will be named g-g'; it is related to the structure of hexagonal graphite.

The relations exemplified by these two pairs of surfaces led the author to define *two complementary minimal surfaces* as a pair of intersection-free IPMS which have the property that the set of all straight lines lying in either surface is the same. For each of the known pairs of complementary IPMS, the space group – but not the genus – is the same for the two surfaces. (Cf. ref. 12, for a discussion of König's theorem: "any connected graph may be embedded in an orientable surface so as to form the vertices and edges of a map.")

A third example of a pair of complementary IPMS is provided by Schwarz's surface H (genus 3) and the surface C(H) (genus 7). In this case, unlike the other two, the embedded lines do not form a connected graph; instead, they form an infinite set of parallel replicas of the infinite plane graph composed of the edges of the regular tessellation {3,6} of equilateral triangles. Thus, the graph is the collection of all the lateral* edges of a space-filling assembly of equilateral triangle right prisms. It is almost certainly true that the existence limits of H and C(H) do not coincide, i.e., there probably exists a range of proportions for the cell Π_5 for which H exists but C(H) does not exist (or vice versa). Thus, the complementary relation between these two surfaces is restricted to the interval on the relative altitude of Π_5 for which both surfaces are defined.

The fact that the complements of P, D, and H are of higher genus than P, D, and H, respectively, may be picturesquely illustrated by comparing appropriate portions of each surface and of its complement which are orthogonally bounded by the interior faces of a given suitably chosen polyhedral cell. If the cells are chosen to be a *cube* for P and C(P), a *tetragonal disphenoid* for D and C(D), and a *rhombic prism* (equal to two adjoining cells of type Π_5) for H and C(H), then it is found that whereas P, D, and H are represented by surface modules having *one* curved edge (plane line of curvature) per cell face, their complements are represented by surface modules having *two* curved edges per cell face. It seems likely that no *other* singularity-free minimal surface modules, containing the same straight line segments, can be bounded by the interior faces of these cells. Each of these cells is a fundamental region for a group of reflections. In the case of D, the group is the complete group of reflections for D. In the case of P and also of H, the group is a subgroup of the complete group of reflections for the surface.

There exists an infinite symmetric graph of degree six, which contains all the vertices of the f.c.c. graph of degree twelve, but only half as many edges; the edges incident at each

* By "lateral edges" is meant edges perpendicular to the prism axes.

vertex lie in a plane. This graph can be embedded in either P or in D. If each of the regular skew hexagons, defined by a circuit of six edges of the graph, is spanned by a minimal surface, P is the resulting IPMS. If each of the regular skew quadrilaterals, defined by a circuit of four edges of the graph, is spanned by a minimal surface, D is the resulting IPMS. Because the sets of *all* straight lines, in P and D, include other lines besides those in this graph of degree six, D and P are not considered to be complementary surfaces. (These other lines are not the same for P and D.)

Finally, CLP is found to be *self-complementary*: if the surface is subjected to a translation by one-half of the elementary lattice distance along the c-axis (tetragonal symmetry axis), the graph composed of all straight lines lying in the untranslated surface coincides with the corresponding graph for the translated surface (Figure 6).

VIII. THE GYROID

This surface appears to be the only known example of an intersection-free IPMS which contains neither straight lines nor plane lines of curvature. Thus, its symmetry group includes no mirror reflections, and the axes of rotational symmetry do not lie in the surface. The gyroid belongs to the *cubic* crystal system; its space group is $I4_1/2\bar{3}/d$. A few descriptive remarks concerning this surface and its relation to the P and D surfaces of Schwarz appear in references 5 and 6. Because a detailed analysis of the gyroid will shortly be published elsewhere, only a few summarizing remarks will be made here.

The gyroid G has a body-centered cubic (b.c.c., or cubic *I*) Bravais lattice. It is associate to D, which has a face-centered cubic (f.c.c., or cubic *F*) lattice, and to P, which has a primitive cubic (cubic *P*) lattice. The angle of associativity (see Appendix I) for G, computed with respect to D, is found to be

$$\theta_G = \mathrm{ctn}^{-1}(K'/K) \cong 38.0147740^\circ \; ; \tag{2}$$

$K' \equiv K'(1/2)$ and $K \equiv K(1/2)$, which are complete elliptic integrals of the first kind, with modulus $k = 1/2$, are the two fundamental periods of the elliptic functions in terms of which Schwarz (ref. 1) expressed the parametric solutions for D and P. The parametrization of the gyroid, therefore, is given by the following equations:

$$x = \mathrm{Re}\int \exp(i\theta_G)F(\tau)(1 - \tau^2)\, d\tau, \tag{3}$$

$$y = \mathrm{Re}\int i \exp(i\theta_G)F(\tau)(1 + \tau^2)\, d\tau, \tag{4}$$

$$z = \mathrm{Re}\int 2 \exp(i\theta_G)\tau F(\tau)\, d\tau, \tag{5}$$

where

$$F(\tau) = (1 - 14\tau^4 + \tau^8)^{-1/2}. \tag{6}$$

The skeletal graphs of the two enantiomorphous labyrinths of G are mirror-symmetric *Laves graphs* of degree three (refs. 5,13).

The nearly *circular* plane "holes" in P (shown by Schwarz to have radius variations of only ~ ± 0.4%) correspond to nearly *helical* geodesics, on G, which have radius variations, with respect to cylindrical helices, of only ~ ± 0.5%.

P, D, and G may be thought of as metric realizations of the following *regular maps with holes* (refs. 5,12,14): {6,4|4}, {4,6|4}, and {6,6|3}. These regular maps are reflexive (ref. 12) in P and in D; they are non-reflexive in G.

A most convenient way of representing the group of isometries by which one can construct any surface associate to P and D, using congruent replicas of a face of any one of the three regular maps listed above, is to construct a group of left- and right-handed screw isometries. Based on the map {6,4|4}, for example, the four-fold screw isometries collapse to a screw of *zero* pitch (but *finite* "hole" diameter) for P, and reach a limit of *finite* pitch (but *zero* "hole" diameter) for D. The images of these hole curves in P and G are straight lines in D. Figure 16 shows computer-generated stereoscopic drawings of a single lattice fundamental region in D, G, and P, respectively. The transformation of the quasi-circular holes in P into straight line holes in D, via intermediate quasi-helical holes of the type which appear in G, is illustrated by the example of the line segment which is shown extending from left to right along the central axis of the fundamental region of D. This line segment corresponds to a single pitch of the general quasi-helical hole curve. The diameter of such a quasi-helix is defined as the diameter of the closely similar circular helix which passes through the vertices of the regular map {6,4|4} shown in the figure. Thus, the quasi-helix may be described as the *circum-helix* of the *regular helical polygon*, having a four-fold screw

isometry, which is a *hole* of the regular map {6,4|4} in the regular warped polyhedron (ref. 5) which is homeomorphic to G.

While P and D are not the only adjoint pair of intersection-free IPMS (the intersection-free IPMS CLP and its homeomorphic adjoint are essentially the "same" surface, aside from a change in tetragonal proportions), no example of *three* intersection-free associate IPMS, aside from the case of P, D, and G, has been found. It is considered highly unlikely that any other intersection-free IPMS containing neither straight lines nor plane lines of curvature will be found. No examples, aside from P, D, and G, of intersection-free IPMS in which regular maps can be embedded, are known.

The three infinite regular skew polyhedra (ref. 14) of Coxeter and Petrie correspond to those three, among the six regular maps which can be embedded in P and D, whose edges cannot be drawn on P and D as line segments. Thus, the regular skew polyhedra have the same vertices as the corresponding regular maps in P and D, but a pair of adjacent vertices in the regular skew polyhedra is joined by straight edges instead of by the curved edges which join them in P and D. When adjacent vertices of any of the three regular maps in G are joined by line segments, the faces of the regular map become regular *skew* polygons, not regular *plane* polygons as in the case of P and D.

In its general morphology, G has a kind of hybrid character with respect to P and D: G has open round "tunnels" (in either labyrinth) which are centered on cube axes, or (100) directions, as does P. G also has open round "tunnels" (in either labyrinth) centered on cube body-diagonal axes, or (111) directions, as does D. (These "tunnels" in D, however, are not "straight", i.e., they conform to the diamond-branched labyrinths of D.)

The general example of a surface associate to P and D is not periodic, i.e., its symmetry group is continuous, not discrete. Only a countably infinite number of surfaces associate to P and D are periodic; among these, G is the only example without self-intersections. The non-periodic surfaces can be described as having infinitely many self-intersections in each finite region of space. Each of the *periodic* surfaces, on the other hand, must satisfy certain commensurability constraints; it is convenient to express these constraints in terms of the proportions (pitch and diameter) of the approximately helical "holes" (refs. 5,14) of the regular map {6,4|4} inscribed in the surface. These commensurability constraints imply that the set of periodic surfaces associate to P and D can be put into one-to-one correspondence with the set of positive rational numbers. If θ is the angle of associativity (see Appendix I),

with respect to D, of a periodic associate surface, than it is found that the allowed values of θ are given by the relation

$$\theta_{p,q} = \mathrm{ctn}^{-1}[(p/q)(K'/K)]; \qquad (7)$$

p and q are any two coprime positive integers; $K' \equiv K(1/2)$ and $K \equiv K(1/2)$ are the complete elliptic integrals appearing in Eq. (2). For the gyroid, p = q = 1 (see Eq. 2).

The countably infinite set of self-intersecting surfaces associate to P, D, and G may be regarded as being related to P, D, and G in somewhat the same way as the four self-intersecting Kepler-Poinsot polyhedra are related to the five Archimedean regular polyhedra. On any of these self-intersecting minimal surfaces, the three regular maps {6,4|4}, {4,6|4}, and {6,6|3} may be inscribed (refs. 5,12,14). The "simplest" of these self-intersecting surfaces is the one with p = 1 and q = 2 (see Eq. 7); in this case, the regular map {6,4|4} has a particularly simple relation to the structure of self-intersections. This surface has been named dh, for *diamond honeycomb*.

Schwarz made repeated references (ref. 1) to the bending of minimal surfaces according to Bonnet's associate surface transformation (ref. 3), in his discussion of P and D, but he does not appear to have made any investigation of the global properties of actual surfaces associate to P and D. Thus, the gyroid appears not to have been identified before now; furthermore, the results summarized by Eq. (7) also appear to be new.

If a lattice fundamental region for each of the three surfaces P, D, and G is chosen to have the highest possible *point group* symmetry, then the respective point groups may be listed as follows:

P: $\frac{4}{m}\,\bar{3}\,\frac{2}{m}$ (cubic)

D: $\bar{4}\,3\,m$ ([regular] tetrahedral)

G: $\bar{3}2$ (trigonal).

Correlated with this sequence of reduced symmetry of the point group is a monotonic increase in the normalized surface-to-volume ratio $S/V^{2/3}$, per lattice fundamental region, for the sequence P → D → G. (For comparison, it should be noted that the corresponding value of $S/V^{2/3}$ for the regular skew polyhedron {6,4|4} is $(3/2)\sqrt{3} \cong 2.5987$.)

The computed values of $S/V^{2/3}$ for P, D, and G are given below:

Surface	$S/V^{2/3}$
P	$3(K/K') \cong 2.3451$
D	$(3/2^{2/3})(K'/K) \cong 2.4177$
G	$(3/4^{2/3})(K'/K)[1 + (K/K')^2] \cong 2.4533$

For C(P), the only other example for which the necessary data are available, $S/V^{2/3}$ is found to have the value $3K'/K \cong 3.51048$; in this case, the modulus $k = 1/\sqrt{3}$. Related results for C(D) would be of some interest, but the difficulty of obtaining a parametrization of this surface appears formidable.

Kelvin considered the following isoperimetric problem: what space-filling polyhedron (not restricted to be convex) has the smallest surface area for a given value of the volume? Kelvin found that a modification of the truncated octahedron in which the edges are slightly curved, all faces being minimal surfaces, leaves the volume unchanged, while the surface area is reduced by roughly one part per thousand. No example with a smaller value of $S/V^{2/3}$ is known, but it has not been proved that the Kelvin solution is optimum.

A different isoperimetric problem may be described as follows: among all intersection-free surfaces in R^3 which have the translational periodicity of a 3-dimensional lattice and which partition R^3 into two congruent regions, which has the smallest value of $S/V^{2/3}$? In this case, S is the area of a single lattice fundamental region of the surface, and V is the volume of a primitive cell of the lattice. It appears quite possible that the periodic minimal surface P is the optimum example of such a surface. Both P and D can be transformed into space-filling assemblies of Kelvin polyhedra by the following construction rule: Add lamellae to the IPMS by spanning all *closed geodesics* with minimal surfaces; then deform the resulting configuration homeomorphically until all surface intersections satisfy the requirements of equilibrium under surface tension. In this final state, the angles of intersection of the three lamellae which intersect along every curved edge are each $2\pi/3$, and the four curved edges which intersect at every vertex meet each other at the angle $\cos^{-1}(-1/3) \cong 109°28'$.

If this construction rule is applied to G, it is found that when the minimal surface lamellae are added, R^3 is partitioned into congruent 17-faced curved polyhedra *which are homeomorphic to the Dirichlet cells of the vertices of the two skeletal*

Laves graphs of G. (In the case of both P and D, also, the Dirichlet cells [truncated octahedra] of the vertices of the two skeletal graphs are homeomorphic to the curved polyhedra which result from this construction.) It is not known whether this construction can be carried to completion in the case of G, i.e., whether the added lamellae, which are curved decagons, together with the quadrilateral and hexagonal faces formed on G by the intersections of the closed geodesics, can be deformed into a homeomorphic configuration of minimal surfaces whose intersections satisfy the laws of equilibrium under surface tension. However, if such an equilibrium state does exist, the examples of P and D suggest that the derived cell is unlikely to have a very much smaller value of $S/V^{2/3}$ than the corresponding Dirichlet cell. For the 17-faced Dirichlet cell in the case of G, $S/V^{2/3} \cong 5.644680$; for the truncated octahedron, $S/V^{2/3} \cong 5.314740$. Hence, it appears likely that *if it exists*, the analog to the Kelvin polyhedron which is derived from the gyroid by the empirical construction rule given above has a *larger* value of $S/V^{2/3}$ than does the Kelvin polyhedron.

These considerations are hardly conclusive, since they are based on an incomplete analysis, but they provide weak additional evidence in support of the Kelvin polyhedron as the solution of the classical $S/V^{2/3}$ isoperimetric problem.

It appears that G may be unique in a *symmetrical* sense: in contrast to P and D, for which variants of lower point group symmetry may easily be proved to exist, G may not have any variant forms of lower symmetry. This statement is based on the discussion which follows.

P is one of two distinct minimal surfaces which may be derived, by means of the construction algorithm of Section V, from the kaleidoscopic cell Π_1 in its most symmetrical form: the cube. The surface module M_α^*, in this case, is a face of the regular map $\{6,4|4\}$ on P. M_α is a face of the regular map $\{6,4|4\}$ on D; the six edges of equal length which form the boundary of M_α correspond to a solution $|\hat{U}_r|$ = constant in Eq. (1). The other solutions of Eq. (1) in this case give rise to a two-parameter family of adjoint surfaces which *resemble* both P and D, but which have lattices of lower symmetry (either tetragonal or monoclinic). By considering the inverse relations which hold between the relative dimensions of the parallelopiped Π_1^*, spanned by a hexagonal face of P in its most general orthorhombic form, and the relative dimensions of the parallelopiped Q_α, from which a subset of six edges forms the boundary W_α of a hexagonal face of D in its most general orthorhombic form, it is possible to show that *except when* $|\hat{U}_r|$ = *constant in Eq. 1, no intersection-free associate surface on a body-centered lattice, corresponding to the gyroid, exists.* This result suggests the

possibility that there does not exist *any* body-centered *orthorhombic* version of G, however it is obtained. In any case, if such an IPMS does exist, it cannot be obtained from lower symmetry variants of P and D by the associate surface transformation. It is not known whether surfaces derived from the gyroid, with *non-zero* constant mean curvature, exist.

If oblique sets of basis vectors for the cubic lattices *P* and *F* are constructed for suitably chosen simply-connected lattice fundamental regions of P and D, respectively, then it is possible to construct a representation of the bending of either fundamental region into the other, in which each basis vector describes an elliptical trajectory centered on the origin fixed in the surface. When $\theta = \theta_G \pmod{\pi}$, the image of this set of vectors is a set of basis vectors for the cubic *I* lattice of the gyroid. (When $\theta = \theta_G \pmod{\pi}$, the gyroid is again generated, but the three vectors lie in a plane.) If $[\hat{u}(\theta), \hat{v}(\theta), \hat{w}(\theta)]$ is this set of vectors, then the determinant $|uvw|$ defines the volume of a lattice primitive cell for D, G, and P, when $\theta = 0$, θ_G, and $\pi/2$, respectively. These volumes are simple functions of the complete elliptic integrals appearing on p. 52.

IX. SEVENTEEN INTERSECTION-FREE IPMS

In this section, we provide a list of the seventeen surfaces which are the subject of this note. We will assume here that all of these surfaces are free of self-intersections, i.e., we will disregard the possibility that any of them contains any "extended loops" of the type described earlier. In Table I, these surfaces are listed according to their assigned names, in order of increasing genus. (The genus of each surface was computed by applying Hopf's theorem (ref. 15), which states that the Euler-Poincaré characteristic of a compact orientable surface is equal to twice the degree of the Gauss mapping, to a lattice fundamental region of the surface.)

For each of the 14 surfaces for which a single "Flächenstück" M_α^* can be orthogonally bounded in the interior of one (or more) of the seven kaleidoscopic cells, the identity and the number of faces m of the cell Π_i are listed, and the number m' of (plane line of curvature) edges of the surface M_α^* contained in Π_i^* is also given. Whenever the application of the construction algorithm of Section V allows the generation of that surface in more than one of the kaleidoscopic cells, the values of m and m' are given for each such cell. The number of the figure (if any) in which the surface is shown is also listed.

Table II provides a list of descriptive remarks, concerning each of the seventeen surfaces, which are sufficiently specific

to assist the reader to some degree in identifying each surface, even in those cases where no illustration has been provided.

Table III lists the crystal system and space group symbol for each of these seventeen surfaces. The space group is also identified by its number in the *International Tables for X-ray Crystallography* (ref. 16).

TABLE I.- SEVENTEEN INTERSECTION-FREE INFINITE PERIODIC MINIMAL SURFACES

Fig. No.	Name of Surface	Genus	Kaleidoscopic Cell Π_i	Number m of Faces of Π_i	Number m' of Boundary Curves of Surface Module M_α^*
2	P	3	$\Pi_4;\Pi_6;\Pi_1$	$4(\Pi_4);5(\Pi_6);6(\Pi_1)$	$4(\Pi_4);5(\Pi_6);6(\Pi_1)$
1	D	3	Π_2	4	4
7	G	3	—	—	—
5	H(=R_I)	3	Π_5	5	5
6	CLP	3	Π_1	6	6
13	H'-T	4	Π_7	5	5
—	S'-S"	4	Π_6	5	5
—	H"-R	5	Π_7	5	5
—	T'-R'	6	Π_7	5	5
10	F-RD	6	Π_3	4	4
11	C(H)	7	Π_5	5	7
9	I-WP	4	Π_4	4	4
3,4	C(P)	9	$\Pi_4;\Pi_1$	$4(\Pi_4);6(\Pi_1)$	$4(\Pi_4);12(\Pi_1)$
—	R_{II}	9	—	—	—
12	O,C-TO	10	Π_4	4	5
—	R_{III}	13	—	—	—
8	C(D)	19	Π_2	4	8

TABLE II.- DESCRIPTIVE REMARKS CONCERNING THE SEVENTEEN INTERSECTION-FREE INFINITE PERIODIC MINIMAL SURFACES

1. P — *Primitive* surface of Schwarz (ref. 1)

2. D — *Diamond* surface of Schwarz (ref. 1)

3. G — *Gyroid*, associate to P and D (cf. Section VIII and refs. 5,6)

4. H(=R_I) — *Hexagonal graph* surface of Schwarz (ref. 1). This surface is also designated R_I, to indicate that it can be constructed from doubly-connected fundamental regions ("ring-like surfaces"), bounded by the opposite parallel equilateral triangles of a prism of type Π_5. The hexagonal graph comprises all of the the lateral edges (i.e., edges perpendicular to the c-axis) of a space-filling assembly of congruent regular hexagon right prisms, as well as one-half of all the other edges of such an assembly. Specifically, these latter edges ("altitude" edges) may be described as the set of *alternate* axial edges of a honeycomb of infinitely long congruent regular hexagon right prisms obtained by removing the hexagonal faces from the honeycomb of finite hexagonal prisms.

5. CLP — *Crossed layers of parallels* surface: This Schwarz surface (ref. 1) may be described in terms of two congruent skeletal graphs, each of which is called "crossed layers of parallels." This graph, which belongs to the tetragonal crystal system, is constructed from equidistant parallel layers of parallel lines. Each layer lies in a plane perpendicular to the tetragonal axis (c-axis), and is made up of an infinite set of equidistant parallel lines. All pairs of adjacent layers are equidistant; the lines in adjacent layers are orthogonal ("crossed"). Every pair of lines in adjacent layers is joined by an edge, parallel to the c-axis, which is the line segment of smallest length connecting the pair of lines. Alternatively, CLP may be described in terms of the smallest straight-edged polygon which may be inscribed in the surface: a hexagon, visible in Figure 6, whose edges are a subset of the edges of a square prism. For the model shown in Figure 6, the square prism is a cube; the space group is not affected by the choice between cube and general square prism.

6. H'-T — *Hexagonal graph – Triangle graph* surface: the skeletal graph of one labyrinth (hexagonal) consists

of all of the edges of a space-filling assembly of congruent regular hexagon (right) prisms; the skeletal graph of the dual labyrinth (triangular) consists of all of the edges of a space-filling assembly of congruent equilateral triangle prisms.

7. S'-S" *Large square graph — Small square graph* surface: the skeletal graph of one labyrinth (S') is made up of parallel layers of identical square tessellations, adjacent layers being joined at edge midpoints by edges perpendicular to the layers; the skeletal graph of the dual labyrinth (S") is made up of layers of identical square tessellations, halfway between and parallel to the other layers; each square in S" has one-half the area of a square in S'. The squares in S" are joined by edges, perpendicular to the layers, at alternate vertices; these edges pass through the centers of the squares in S'.

8. H"-R *Hexagonal graph — Rhombic graph* surface: H" is the collection of all lateral edges of a space-filling assembly of congruent regular hexagon (right) prisms, plus edges, perpendicular to the hexagonal layers, which join neighboring layers at the mid-points of the hexagon edges. R is a graph whose identical layers are rhombic plane tessellations, each rhombus being the "sum" of two adjacent equilateral triangles. The connections between adjacent rhombic layers are edges, perpendicular to the layers, which join *acute* rhombic vertices. Rhombus Area = (1/3)(Hexagon Area).

9. T'-R' *Triangular graph — Rhombic graph* surface: T' is the collection of all lateral edges of a space-filling assembly of congruent equilateral triangle (right) prisms, plus edges, perpendicular to the triangle layers, which join neighboring layers at the midpoints of the triangle edges; R' is a graph whose identical layers are rhombic plane tessellations, each rhombus being the "sum" of two adjacent equilateral triangles. The connections between adjacent rhombic layers are edges, perpendicular to the layers, which join *obtuse* rhombic vertices. Rhombus Area = (2/3)(Triangle Area).

10. F-RD *F-graph — Rhombic dodecahedra graph* surface: (dual of f.c.c.): The F-graph is the symmetric graph, of degree 12, constructed by joining all nearest neighbor points of a f.c.c. lattice, by an edge. The RD-graph is constructed by joining the centroids

of all facially adjacent polyhedra by edges, in a cubically symmetrical packing of regular octahedra and regular tetrahedra. Also, the RD graph is the assembly of all the edges of a space-filling assembly of rhombic dodecahedra. F-RD is the adjoint of a surface partly analyzed by Stessmann (ref. 8).

11. C(H) *The complement of H*. This surface is a trigonally symmetrical analog of C(P): if the cell Π_1, in its *cube* form, contains an orthogonally bounded 12-gon face (with curved edges) of C(P), and the cell is continuously sheared until it assumes the shape of a rhombic prism which is congruent to the "sum" of two equilateral triangle prisms, then the 12-gon face of C(P) is transformed into a 12-gon face of C(H).

12. I-WP *I-graph — Wrapped Package graph* surface: the I-graph is the symmetric graph, of degree eight, constructed by joining by an edge all nearest neighbor points of a b.c.c. lattice; the WP graph is constructed by joining by an edge the centers of opposite edges of each square face of every cube in a space-filling assembly of cubes. (The name WP is chosen because of the resemblance of finite portions of the graph to the arrangement of string on a simply wrapped package.) I-WP is the adjoint of a surface partly analyzed by Stessmann (ref. 8).

13. C(P) *The complement of P*, analyzed by Neovius (refs. 4,6).

14. R_{II} An IPMS assembled from *"ring-like* surfaces", each bounded by the opposite parallel triangles ($\pi/2$, $\pi/4$, $\pi/4$) of a prism of type Π_6.

15. O,C-TO *Octahedra — cuboctahedra graph — tetragonal octahedron graph* surface: O,C is a symmetric graph of degree eight which comprises the edges of a space-filling assembly of regular octahedra and cuboctahedra; TO is constructed from the edges of a space-filling assembly of tetragonal octahedra. This octahedron consists of an assembly of four tetragonal disphenoids, joined along a common *long* edge lying along the 4-fold axis of the octahedron. Each tetragonal disphenoid is congruent to the kaleidoscopic cell π_2. This IPMS may be regarded as a kind of hybrid version of P and I-WP: the large cubically-symmetrical "chambers" of the TO labyrinth may be

described picturesquely as spherical bubbles which have sprouted tubules outward to the *faces* (cf. P) and also to the *corners* (cf. I-WP) of an enclosing cube. This description, based on the morphology of a lattice fundamental region of the surface, is reinforced by the fact that the boundary of a pentagonal surface module M_α, which is adjoint to the module M_α^* of O,C-TO, can be expressed as a kind of *linear combination* of the boundaries of quadrilateral surface modules M_α of P and I-WP (cf. Section VI). The *existence* of this IPMS is supported by the experimental observation that a soap-film model of M_α^*, formed in the interior of the kaleidoscopic cell Π_4, is *stationary*, and therefore appears to satisfy the requirements of unstable equilibrium for a minimal surface which is orthogonally bounded by the interior of a convex polyhedron. The relative lengths of the edges of the pentagonal module for this surface were derived from measurements of the soap film M_α^*.

16. R_{III} An IPMS assembled from "*ring-like* surfaces", each bounded by the opposite parallel triangles ($\pi/2$, $\pi/3$, $\pi/6$) of a prism of type Π_7.

17. C(D) *The complement of D* (ref. 6). The skeletal graphs of C(P) and C(D) may be derived according to a simple rule from the skeletal graphs of P and D, respectively; this rule is described in Appendix II.

TABLE III.- CRYSTAL SYSTEMS AND SPACE GROUPS OF THE SEVENTEEN INTERSECTION-FREE INFINITE PERIODIC MINIMAL SURFACES

Name of Surface	Crystal System	Space Group Symbol	Space Group Number
P	Cubic	$P\ \frac{4}{m}\ \bar{3}\ \frac{2}{m}$	221
D	Cubic	$F\ \bar{4}\ 3\ m$	216
G	Cubic	$I\ \frac{4_1}{a}\ \bar{3}\ \frac{2}{d}$	214
H	Trigonal	$P\ \bar{3}\ \frac{2}{m}\ 1$	164
CLP	Tetragonal	$P\ \bar{4}\ 2\ m$	111
H'-T	Hexagonal	$P\ \frac{6}{m}\ \frac{2}{m}\ \frac{2}{m}$	191
S'-S"	Tetragonal	$P\ \frac{4}{m}\ \frac{2}{m}\ \frac{2}{m}$	123
H"-R	Hexagonal	$P\ \frac{6}{m}\ \frac{2}{m}\ \frac{2}{m}$	191
T'-R'	Hexagonal	$P\ \frac{6}{m}\ \frac{2}{m}\ \frac{2}{m}$	191
F-RD	Cubic	$F\ \frac{4}{m}\ \bar{3}\ \frac{2}{m}$	225
C(H)	Trigonal	$P\ \bar{3}\ \frac{2}{m}\ 1$	164
I-WP	Cubic	$I\ \frac{4}{m}\ \bar{3}\ \frac{2}{m}$	229
C(P)	Cubic	$P\ \frac{4}{m}\ \bar{3}\ \frac{2}{m}$	221
R_{II}	Tetragonal	$P\ \frac{4}{m}\ C\ C$	124
O,C-TO	Cubic	$P\ \frac{4}{m}\ \bar{3}\ \frac{2}{m}$	221
R_{III}	Hexagonal	$P\ 6\ 2\ 2$	177
C(D)	Cubic	$F\ \bar{4}\ 3\ m$	216

The lower-symmetry variants of P and D are given below:

P_T	Tetragonal	$P\ \frac{4}{m}\ \frac{2}{m}\ \frac{2}{m}$	123
P_O	Orthorhombic	$P\ \frac{2}{m}\ \frac{2}{m}\ \frac{2}{m}$	47
D_T	Tetragonal	$I\ \bar{4}\ m\ 2$	119
D_O	Orthorhombic	$F\ 2\ 2\ 2$	22

X. THE EIGHT PENTAGONAL MINIMAL SURFACES WHICH ARE "FLÄCHENSTÜCKE" FOR IPMS ON NON-CUBIC BRAVAIS LATTICES

Schoenflies (ref. 8) proved that there are only six minimal surfaces spanned by straight-edged quadrilaterals from which IPMS can be constructed. In all of these six examples, the edges of the quadrilaterals are either cube edges or cube face diagonals. While there is an infinite number of polygons of any higher order, including pentagons, which bound minimal surfaces from which IPMS can be constructed, *the number of pentagons is restricted to eight, if only IPMS having non-cubic Bravais lattices are allowed*. These correspond to the eight ways of constructing pentagons from the edges of any of four triangular (right) prisms. The triangle faces of these prisms are:

(a) 30° - 60° - 90°

(b) 60° - 60° - 60°

(c) 120° - 30° - 30°

(d) 90° - 45° - 45°

XI. A NON-ORIENTABLE IPMS

A non-orientable IPMS has been constructed in which self-intersections occur only along the branch lines, associated with simple branch points, of the skew-hexagram-like faces of which it is composed. A single fundamental region of this surface is shown in Figure 15. The Bravais lattice of this surface is P (primitive cubic). The elementary skew polygon which is a fundamental region for the group of two-fold rotational isometries of the surface is a pentagon; 48 such pentagonal faces are contained in a single fundamental region of the surface. A representative pentagonal face has consecutive vertices at the positions (0 0 0), (- 1 0 1), (- 1 1 2), (- 1 4 - 1), and (0 4 0).

This surface partitions R_3 into two directly congruent labyrinths, for either of which the skeletal graph may be described as a symmetric graph of degree three which is homeomorphic to the *Laves graph* of degree three (ref. 13), but which is more specifically described, metrically, as being derived from the diamond graph by symmetrically removing a single edge from the set of four edges incident at each vertex.

The non-orientable character of this surface is easily verified by identifying an appropriate closed path along six contiguous pentagonal faces. As is clearly shown by a stereo-

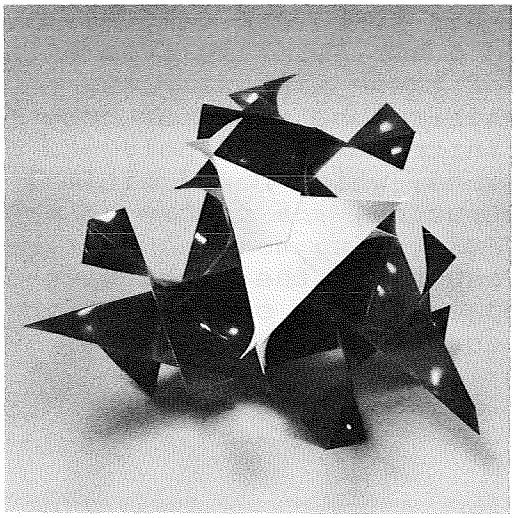

a. View along (111) axis.

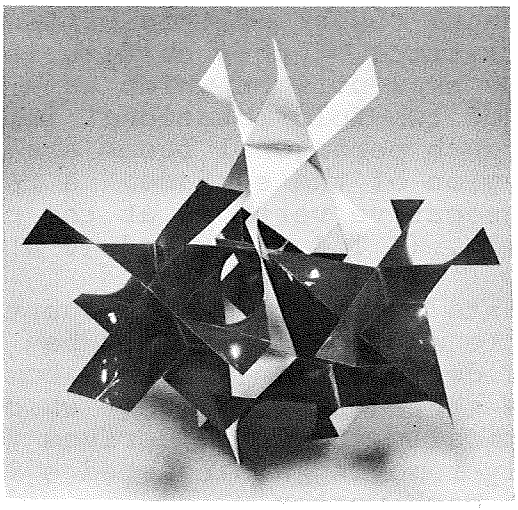

b. View along (110) axis.

Figure 15.- A *non-orientable* infinite periodic minimal surface. Shown here is a single lattice fundamental region.

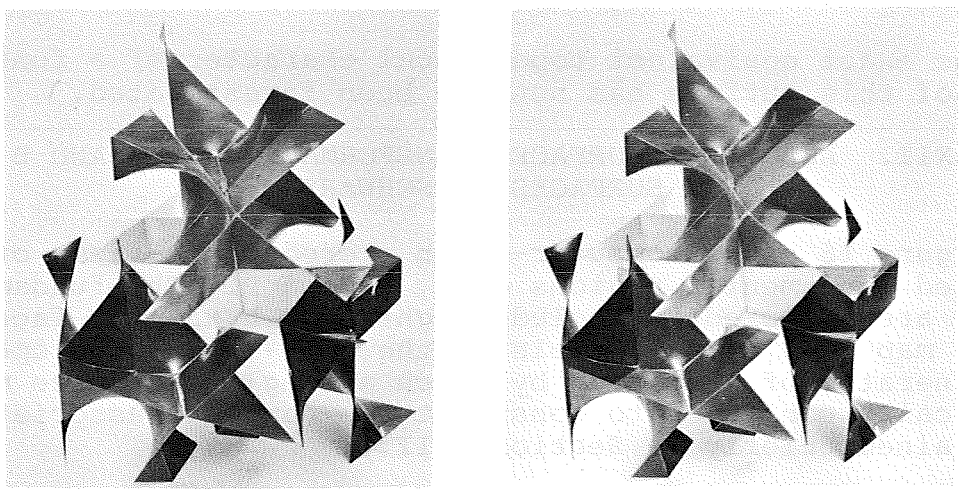

c. Right-left stereoscopic views of *non-orientable* surface.

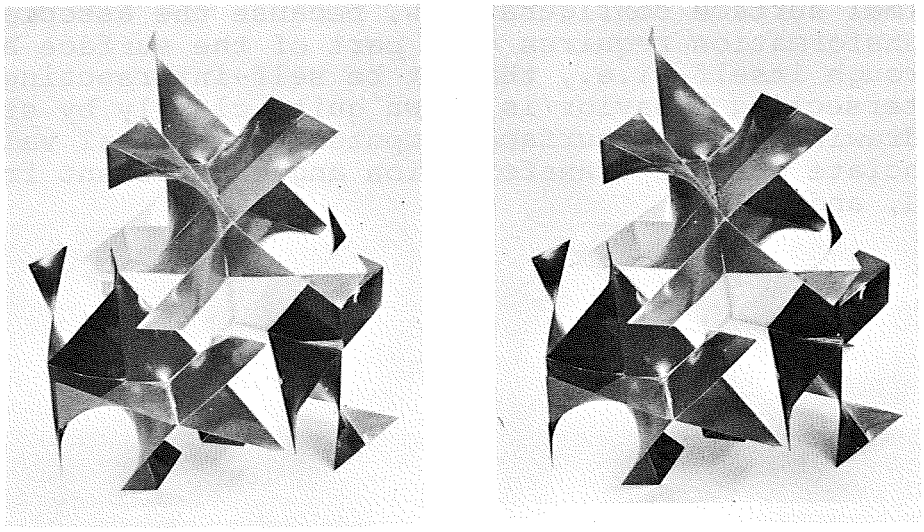

d. Left-right stereoscopic views of *non-orientable* surface.

Figure 15.- Concluded.

graphic projection of the Gauss map for these six faces, the normal to the surface is defined at any point with the ambiguity proper to a non-orientable surface.

The exact equivalent topological character of a fundamental region of this surface has not yet been investigated.

XII. ASSOCIATE SURFACE TRANSFORMATION OF P AND D SURFACES OF SCHWARZ

Figure 16 shows computer-drawn stereoscopic views of simply-connected fundamental regions of D, G, and P. The fundamental regions are selected to include eight skew hexagonal faces of the regular map $\{6,4|4\}$. The role of the four-fold screw operator, as a generator of the group by which a single such face may be analytically continued to construct the complete associate IPMS, is explained briefly in Section VIII.

Using plastic models of the surfaces shown in Figure 16, one can literally bend each of these surfaces into either of the others. (The fundamental regions for G and for P require appropriate *cuts* in order to be simply-connected. The cut for G separates the hexagonal faces which have a common point near the top center of Figures 16b and 16e. The cut for P is along the approximately semi-circular arc which joins the upper-front pair of hexagonal faces to the upper-rear pair of hexagonal faces, in Figures 16c and 16f.) During much of this bending, it is necessary for the surface models to depart somewhat from the minimal surface configurations, because the associate surface transformation requires that part of the surface actually pass through itself, i.e., that it be self-intersecting. This self-intersecting behavior is shown quite clearly by stereoscopic drawings of the surface computed for several values of the associate surface transformation angle different from those for D, G, and P.

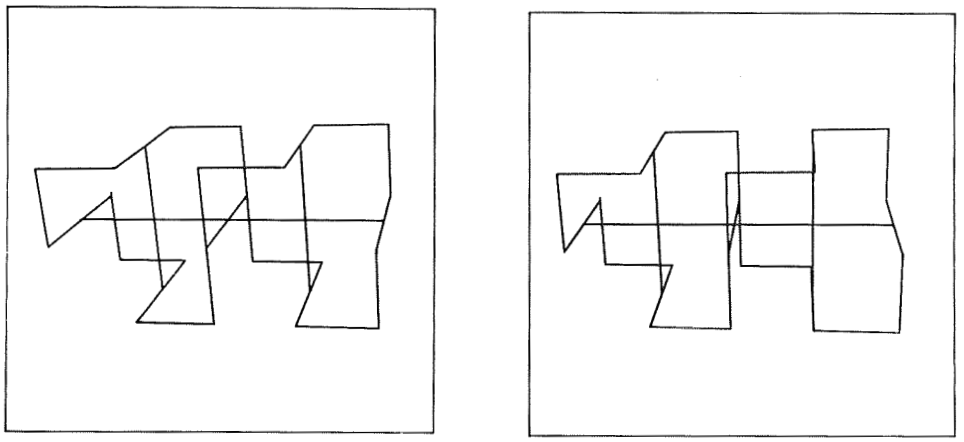

a. D

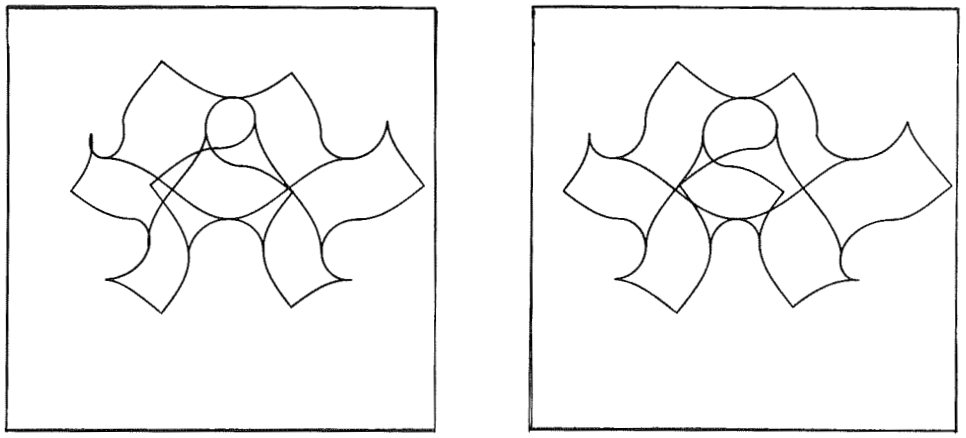

b. G

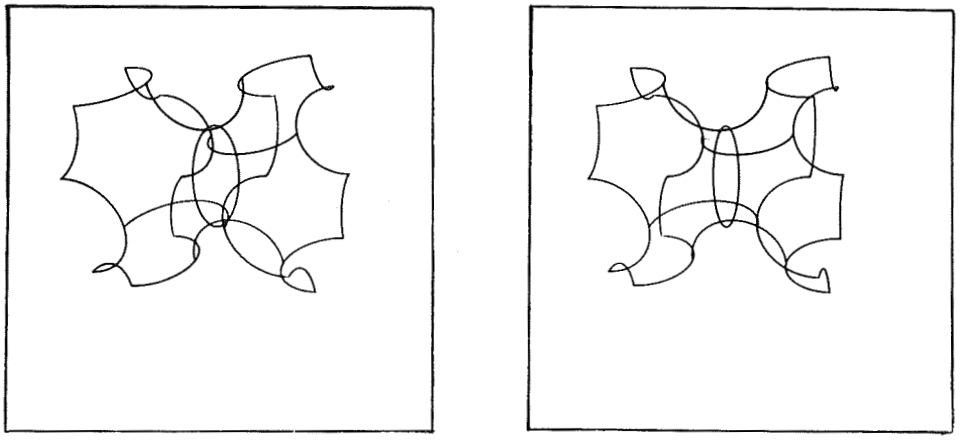

c. P

Figure 16.- Right-left stereoscopic views of fundamental regions of D, G, and P, respectively. The centroid of D is the fixed point; all other points of the fundamental region describe elliptical trajectories centered on the fixed point, throughout this bending transformation.

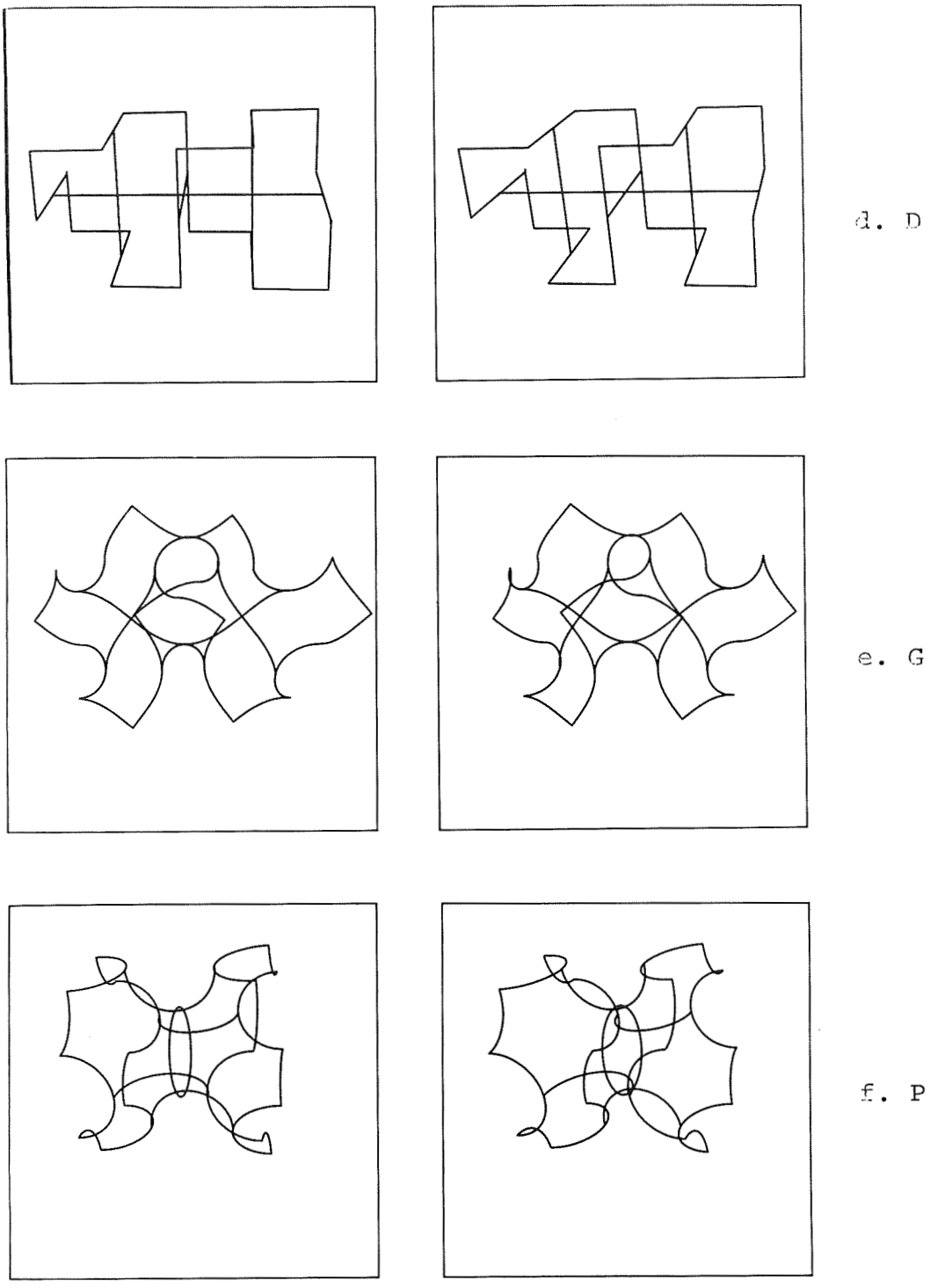

Figure 16.- Left-right stereoscopic views of the fundamental regions of D, G, and P, respectively. Concluded.

APPENDIX I

SOME ASPECTS OF BONNET'S ASSOCIATE SURFACE TRANSFORMATION, AND RELATED TOPICS

Any minimal surface M can be parametrized in the form

$$x = \mathrm{Re}\int (1 - u^2)F(u)\, du, \tag{1}$$

$$y = \mathrm{Re}\int i(1 + u^2)F(u)\, du, \tag{2}$$

$$z = \mathrm{Re}\int 2uF(u)\, du, \tag{3}$$

where $\hat{r}(u) \equiv [x(u), y(u), z(u)]$ is the position of a point on the surface, and $F(u)$ is any analytic function of the complex variable u.

If $F(u)$ is replaced in Eqs. (1-3) by the function $F(u) \exp(i\theta)$, where θ is an arbitrary real constant, then the resulting expressions for $\hat{r}(u)$ define the parametrization of a minimal surface *associate* to M. Each such associate surface can be obtained by bending M in such a way as to preserve the orientation of the tangent plane at every point of the surface. In particular, when $\theta = \pi/2$ or $-\pi/2$, the parametrized surface M^* is called the surface *adjoint* to M, with coordinates

$$x^* = \pm\, \mathrm{Re}\int i(1 - u^2)F(u)\, du, \tag{4}$$

$$y^* = \mp\, \mathrm{Re}\int (1 + u^2)F(u)\, du, \tag{5}$$

$$z^* = \pm\, \mathrm{Re}\int 2iuF(u)\, du; \tag{6}$$

the choice between upper and lower signs in Eqs. (4-6) corresponds to the choice between $\theta = \pi/2$ and $\theta = -\pi/2$, respectively.

For arbitrary values of θ, the coordinates of the associate surface can be written

$$x(\theta) = x \cos\theta + x^* \sin\theta, \tag{7}$$

$$y(\theta) = y \cos\theta + y^* \sin\theta, \tag{8}$$

$$z(\theta) = z \cos\theta + z^* \sin\theta, \tag{9}$$

if the first choice of signs is made in Eqs. (4-6). Eqs. (7-9) show that as θ varies, the origin remains fixed, and every point of the surface describes an ellipse whose center is this fixed point.

Schwarz's collected works (ref. 1) include a brief note by E. E. Kummer, who described a minimal surface bounded by the four planes of a tetrahedron (*tetragonal disphenoid*) which is one of the seven kaleidoscopic cells listed in Section IV of this note. This minimal surface, which is illustrated by a drawing (ref. 1), is described as a portion of Schwarz's primitive surface; it is adjoint to the surface bounded by a circuit of four edges (a Hamilton line) in a regular tetrahedron. This latter surface is a face, bounded by *linear asymptotics*, of the regular map $\{4,6|4\}$ on D. The orthogonal relationship between the boundaries of these two quadrilateral surface modules provides an illustration of the following lemmas concerning properties of adjoint minimal surfaces (proofs are given in ref. 11):

Lemma (1) The asymptotic lines on either of two adjoint minimal surfaces correspond to the lines of curvature on the other surface;

Lemma (2) On two adjoint minimal surfaces, at corresponding points P and P^*, the tangents to corresponding curves are perpendicular.

It follows immediately from Lemmas (1) and (2) that

Lemma (3) If the *asymptotic* C on a minimal surface M is a *straight line*, then its image C^* on the adjoint surface M^* is a *line of curvature* lying in a *plane* f which is perpendicular to C.

Furthermore, using Lemma (3) and also the fact that the tangent planes at P and P^* are parallel, we have the following Lemma:

Lemma (4) Consider two adjoint minimal surfaces M and M^*. If P is any point of a linear asymptotic C on M, and P^* is the image of P on the plane line of curvature, C^*, which is the image of C on M^* and which lies in the plane f, then the tangent plane to M^* at P^* is perpendicular to f; hence M^* meets f perpendicularly everywhere along its length.

(H. Blaine Lawson, Jr.* has used complex analysis to prove Lemmas (3) and (4), together with a generalization of these results which applies to conjugate minimal surfaces embedded in

*Private communication

the Euclidean 3-sphere; he has also treated the related problem of the construction of surfaces of constant mean curvature in Euclidean 3-space.)

We will now make use of a theorem of Weierstrass, which — combined with Lemma (4) — serves as the basis for the algorithm (treated in Section V of this note) for constructing minimal surfaces which are fundamental regions for groups of reflections. Such surfaces do not necessarily contain any straight lines. Weierstrass (ref. 1) proved the following results:

Lemma (5) Every straight line lying on a minimal surface M is an axis of two-fold rotational symmetry of the minimal surface M which results from analytic continuation of M;

Lemma (6) If a plane curve lies in a minimal surface M, and the angle formed by the intersection of the plane of this curve and the tangent plane of the surface along the curve is a right angle everywhere along the curve, then the plane of the curve is a *plane of reflection symmetry* for the minimal surface M which is obtained by analytic continuation of M.

Lemmas (3) - (6) provide the basis for deriving examples of IPMS, including cases which apparently were not previously recognized. The mathematical basis for the surface construction algorithm will now be discussed in further detail.

Let W_α be any straight-edged skew polygon with directed edges $\hat{U}_1, \hat{U}_2, \ldots, \hat{U}_m$. These edges form a closed circuit, according to the sequence $\hat{U}_1, \hat{U}_2, \ldots, \hat{U}_m$; hence

$$\sum_{r=1}^{m} \hat{U}_r = 0. \tag{10}$$

Assume that there exists a plane on which W_α has a parallel or central projection which is a simply covered convex curve; this property (ref. 17) is sufficient to guarantee that there exists a unique minimal surface, M_α, which spans W_α. (No loss of generality results from making this restriction, because for each of the cases of intersection-free IPMS which can be derived by application of the construction algorithm, the polygon W_α, which forms the boundary of the adjoint surface M_α, has this convex projection property. For other examples of intersection-free IPMS, for which the surface module M_α^* bounded by the faces of a kaleidoscopic cell has more than one bounding arc on at least one face of the cell, the convex projection property does not always hold for W_α. Furthermore, the polygon W_α in each of these latter cases is not a circuit of edges of a polyhedron

which is of the same type as the kaleidoscopic cell, in contrast to the examples which follow from the algorithm. For all of these more complex examples, nevertheless, it appears that M_α is unique. The present discussion will be confined to the cases derivable from the construction algorithm; similar considerations apply to the other cases, but these will not be described further in this note.)

If M_α^* is the surface adjoint to M_α, then from Lemma (3) it follows that the adjoint image of each directed edge $\hat{U}_r$ of M_α is a plane line of curvature $C_{\alpha,r}$ in M_α^*, lying in a plane perpendicular to $\hat{U}_r$. Consider any two consecutive edges $\hat{U}_r$, $\hat{U}_{r+1}$ of M_α, and their respective images $C_{\alpha,r}$, $C_{\alpha,r+1}$ in M_α^*. $C_{\alpha,r}$ and $C_{\alpha,r+1}$ lie in planes f_r and f_{r+1}, respectively, where f_r is perpendicular to $\hat{U}_r$, and f_{r+1} is perpendicular to $\hat{U}_{r+1}$. Let the *positive* side of f_r be defined as the side from which the normal vector $\hat{U}_r$ is directed *outward*, the same sign convention applying also to the planes orthogonal to the remaining edges of W_α. Then, from the preceding results, making use of the fact that M_α and M_α^* are orientable simply-connected surfaces, it follows that there are two possibilities for the location of that portion of M_α^* which is bounded by $C_{\alpha,r}$ and $C_{\alpha,r+1}$, with respect to the four distinct regions of space formed by the intersection of the boundary planes f_r and f_{r+1}: either this portion of M_α^* lies in the region bounded by the *positive* sides of both f_r and f_{r+1}, or else it lies in the region bounded by the *negative* sides of both f_r and f_{r+1}. By applying this argument to all of the pairs of adjacent edges of W_α, it is found that *M_α^* may be constructed so as to lie either on the positive side of every one of its boundary planes, or else on the negative side of every one of its boundary planes*. These two cases correspond, respectively, to two specimens of M_α^* which are related to each other by inversion; thus, each specimen is a mirror image of the other. They are associated with the values $\theta = \pi/2$ and $\theta = -\pi/2$, respectively, in Eqs. (4-6).

If W_α is derived from a kaleidoscopic cell Π, according to the procedure described in the algorithm at the beginning of Section V, then the adjoint minimal surface M_α^* is bounded by arcs $C_{\alpha,r}$ lying in the planes f_r of a convex polyhedron which is a kaleidoscopic cell Π^* of the same type as Π, but with proportions which are determined by the relative lengths of the edges $\hat{U}_r$ of W_α. If Π is one of the three tetrahedral cells described in Section IV, then Π and Π^* are congruent, because Eq. (1) is satisfied for only one set of relative lengths of the $\hat{U}_r$ for the case of tetrahedra. For the four non-tetrahedral cells, the proportions of Π depend on the relative lengths of the $\hat{U}_r$ in the way described in Section V.

The *existence* of a periodic minimal surface M_α derived from M_α^* as fundamental region is guaranteed by the fact that the group of reflections for Π^* is the same as the group of reflections for M_α^*; this result follows from Lemma (6), since all of the boundary arcs $C_{\alpha,r}$ of M_α^* lie in faces of Π^*. The *absence of self-intersections* in M_α, on the other hand, requires also that there be no "extended loops" among the boundary arcs $C_{\alpha,r}$ of M_α^*, as mentioned in Section V. Each vertex of M_α^* is constrained to lie in the surface of the corresponding cell Π^*, in fact, along an edge of Π^*; however, the possibility that a given arc $C_{\alpha,r}$ may form an "extended loop", i.e., the possibility that a portion of $C_{\alpha,r}$ lies outside of Π^*, can be excluded only by detailed investigation. By making use of lemma (4) and also of the bounds on the orientation of the normal vector along the boundary of M_α (and, therefore, also of M_α^*) which are implied by the fact that *a minimal surface is wholly contained in the convex hull of its boundary curve* (ref. 17), it can be proved that the arcs $C_{\alpha,r}$ do not form extended loops in *most* of the faces of each M_α^* which is generated by using the construction algorithm of Section V. However, aside from the five examples P, D, C(P), H, and CLP, which are already known (from the work of Schwarz and of Neovius) to be intersection-free, H'-T is the only other case, among the eleven surfaces generated from this algorithm, for which it is possible to prove, using only these boundary normal vector arguments, that *all* of the arcs $C_{\alpha,r}$ of M_α^* are free of extended loops, and – therefore – that M_α^* is free of intersections. In each of the remaining five cases, rigorous proof of the absence of self-intersections would require that the complete analytic solution for the surface be obtained. C(D) is easily shown to be intersection-free by using the convex hull argument cited above.

For each of the three surfaces C(H), O,C-TO, and g-g', the number of boundary arcs $C_{\alpha,r}$ is greater than the number of faces of the cell Π^*; arguments based on the preceding discussion and on certain continuity properties may be used to prove the *existence* of a surface module which is a fundamental region of the group of reflections for each of these surfaces. However, not all of the bounding arcs of any of these surface modules have been shown to be free of an extended loop, aside from the evidence provided by the experimental construction of soap film models of surface modules inside kaleidoscopic cells. Thus, although it has been rigorously proved that for each of these examples, there exists a set of relations among the relative lengths of the edges of a polygon W_α, spanned by the adjoint surface M_α, for which the planes of the boundary curves lying in parallel planes *coalesce*, it is still necessary – in the absence of other evidence – to rely on soap film models of M_α^* for evidence that *all* of the boundary arcs are free of "extended loops". Just as in the case of modules M_α^* having only *one* boundary arc per face of Π^*, it is found that plastic models of

M_α^* modules derived from the shapes of these soap films may be satisfactorily bent to produce models of adjoint surface modules M_α, whose boundary curves closely approximate straight line segments, viz., the edges of the polygon W_α.

The relation between the existence of a minimal surface M_α^*, bounded by the faces of a kaleidoscopic cell, and the stability properties of a soap film model of such a surface will be discussed in detail in a future publication*. In brief, Schwarz found that the second variation of the area of such a surface is not positive; this property is related to the fact that a soap film model of such a surface is in unstable equilibrium, when the film is "freely" bounded by the faces of the enclosing kaleidoscopic cell. Experimental observation of such a film depends on the fact that the film is nearly stationary in its position of unstable equilibrium, i.e., in the position corresponding to the minimal surface configuration. When one or more straight line segments lie in the interior of such a surface, one or more fine wires can be strung inside the enclosing cell, coinciding with such segments, in order to prevent the soap film from moving away from its position of equilibrium. In some cases (e.g., H), the use of such a wire makes the film actually stationary, because it is in stable equilibrium. In other cases, where the equilibrium is unstable (e.g., C(H)), the film remains stationary for at least several seconds when a wire is used; without wires, it is extremely difficult to make such films remain stationary long enough to observe the detailed shape of their boundary curves, or even to verify experimentally that they exist in the form of minimal surfaces.

Another aspect of the question of the existence of intersection-free IPMS of specified form can be only briefly mentioned here. It concerns a picturesque method of constructing and classifying hypothetical examples of IPMS without self-intersections. The method is based on the examination of the shape and symmetry of assorted multiply-connected surfaces bounded by the interiors of convex polyhedra. Such polyhedra are either kaleidoscopic cells or symmetrical aggregates of kaleidoscopic cells. As an example, consider a spherical soap bubble with its center at the center of an enclosing cube; in what symmetrical ways can one blow out tubular holes in the bubble, so that the bubble is transformed into a *minimal* surface, with tubular projections, bounded by the interior surface of the cube? An analysis of some examples of IPMS mentioned in this note, according to this mode of description, leads to a classification in which the surfaces are distinguished according to the cube elements (faces, edges, or corners), or combination of cube elements, to which the tubules are attached.

*To be published

For example, the cube elements for five of the IPMS can be listed as follows:

F-RD	4 corners (tetrahedrally distributed)
I-WP	8 corners
C(P)	12 edges
P	6 faces
O,C-TO	6 faces and 8 corners

The principal advantage of this descriptive method is that from the standpoint of morphology, it is in some respects more convenient — paradoxically — to distinguish and classify examples of finite portions of intersection-free IPMS which are *multiply-connected*, instead of the simply-connected elementary modules into which they may be decomposed.

It is necessary to define what is meant by calling two intersection-free IPMS "distinct". Suppose M_1 and M_2 are non-congruent intersection-free IPMS. Let us calculate the genus of a lattice fundamental region for M_i; this lattice has a primitive cell of minimum volume, i.e., its translational symmetry group is the same as that of M_i. Let $p(M_i)$ denote the genus of M_i, and $G(M_i)$ the space group of M_i. Then we adopt the following convention:

1. If $p(M_1) \neq p(M_2)$, or $p(M_1) = p(M_2)$ and $G(M_1) \not\equiv G(M_2)$, then M_1 and M_2 will be regarded as distinct surfaces.

2. If $p(M_1) = p(M_2)$ and $G(M_1) \equiv G(M_2)$, then M_1 and M_2 will be regarded as the same surface.

This classification scheme is consistent with a classification based on the analytic properties of these surfaces. Schwarz briefly discussed (pp. 95-96 of ref. 1) the relation between the analytic and symmetry properties of surfaces derived from D by changing the altitude of a hexagonal module of D along one lattice axis. His examples include the Scherk surface, for which the coordinates may be given as

$$e^z = \cos x/\cos y;$$

in this case, the altitude of a hexagonal module of D is allowed to increase without limit.

It has been found from a detailed study of the examples listed in Table I that any two of the listed surfaces which have

the same genus, in the sense defined above, are globally homeomorphic by a deformation, i.e., by a biunique continuous topological transformation (no surface tearing). (Cf. the classical theorem: if two closed surfaces have the same genus, then either may be deformed into the other.) Thus, for example, any one of the five intersection-free IPMS of genus three — P,D, G,H, and CLP — can be deformed into any of the others. Schwarz (ref. 1) noted that P and D are related by a deformation: either surface may be constructed by joining replicas of a doubly-connected minimal surface which is bounded by two parallel congruent equilateral triangles; the two triangles are related by a 60° screw motion along their common axis. If the triangle separation in P is increased continuously until it reaches twice its original value, then the deformation of P into D is accomplished through a continuum of intermediate minimal surfaces. Thus, P and D are related by a deformation, which is topologically simpler but analytically more complicated than the adjoint transformation: dilatation or compression of the c-axis of the trigonal lattice of the general surface.* The deformations which relate most of the other pairs of IPMS of the same genus, among the examples listed in the Tables, involve more complicated changes of symmetry than the deformation relating P and D, and it is not known whether the mean curvature at every point of the surface can remain zero throughout all of these deformations. It is apparent that P and D are related to their tetragonal and orthorhombic analogs (cf. Table III) by deformations; these can be described loosely as dilatation or compression along one or two of the cube axes of the surface. These deformations preserve the minimal surface property.

The existence of these deformations relating IPMS of the same genus suggests that the concept of a dual pair of skeletal graphs as representatives of a given intersection-free IPMS must be interpreted cautiously. It is not true, for example, that the topological properties of the Laves graph, viz., that three edges meet at every vertex and that the smallest number of edges in any closed circuit of edges ("girth") is ten, correspond to a topologically fundamental property of the gyroid. The association between a pair of skeletal graphs and an IPMS should be viewed as primarily geometrical, in the sense that the symmetry (space group) is the same, and the topological properties are consistent. Thus, it is *topologically* just as reasonable to associate a pair of primitive cubic graphs or a pair of diamond graphs (with curved edges) with the two labyrinths of the gyroid (or those of H or CLP, for that matter) as it is to associate a pair of enantiomorphous Laves graphs with these labyrinths, but of these three kinds of graphs, only the Laves graphs have the *symmetry* of the

*Schwarz did not obtain a solution for the general minimal surface, bounded by two triangles, which is described here.

gyroid. A deformation of one intersection-free IPMS into another of the same genus can be represented by a continuous transformation of the skeletal graphs of the first into the corresponding skeletal graphs of the second. This graph transformation, which may be called elision, may be described by making use of the concept of the tubular graph associated with each skeletal graph (cf. p. 79). The surface deformation defines the deformation of the homeomorphic tubular graphs; the elision of the skeletal graphs may be inferred from these deformations. (In practice, it is usually easier to find a construction for the graph transformation first, and then describe the corresponding surface deformation.) Graph elision may add vertices and edges to the skeletal graph, or subtract them from the graph (hence the name elision). Two infinite periodic graphs are defined as *generically equivalent* if their respective tubular graphs have the same genus per lattice fundamental region. These elision transformations of graphs provide a simple method of describing the required deformations of the corresponding IPMS.

A special property of CLP should be noted: it is related to its adjoint surface by a deformation, and both surfaces have (in general) the same space group.

Some examples of intersection-free IPMS for which the smallest simply-connected surface module is a *straight-edged polygon* appear to have been omitted from Tables I-III. At least some of these omitted cases, however, may be obtained from listed examples of higher symmetry, simply by changing the relative scale lengths along the various lattice axes so as to eliminate one or more classes of two-fold rotational symmetry elements from the space group — and, therefore, one or more straight lines from the listed IPMS.

The question of whether lower-symmetry variants of a given intersection-free IPMS exist is too extensive to be treated thoroughly here. Nevertheless, it may be useful to make some general remarks on this subject. In many cases, the removal of symmetry elements from the space group of a given intersection-free IPMS by a suitable deformation makes it impossible to isolate a simply-connected surface module which is bounded either by line segments or by plane lines of curvature, or by both. In such cases, the existence of the hypothetical surface of lower symmetry depends on the existence of a finite *multiply*-connected minimal surface, and this question is in general a difficult one. The particularly interesting question of the possible existence of lower-symmetry variants of the gyroid is briefly discussed in Section VIII. The impossibility of obtaining a body-centered orthorhombic variant of the gyroid by bending a suitable orthorhombic variant of P or D suggests caution in speculating on the existence of variants of certain examples of minimal surfaces.

APPENDIX II

THE CONCEPT OF DUAL INFINITE PERIODIC GRAPHS, AND THE "PARTITIONING ALGORITHM" FOR THE CONSTRUCTION OF A DUAL GRAPH

INTRODUCTION

It is well known in the theory of graphs that the concept of *dual* graph is well-defined only for planar graphs. Recently (ref. 10), the author attempted to develop the idea of a dual relation which was restricted to certain types of three-dimensional periodic *non*-planar graphs, having straight edges, by making use of a concept described by P. Pearce: the *saddle polyhedron* (ref. 18). We will consider a saddle polyhedron to be any curved polyhedron, homeomorphic to the sphere, whose faces are minimal surfaces spanning skew polygon boundaries. Such polyhedra may have two-valent vertices, but they need not do so. The skewness of one or more faces of the polyhedron may vanish, in which case the face is plane. Both Pearce and the author have constructed a large variety of saddle polyhedra which fill space without voids, either singly (unary space-filling) or multiply (n-ary space-filling). Many examples of these polyhedra will be described and illustrated in a forthcoming book by Pearce (ref. 19).

The author of this note found that for each of the examples then known to him of infinite *symmetric* graphs (infinite periodic graphs, having the translational periodicity of a three-dimensional lattice, with symmetrically equivalent vertices and symmetrically equivalent edges) and also for a larger number of other infinite periodic graphs, an empirically developed algorithm made it possible to derive a unique *dual* graph. (*Unique* here means unique aside from deformations which leave the topology and space group of the graph unchanged.) The dual graph, in turn, when subjected to the construction specified in the algorithm, led back to the original graph, thereby meeting the minimum requirements of any reasonable notion of a dual relation, viz., that it be *symmetric*. Because of the *ad hoc* character of this dual graph algorithm, an effort was made to find a counterexample, i.e., an infinite symmetric graph for which the algorithm leads either to an ambiguous result, or to no result at all! Before such a counterexample was found, the algorithm was described in a published abstract (ref. 10) in its original form. An "improvement" in the algorithm was then made, and it is this "improved" version of the algorithm which is given below. The saddle polyhedron is the device whose construction according to this algorithm underlies the dual

graph relation. This algorithm will hereafter be called the *partitioning algorithm*.

After continued investigation of many examples of both infinite symmetric graphs and also other infinite periodic graphs, the author found an example of an infinite symmetric graph for which the partitioning algorithm failed to generate any dual graph. (A close study of this example led to the discovery of the gyroid, which is described in Section VIII of this note.) As a result of this failure of the algorithm, the class of graphs considered subjects for the algorithm was slightly restricted (see next subsection) so as to eliminate the offending graph from consideration! This is an awkward solution to the problem, especially since the algorithm performs quite satisfactorily for a large number of infinite graphs which are merely periodic, but not symmetric. In any event, this aspect of the case illustrates the basic difficulty of attempting to construct a satisfactory dual graph relation by using admittedly *ad hoc* methods, not derived from first principles.

The "improved" form of the partitioning algorithm is summarized below, for whatever intrinsic interest it may have. The algorithm appears thus far to serve a useful purpose by providing the basis for a self-consistent description of the dual skeletal graphs for the two labyrinths of every one of the intersection-free IPMS mentioned in this note (see Section III).

The essential idea of the partitioning algorithm is the following: for at least many examples of infinite symmetric graphs — and also for many examples of infinite graphs which are merely periodic but not symmetric — *one can associate with each vertex of the graph a unique saddle polyhedron which contains the vertex in its interior, and which has the same number of faces as the number of edges incident at the vertex; furthermore, each of these faces is penetrated at a single interior point by one of these edges*. This saddle polyhedron is called a *symmetry domain* of the vertex. The edges of a space-filling assembly of all the symmetry domains associated with a given graph define a second periodic graph, the dual graph. Even when the original graph is a symmetric graph, the second graph is not necessarily a symmetric graph, i.e., it may have inequivalent edges and/or inequivalent vertices. It is assumed throughout this discussion that the edges of an infinite periodic graph are line segments, and that every vertex of such a graph has at least three incident edges.

For some examples of infinite symmetric graphs, the *Voronoi polyhedron** associated with a given vertex of the original graph (i.e., the polyhedron which consists of all the points which are as near to the given vertex as to any other vertex) does have the property of having exactly as many faces as the number of edges incident at the graph vertex in its interior. More often, however, the Voronoi polyhedron has additional faces; these extra faces are produced by the truncating effects of other nearby vertices in the graph, i.e., vertices which are not joined by edges to the given vertex. No method is known for constructing any *other* convex polyhedron — for an arbitrary infinite symmetric graph G — which exhibits a one-to-one correspondence between its faces and the edges incident at each vertex of G.

The study of Voronoi polyhedra for a large number of different examples of infinite periodic graphs has led to the discovery, by the author, of examples of 17-, 18-, and 20-faced convex polyhedra which form unary space-fillings. In fact, infinite families of 17- and 20-faced convex polyhedra of this type have been found, by constructing the Voronoi polyhedron for the vertices of certain infinite symmetric graphs which are subjected to a kind of homogeneous "collapsing" transformation (refs. 21,22). In this transformation, the topology of the graph is preserved, and the graph remains symmetric throughout the transformation, but the geometrical character of the graph changes continuously. A detailed analysis of examples of this transformation will be included in a future report.** Voronoi proved that for convex *parallelohedra* in R^3, the maximum possible number of faces is 14†; the corresponding upper limit is not known for the more general case, where it is not required that the polyhedra be parallelohedra, i.e., that they be equivalent under translation.

The algorithm for the construction of symmetry domains for a given infinite periodic graph requires, first, that saddle polyhedra, called *interstitial domains*, be constructed. The boundaries of the faces of these interstitial domains are circuits of edges of the original graph, chosen according to

---

*Voronoi applied this polyhedron construction to the points of a lattice, not to the points of a *regular system*, which is an array of points in R^3 which are symmetrically equivalent under some more general symmetry element of the full space group than a lattice translation (see ref. 20). *Voronoi polyhedron* is simply another name for *Dirichlet cell* (cf. Section VIII).

**To be published

†Voronoi showed that this number is $2(2^n-1)$ in R^n (see ref. 23).

a recipe given in the next subsection. Next, a vertex of the dual graph is constructed in the interior of each interstitial domain; the rule for choosing the position of this dual graph vertex is also given in the next subsection. Then these dual graph vertices are joined in pairs by edges, each such vertex being connected only to those in the interior of *adjacent* interstitial domains. Finally, the faces of the symmetry domains are chosen by the same rule as the one, given in the next subsection, which governed the initial construction of the faces of the interstitial domains.

The interstitial domains are so named because they occupy the interstices of the original graph. The naming of the symmetry domains derives from the fact that they have the same point-group symmetry as does the infinite graph itself, with respect to the graph vertex in the interior of a single symmetry domain. Because of the dual relation between the two graphs underlying this construction, the saddle polyhedra which are *interstitial domains* with respect to the original graph are *symmetry domains* of the dual graph, and the saddle polyhedra which are *interstitial domains* of the dual graph are *symmetry domains* of the original graph.

Before describing the partitioning algorithm in detail, it should be explained that the duality relationship between the two skeletal graphs of an intersection-free IPMS is based also on the following construction: Assume that the skeletal graph is given for one labyrinth of a particular intersection-free IPMS. Let each edge of the skeletal graph be replaced by a thin open tube, and let these tubes be smoothly joined (without intersections) around each vertex so that the whole *tubular graph* forms a single infinitely multiply-connected surface, which contains the skeletal graph in its interior. Such a tubular graph is globally homeomorphic to the corresponding minimal surface. If the tubular graph is sufficiently "inflated", it becomes deformed into a *dual* tubular graph which contains in its interior the skeletal graph of the other labyrinth of the surface. The "outside" of the first tubular graph is the "inside" of the second tubular graph. The two skeletal graphs for a given IPMS are required to have the same space group as the IPMS, and to correspond, respectively, to two tubular graphs which are globally homeomorphic to the IPMS.

This prescription for deriving a skeletal graph from its dual graph gives the same result, for all the known examples of intersection-free IPMS, as the partitioning algorithm. In spite of the fact that the tubular graph construction is less complicated to describe than the partitioning algorithm, it is probably somewhat easier to apply the partitioning algorithm

to actual examples. Neither construction has a rigorous foundation; furthermore, the whole concept of dual periodic graphs is not essential to the development of the theory of intersection-free IPMS. However, the underlying idea of dual skeletal graphs provides a unified basis for an abstract "morphological" description of all presently known examples of intersection-free IPMS. Furthermore, as already mentioned in Sections III and VI, the skeletal graph is a convenient device for suggesting hypothetical examples of intersection-free IPMS and also of infinite periodic surfaces of non-zero constant mean curvature.

The above description of the duality relationship between two skeletal graphs shows that whenever one of the graphs has an intrinsic *handedness* (cf. a Laves graph in either labyrinth of the gyroid), the other graph must have the opposite handedness, on account of the *eversive* character of the transformation which expresses the duality.

ALGORITHM FOR THE CONSTRUCTION OF AN INFINITE PERIODIC GRAPH WHICH IS THE DUAL OF A GIVEN INFINITE SYMMETRIC GRAPH *("PARTITIONING ALGORITHM")*

1. Consider any infinite graph G, having straight edges, which has the following properties:

   a. All edges of G are symmetrically equivalent, i.e., there exists an element of the space group of G which is transitive on the edges.

   b. All vertices of G are symmetrically equivalent, i.e., there exists an element of the space group of G which is transitive on the vertices.

   c. Each vertex of G is joined by an edge to every one of the Z nearest neighbor vertices (the graph is described as being of *maximum degree* with respect to the vertices).

   d. Each vertex lies at the centroid of the positions of the Z nearest neighbor vertices (the graph is described as being *locally centered*).

2. Consider any circuit of edges K_i which forms a simply-connected closed curve (no self-intersections) having a convex central or parallel projection. (This property of K_i insures that there exists a *unique* minimal surface spanning K_i.) Span K_i by the minimal surface $S(K_i)$, and also span every image of K_i, $I_j(K_i)$, i.e., every symmetrically equivalent replica of K_i, by a minimal surface $S[I_j(K_i)]$. Determine whether there exist any two images of K_i — say, $I_\ell(K_i)$ and $I_m(K_i)$ — for which the minimal

surfaces $S[I_\ell(K_i)]$ and $S[I_m(K_i)]$ intersect along a curve not made up of edges of G which are common to the boundaries of $I_\ell(K_i)$ and $I_m(K_i)$. (Such a non-boundary-edge curve is called a *disallowed intersection curve*.) If no such image pairs exist, then K_i is described as a *non-self-intersecting polygon* $K_i^{\dagger}$.

3. For every non-self-intersecting polygon $K_i^{\dagger}$, determine whether there exists any other non-self-intersecting polygon $K_j^{\dagger} \neq I(K_i^{\dagger})$ with at least one image $I_r(K_j^{\dagger})$ such that $S(K_i^{\dagger})$ and $S[I_r(K_j^{\dagger})]$ intersect along a disallowed intersection curve. If no such polygon $K_j^{\dagger}$ exists, then $K_i^{\dagger}$ is described as a *non-intersecting polygon* $K_i^{\dagger\dagger}$.

4. For every $K_i^{\dagger\dagger}$, span all images of $K_i^{\dagger\dagger}$, $I_j(K_i^{\dagger\dagger})$, with minimal surfaces $S[I_j(K_i^{\dagger\dagger})]$.

R^3 is now partitioned by a n-ary assembly of finite closed cells, i.e., by finite closed cells having n symmetrically inequivalent forms.

5. Remove all minimal surfaces $S'(K_t^{\dagger\dagger})$, together with all images of $S'(K_t^{\dagger\dagger})$, $I[S'(K_t^{\dagger\dagger})]$, whose omission merely leads to a reduction in the total number of closed finite cells which partition any given "large" finite portion of R^3 (*large* means large with respect to the dimensions of a lattice fundamental region). *The resulting cells are the interstitial domains of the graph G.*

6. Construct a vertex $\overline{V}$ in the interior of each interstitial domain of G. The position of $\overline{V}$ is determined by the following rule: the point group of the union of $\overline{V}$ with the interstitial domain in which it lies is the same as the point group of the interstitial domain itself.

7. Join each vertex $\overline{V}_r$ by an edge $\overline{E}_{rj}$ to the vertices $\overline{V}_j$ in each of the interstitial domains adjacent to the r^{th} domain (the one which contains $\overline{V}_r$); these adjacent interstitial domains are those which have a face S_{rj} in common with the r^{th} domain.

The graph $\overline{G}$ of vertices $\overline{V}$ and edges $\overline{E}$ is defined as the graph dual to G.

8. Apply steps 1-5 to the graph $\overline{G}$. The resulting cells partition R^3 into congruent saddle polyhedra, which are the *symmetry domains* of G.

DISCUSSION

Among infinite symmetric graphs of maximum degree, no examples have been found for which the partitioning algorithm fails to generate an unambiguous dual graph. More than twenty

examples of infinite symmetric graphs have been studied; not all of these graphs can be shown to be skeletal graphs of intersection-free IPMS. In addition, a much larger number of infinite graphs which are periodic but not symmetric have been studied and found to yield unambiguous dual graph results. Nevertheless, it has so far not been possible to establish the partitioning algorithm on a rigorous basis. The minimal surface as a boundary-spanning device should be regarded as a useful "convenience."

An example of a graph which would be considered a counter-example to the partitioning algorithm, if the restriction had not been made to allow only infinite symmetric graphs *of maximum degree*, is the infinite periodic graph whose vertices are those of the regular map $\{4,6|4\}$ on the gyroid (see Section VIII), and whose edges are line segments (instead of the curved geodesics of this regular map embedded in G). This graph can be regarded as a "defective" graph (i.e., a graph of less than maximum degree) on the points (vertices) of a *body-centered cubic lattice*; two of the eight edges of the "standard" b.c.c. graph, in which each vertex is joined by an edge to its eight nearest neighbor vertices, are omitted at each vertex of this graph. When an attempt is made to apply the dual graph algorithm to this case, it is found that after step 4 is carried out, R^3 is partitioned into two *infinite* cells, which are homeomorphic, respectively, to the two labyrinths of the gyroid. The algorithm cannot be applied further, in this case, to yield a construction for a symmetry domain. However, a saddle polyhedron has been found which exhibits the essential property of a symmetry domain for this graph of degree six: it is a unary space-filler, it has six faces, and it has the same point group isometries as the graph, with respect to its centroid. This figure was constructed by essentially trial and error methods. It can be generated by an appropriate superposition of the non-orientable IPMS, shown in Figure 15, on its enantiomorphous image; such a superposition of enantiomorphous surfaces partitions R^3 into an infinite periodic assembly of these six-faced cells. The Voronoi polyhedron for a vertex of this graph is the *truncated octahedron*, with fourteen faces. Moreover, the symmetry domain for the symmetric graph of degree eight (maximum degree) on the vertices of this graph is a saddle polyhedron (the "*expanded octahedron*") with eight faces, each of which is congruent to a face of the regular map $\{6,4|4\}$ on the Schwarz surface D (Figure 1).

A second "defective" infinite symmetric graph, which is also locally-centered, is a graph of degree six on the vertices of a *face-centered cubic lattice*. This graph, when constructed with straight edges, can be embedded in either P or D (see Section VII). Application of the partitioning algorithm to this example is straightforward and yields a (non-symmetric) dual graph of degree ten.

Finally, a third infinite symmetric graph which is not of maximum degree and is not locally-centered is a graph of degree three on the vertices of a *simple cubic lattice*. This graph is homeomorphic to the Laves graph of degree three (see Section VIII and ref. 13), and the partitioning algorithm leads to results similar to those obtained for the Laves graph: the symmetry domains and interstitial domains are enantiomorphous (a saddle trihedron, each face being a non-regular skew decagon), and the graph and its dual are also enantiomorphous.

These few special examples have been described in order to illustrate the extremely varied properties of infinite symmetric graphs, when they are viewed in the context of the partitioning algorithm. As a further example, consider the saddle polyhedra, shown in Figures 4e and 8c, which are both symmetry domains and interstitial domains for the self-dual skeletal graphs of C(P) and C(D), respectively. These graphs, which are periodic but not symmetric, can be derived by an elementary construction based on the polyhedra which are both symmetry and interstitial domains for the self-dual skeletal graphs of the respective complementary surfaces, P and D. These latter symmetry domains are the *cube* (skeletal graph of P) and the *expanded tetrahedron*, a saddle polyhedron having four regular skew hexagonal faces, with face angles $\theta = \cos^{-1}(-1/3)$ (skeletal graph of D); thus, the skeletal graph for P or D is comprised of the edges of a honeycomb of cubes or expanded tetrahedra, respectively. The skeletal graph for the surface complementary to P or D can also be formed from the same honeycomb as for P or D itself, as follows: join every vertex V of the honeycomb by a straight edge to each of the vertices obtained by inversion of V in the centers of the incident faces of the honeycomb. The simplicity of these rules for P, D, C(P), and C(D) is paralleled by an algorithm (ref. 6) for the construction of C(P) and C(D), based on the theory of Petrie polygons for reflexive regular maps (ref. 7).

A detailed description of the symmetry domains and interstitial domains for the two skeletal graphs of the other IPMS listed in Table I will be provided in a detailed report*, which will also include other examples of applications of the partitioning algorithm.

Coxeter (ref. 24) has described the "reciprocal" relations between packings of regular and uniform convex polyhedra. The application of the partitioning algorithm to each of these examples of packings leads to exactly the results described by Coxeter. The partitioning algorithm, moreover, always leads to the Voronoi polyhedron as the symmetry domain for any infinite symmetric graph *whenever the number of faces of the Voronoi polyhedron is equal to the degree of the graph* (ref. 10).

---

*To be published

The application of the partitioning algorithm to specific examples of infinite periodic graphs leads to the construction of a great variety of skew polygons. The edges of such skew polygons do not always coincide with symmetry axes of any space group, even when the graph is symmetric (it was erroneously stated by the author in ref. 10 that this coincidence always occurs for symmetric graphs). If every one of the edges of a given skew polygon lies along a two-fold axis of some space group, then the polygon is a module for an IPMS. If some or all of the edges of a given skew polygon coincide with *three*-fold axes of some space group, any remaining edges being coincident with two-fold axes of the same group, then the polygon can be used as a module for a periodic *integral varifold*, in which three modules intersect along the edges which correspond to three-fold axes. An example of such an integral varifold was first described to the author by Dennis Johnson*; in this case, which is based on the pentagonal module of the surface which is adjoint to Schwarz's H surface (cf. Fig. 5), the integral varifold partitions R^3 into *three* infinite congruent interpenetrating labyrinths. The three-fold intersections occur here along the two parallel edges of each elementary Flächenstück. An example of an integral varifold which partitions R^3 into *four* infinite congruent interpenetrating labyrinths may be derived from the symmetry domain of the defective f.c.c. graph of degree six, which was first mentioned at the end of Section VII. If a unary honeycomb is constructed from an infinite assembly of these "six-pointed starfish" polyhedra, and then all of the quadrilateral faces which are directly congruent to a given single face are removed, the four-labyrinth varifold remains. The original honeycomb is a superposition of two enantiomorphous varifolds of this type. The skeletal graphs** of each of the four labyrinths of this integral varifold are directly congruent Laves graphs of degree three (ref. 13).

The two examples of periodic integral varifolds described in the preceding paragraph, as well as other examples which have been constructed, have the same kinds of equiangular intersections of lamellae and of edges as soap froths of finite cells (cf. Section VIII). Some of these other examples partition R^3

*Private communication

**The concept of skeletal graph is extended to include such examples as this, in which the labyrinth envelope has a singularity along each three-fold intersection of surface modules. The homeomorphism between the tubular graph, derived from a given skeletal graph, and the labyrinth envelope is similar to the case of intersection-free IPMS.

into an infinite number of *infinite* domains. These infinite domains, however, are not labyrinthine in the sense defined here, i.e., they do not have the periodicity of a three-dimensional lattice; instead, the envelope of each such domain is deformable into a cylinder of finite radius and infinite length.

If an IPMS generated from a straight-edged module is self-intersecting, the self-intersections may occur either along the edges of the modules, or else along curves interior to each module as well as along the edges. The Neovius surface adjoint to C(P) and the surface adjoint to I-WP are examples of IPMS in which the self-intersections occur *only* along module edges; these surfaces partition R^3 into infinite assemblies of finite closed cells (saddle polyhedra). Another example of such a surface is the assembly of interstitial or symmetry domains for the Laves graph of degree three. In this case, the elementary surface module is a skew pentagon; four such pentagons join smoothly to form a single skew decagon face of the trihedral interstitial (or symmetry) domain of the Laves graph. The surface adjoint to F-RD, on the other hand, is an example of an IPMS in which the self-intersections occur both along module edges and also along curves in the interior of each module; here also, R^3 is partitioned into finite closed cells by the IPMS.

In Figure II-1 is shown an example of the collapsing transformation on an infinite symmetric graph — the Laves graph of degree three. Figure II-2 shows several examples of Voronoi polyhedra of symmetric graphs. The polyhedron appearing in Figure II-2a is the cell discussed in Section VIII in connection with the gyroid and its relation to the Kelvin isoperimetric problem. Some of these examples of Voronoi polyhedra were originally derived by the author using hand calculations. Others were obtained by means of a computer algorithm developed by the author, with the assistance of R. Lundberg. This computer algorithm also provides for the automatic construction of a pair of stereoscopic views of the Voronoi polyhedron.

Note added in proof: It has been pointed out to the author by J. Milnor that in order for two different intersection-free IPMS to be related by a deformation (cf. pp. 73-74), it is not necessary that the genus per fundamental region have the same value for the two surfaces. Thus, the deformation relations described on pp. 73-74 are merely special cases of quite general deformability relations among all possible examples of intersection-free IPMS.

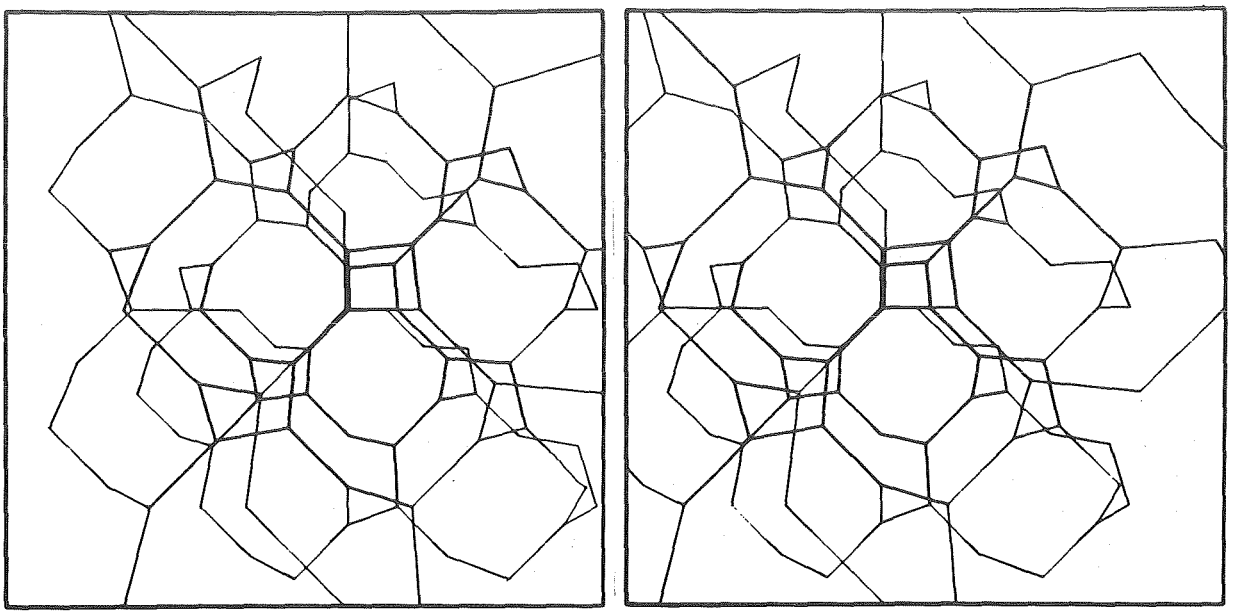

Figure II-1a.- Right-left stereoscopic view of *Laves graph of degree three*. This symmetric graph appears here in its normal "fully-expanded" form, i.e., as a locally-centered graph. In Figures II-1b, c, d, and e, the graph appears in successive stages of partial "collapse". During this transformation, it retains its identity as a symmetric graph with fixed edge length, but it is no longer locally centered (cf. discussion on p. 78). When every edge has completed a 90° plane rotation about either incident vertex, the infinite graph is transformed into a regular tetrahedron; each edge of the graph has become superimposed onto one of the six edges of this tetrahedron. When the edges have completed a 180° plane rotation, the graph enantiomorphous to the original graph is obtained. Throughout the transformation, all vertices of the graph describe elliptical trajectories centered on the origin of the coordinate system in which the transformation is described. Twelve other examples of infinite periodic graphs whose vertices lie in P, D, or G, and whose edges are homeomorphic to arcs lying in P, D, or G can be subjected to a "collapsing" transformation of this kind.

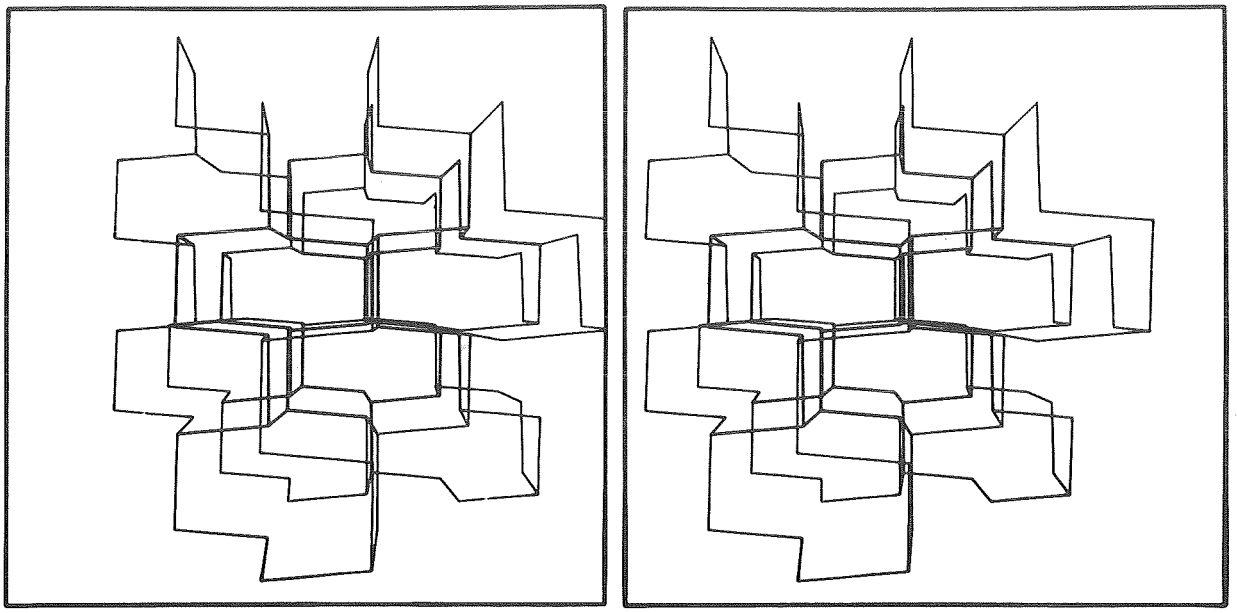

Figure II-1b.- Partially collapsed Laves graph (stage 2).

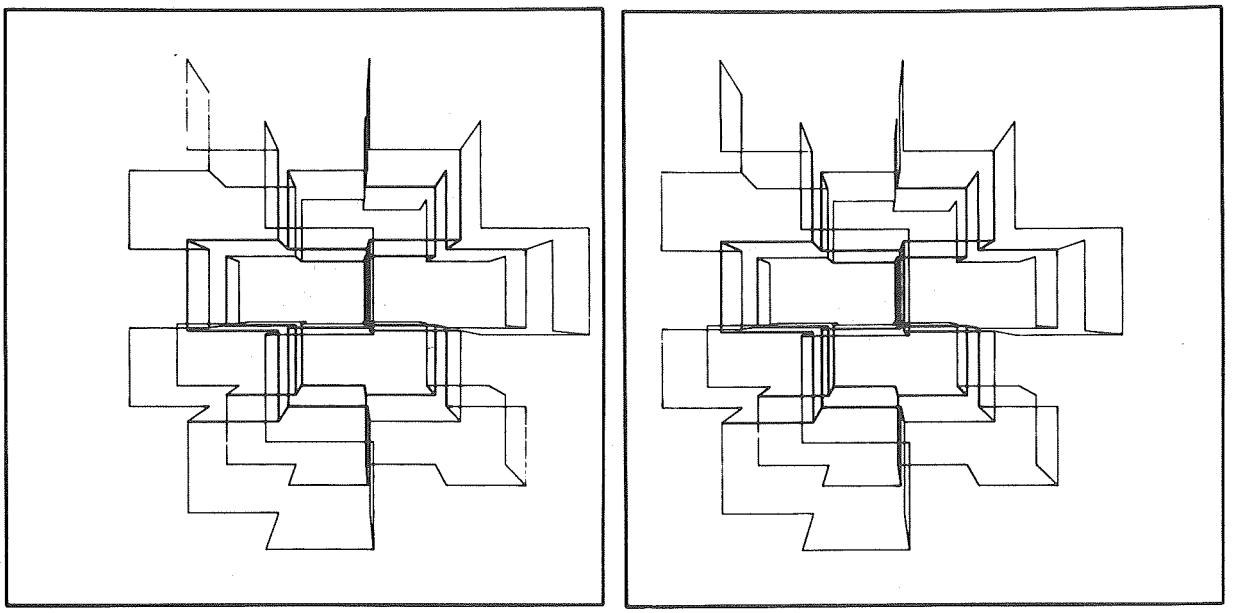

Figure II-1c.- Partially collapsed Laves graph (stage 3); the graph has become transformed into the "defective" simple cubic graph (cf. discussion on p. 83).

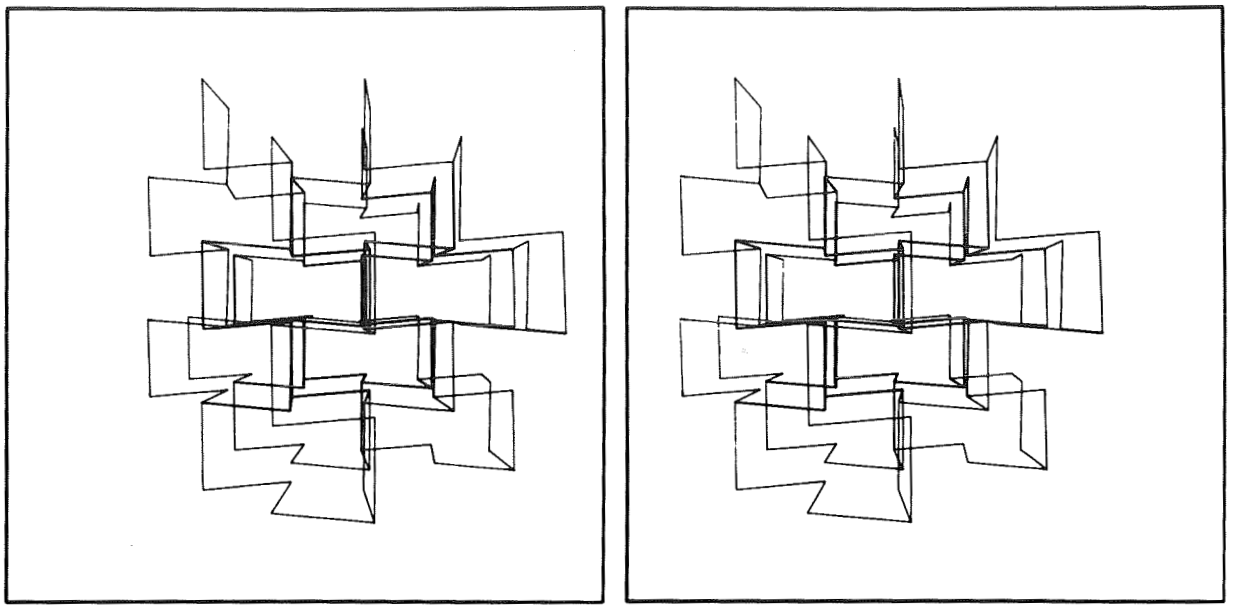

Figure II-1d.- Partially collapsed Laves graph (stage 4).

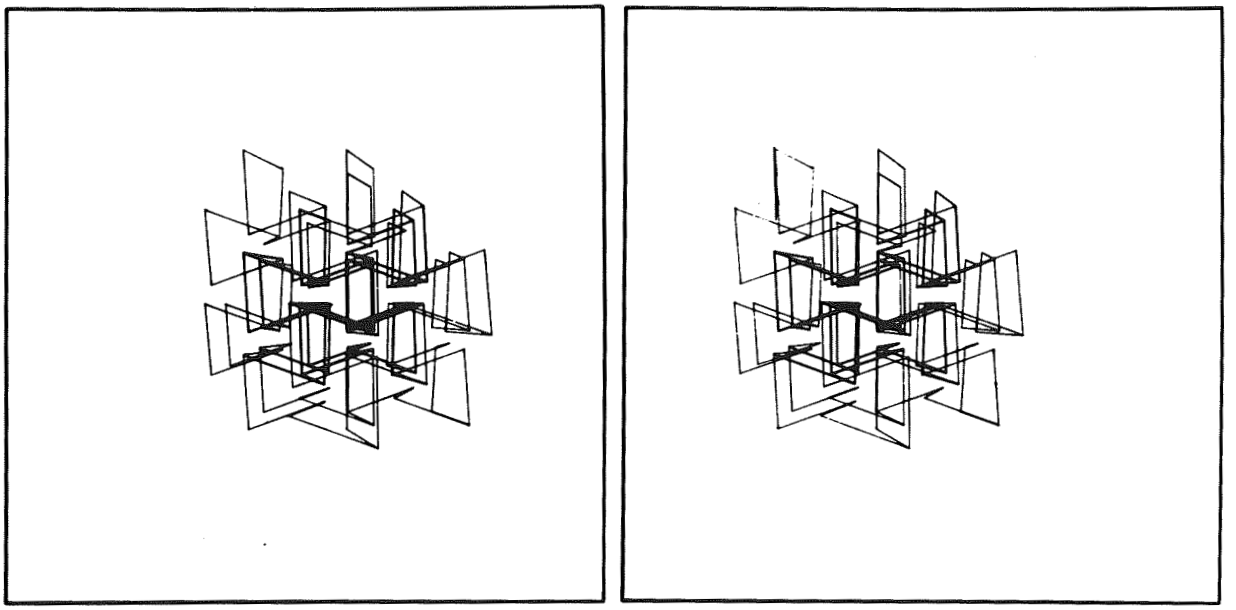

Figure II-1e.- Partially collapsed Laves graph (stage 5).

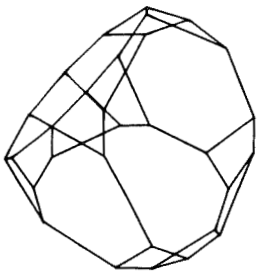

Figure II-2a.- The seventeen-faced *Voronoi polyhedron* of the regular system of points comprising the vertices of two enantiomorphous *Laves graphs of degree three*. These two symmetric graphs are related to one another by inversion, in accordance with their positions as skeletal graphs of the two enantiomorphous labyrinths of the gyroid. (Cf. discussion of the Kelvin isoperimetric problem and the gyroid in Section VIII.)

b.

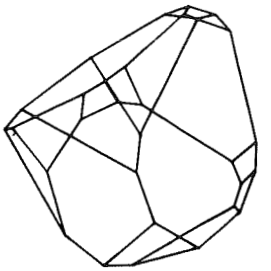

c.

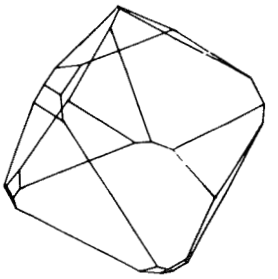

d.

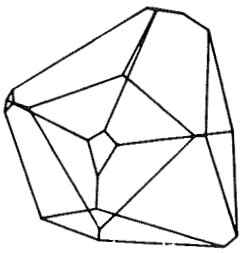

Figure II-2b,c, and d.- Voronoi polyhedra for symmetric graphs in various intermediate stages of collapse.

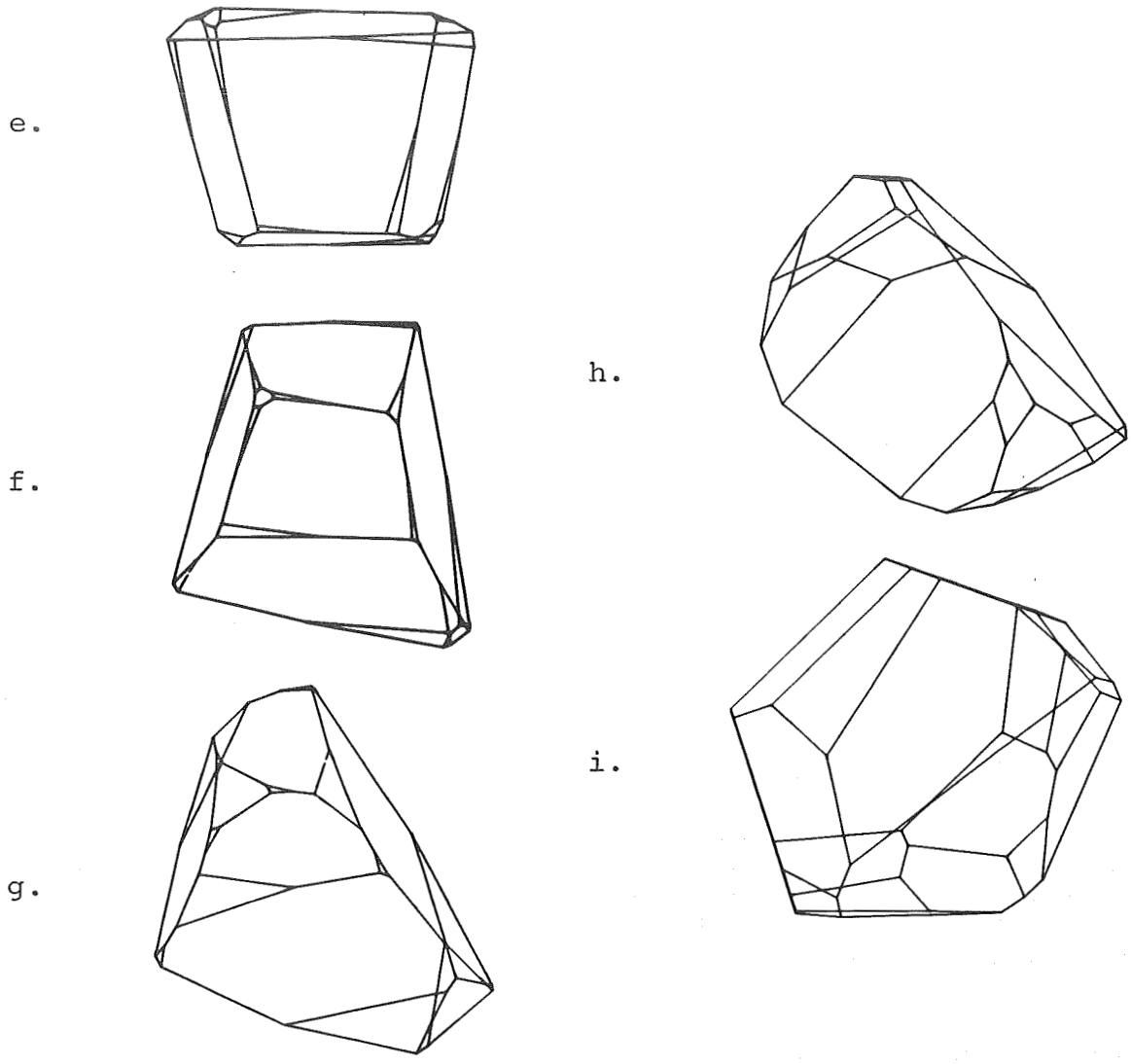

Figure II-2 (Concluded).- Voronoi polyhedra for symmetric graphs in various intermediate stages of collapse.

REFERENCES

1. Schwarz, H.A.: Gesammelte Mathematische Abhandlungen. vol. 1, Julius Springer, Berlin, 1890.

2. Darboux, G.: Leçons sur la Theorie Générale des Surfaces. part 1, Gauthier-Villars, Paris, 1887.

3. Bonnet, O.: Note sur la Théorie Générale des Surfaces. Comptes Rendus, vol. 37, 1853, pp. 529-532.

4. Neovius, E.R.: Bestimmung Zweier Speciellen Periodischen Minimalflächen. Helsingfors, 1883.

5. Schoen, A.H.: Infinite Regular Warped Polyhedra and Infinite Periodic Minimal Surfaces. Not. Amer. Math. Soc., vol. 15, 1968, p. 727.

6. Schoen, A.H.: A Fifth Intersection-Free Infinite Periodic Minimal Surface of Cubic Symmetry. Not. Amer. Math. Soc., vol. 16, 1969, p. 519.

7. Coxeter, H.S.M.: Regular Polytopes. MacMillan, New York, 1963.

8. Stessmann, B.: Periodische Minimalflächen. Math. Zeit., vol. 33, 1934, pp. 417-442.

9. Nitsche, J.C.C.: On New Results in the Theory of Minimal Surfaces. Bull. Amer. Math. Soc., vol. 71, 1965, p. 239.

10. Schoen, A.H.: Homogeneous Nets and Their Fundamental Regions. Not. Amer. Math. Soc., vol. 14, 1967, p. 661.

11. Eisenhart, L.P.: A Treatise on the Differential Geometry of Curves and Surfaces. Dover Publications, New York, 1960.

12. Coxeter, H.S.M. and Moser, W.O.J.: Generators and Relations for Discrete Groups. Springer-Verlag, New York, 1965.

13. Coxeter, H.S.M.: On Laves' Graph of Girth Ten. Can. J. Math., vol. 7, 1955, pp. 18-23.

14. Coxeter, H.S.M.: Regular Skew Polyhedra in Three and Four Dimensions, and Their Topological Analogues. Proc. Lond. Math. Soc., no. 2, vol. 43, 1937, pp. 33-62.

15. O'Neill, B.: Elementary Differential Geometry. Academic Press, New York, 1966, p. 386.

17. Radó, T.: On the Problem of Plateau, Chelsea Publishing Co., New York, 1951.

18. Pearce, P.: Synestructics: The Science of Universal Structure; a Report to the Graham Foundation. Peter Pearce, No. Hollywood, 1966.

19. Pearce, P.: Structure in Nature as a Strategy for Design. The M.I.T. Press, Cambridge, to be published in 1971.

20. Coxeter, H. S. M.: Introduction to Geometry. John Wiley and Sons, Inc., New York, 1961, p. 53.

21. Schoen, A. H.: Infinite Quasi-Regular Warped Polyhedra and Skewness of Regular Polygons. Not. Amer. Math. Soc., vol. 15, 1968, p. 801.

22. Schoen, A. H.: Regular Saddle Polyhedra. Not. Amer. Math. Soc., vol. 15, 1968, p. 929.

23. Bambah, R. P. and Davenport, H.: J. London Math. Soc. t. 27, 1952, pp. 224-229.

24. Rouse Ball, W. W.: Mathematical Recreations and Essays. Revised by H. S. M. Coxeter. The Macmillan Co., New York, 1962, pp. 146-148.

NASA-Langley, 1970 —— 19 C-98

NATIONAL AERONAUTICS AND SPACE ADMINISTRATION
WASHINGTON, D. C. 20546

OFFICIAL BUSINESS

FIRST CLASS MAIL

POSTAGE AND FEES PAID
NATIONAL AERONAUTICS AND
SPACE ADMINISTRATION

POSTMASTER: If Undeliverable (Section 158 Postal Manual) Do Not Return

"The aeronautical and space activities of the United States shall be conducted so as to contribute . . . to the expansion of human knowledge of phenomena in the atmosphere and space. The Administration shall provide for the widest practicable and appropriate dissemination of information concerning its activities and the results thereof."

— NATIONAL AERONAUTICS AND SPACE ACT OF 1958

NASA SCIENTIFIC AND TECHNICAL PUBLICATIONS

TECHNICAL REPORTS: Scientific and technical information considered important, complete, and a lasting contribution to existing knowledge.

TECHNICAL NOTES: Information less broad in scope but nevertheless of importance as a contribution to existing knowledge.

TECHNICAL MEMORANDUMS: Information receiving limited distribution because of preliminary data, security classification, or other reasons.

CONTRACTOR REPORTS: Scientific and technical information generated under a NASA contract or grant and considered an important contribution to existing knowledge.

TECHNICAL TRANSLATIONS: Information published in a foreign language considered to merit NASA distribution in English.

SPECIAL PUBLICATIONS: Information derived from or of value to NASA activities. Publications include conference proceedings, monographs, data compilations, handbooks, sourcebooks, and special bibliographies.

TECHNOLOGY UTILIZATION PUBLICATIONS: Information on technology used by NASA that may be of particular interest in commercial and other non-aerospace applications. Publications include Tech Briefs, Technology Utilization Reports and Technology Surveys.

Details on the availability of these publications may be obtained from:

SCIENTIFIC AND TECHNICAL INFORMATION DIVISION

NATIONAL AERONAUTICS AND SPACE ADMINISTRATION

Washington, D.C. 20546